New Journal of Chemistry

Design, Synthesis and Characterization of Indole based Anion Sensing Receptors

Ramalingam Manivannan[1], Angupillai Satheshkumar[1], El-Sayed H. El-Mossalamy[2,3], Laila M. Al-Harbi[2], Samia A. Kosa[2] and Kuppanagounder P. Elango[1*]

[1]Department of Chemistry, Gandhigram Rural Institute (Deemed University), Gandhigram 624302, India

[2]Chemistry Department, Faculty of Science, King Abdul-Aziz University, Jeddah 21589, P.O.Box: 80203 Saudi Arabia

[3]Chemistry Department, Faculty of Science, Benha University, Benha, Egypt 13518

Supporting Information

Fig.No.	TABLE OF CONTENT	Page No.

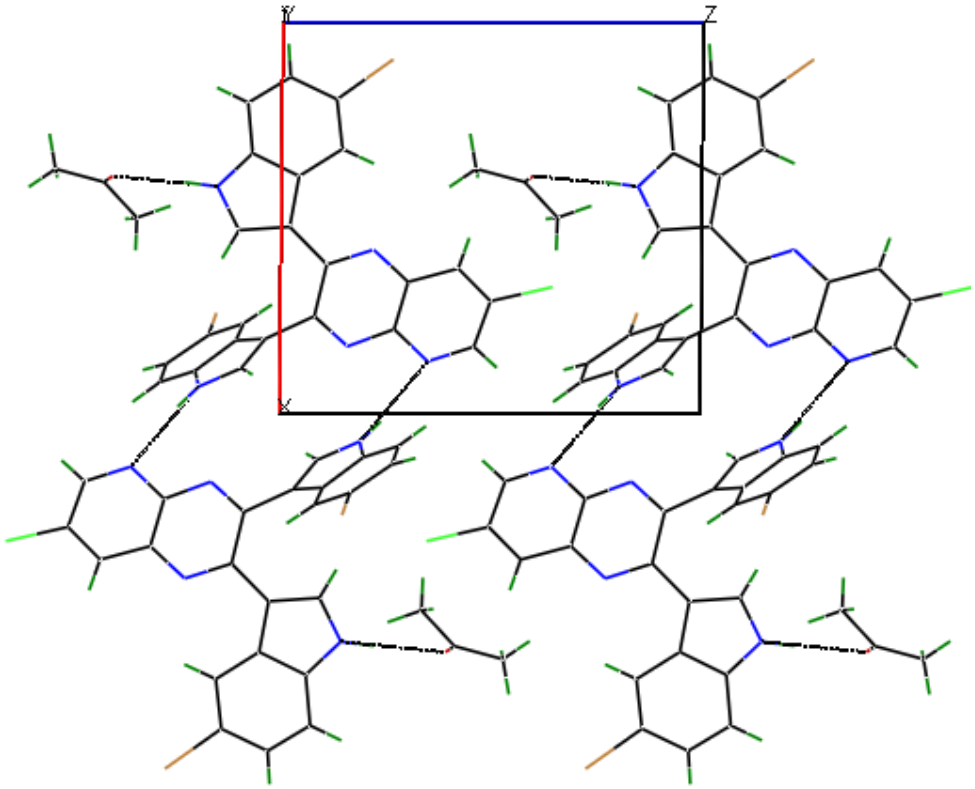

Figure S1. Crystal Packing of R4

Figure S2. Color change of R1-R4 (6.25x10-5 M) with various anions.

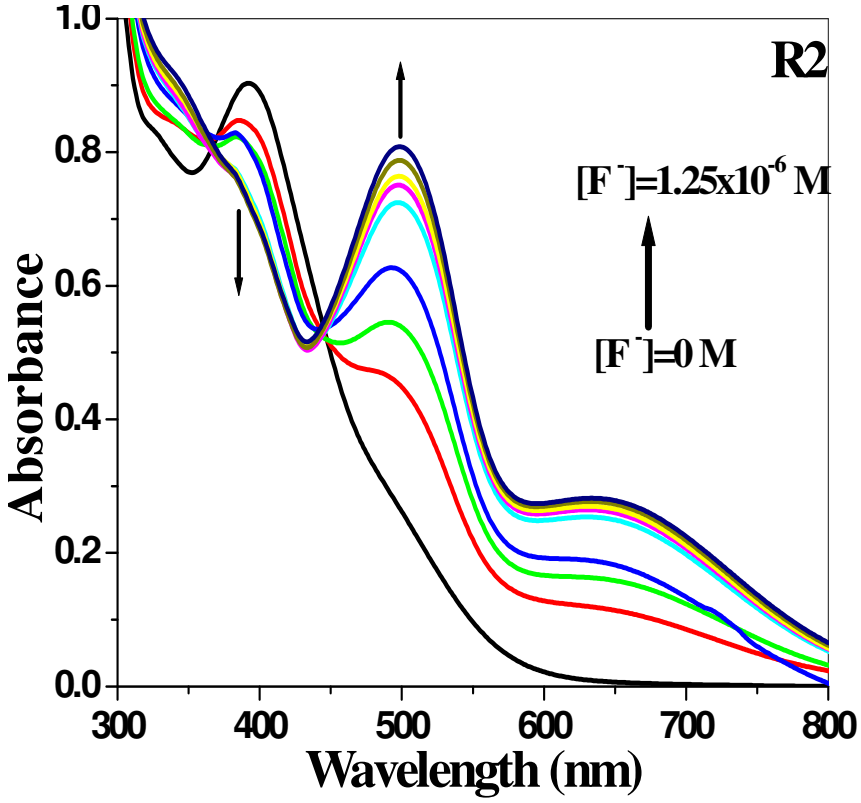
R2
[F⁻]=1.25x10⁻⁶ M
[F⁻]=0 M
Absorbance
Wavelength (nm)
1.0
0.8
0.6
0.4
0.2
0.0
300
400
500
600
700
800

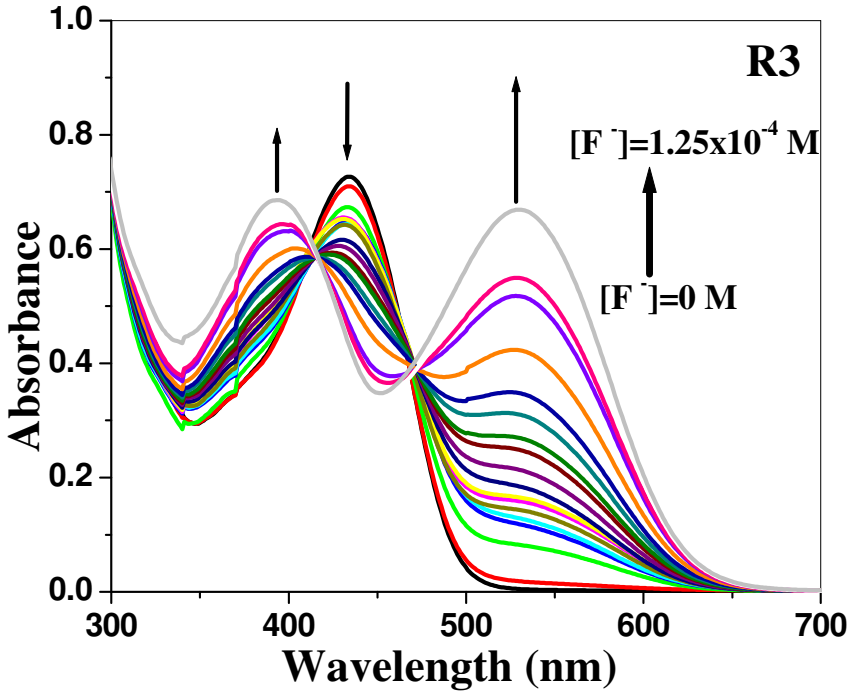
R3
[F ⁻]=1.25x10⁻⁴ M
[F ⁻]=0 M
Absorbance
Wavelength (nm)
1.0
0.8
0.6
0.4
0.2
0.0
300
400
500
600
700

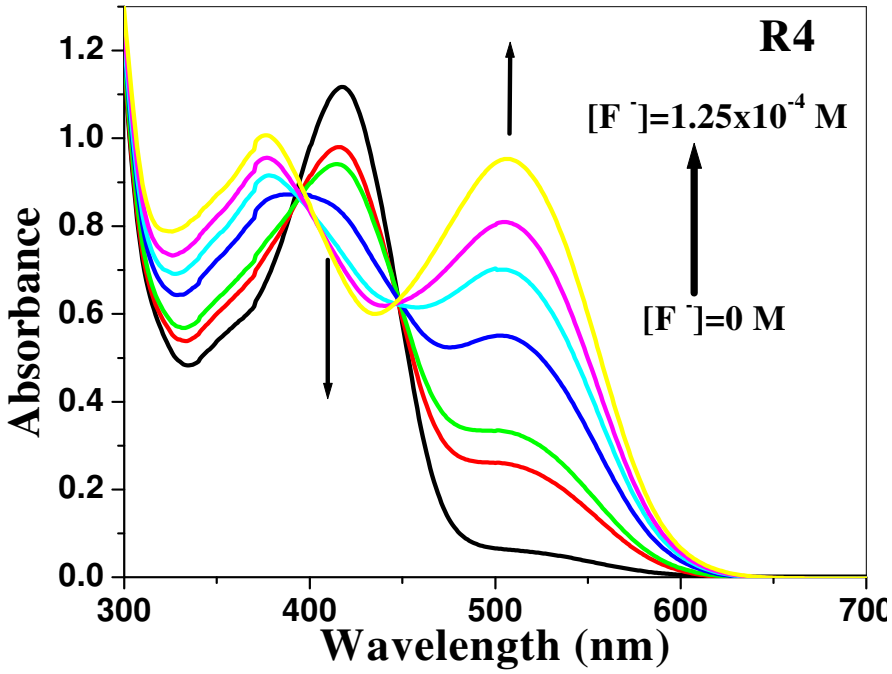
R4
[F ⁻]=1.25x10⁻⁴ M
[F ⁻]=0 M
Absorbance
Wavelength (nm)
1.2
1.0
0.8
0.6
0.4
0.2
0.0
300
400
500
600
700

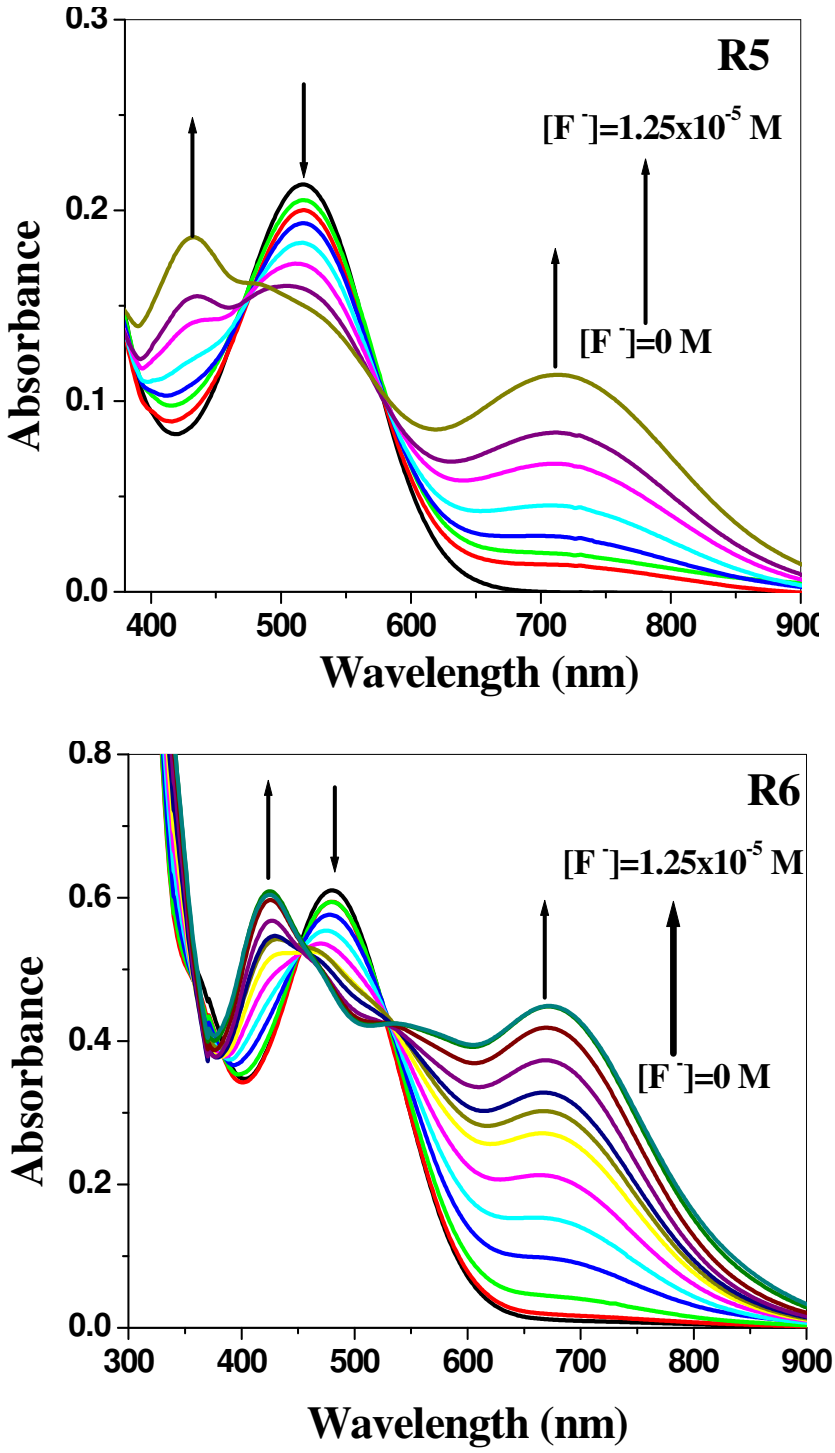

Figure S3. Change in UV-Vis spectra for **R3-R6** (6.25×10^{-5} M) in DMF with the incremental addition of fluoride ions.

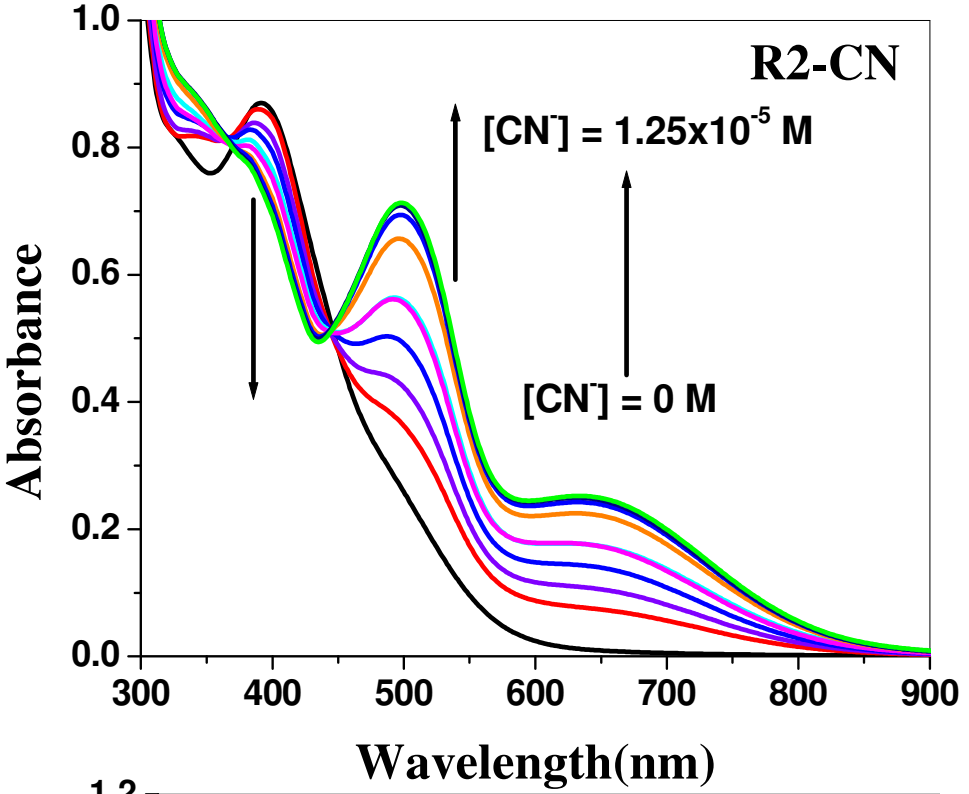
R2-CN
[CN-] = 1.25x10-5 M
[CN-] = 0 M
Absorbance
Wavelength(nm)
1.0
0.8
0.6
0.4
0.2
0.0
300
400
500
600
700
800
900

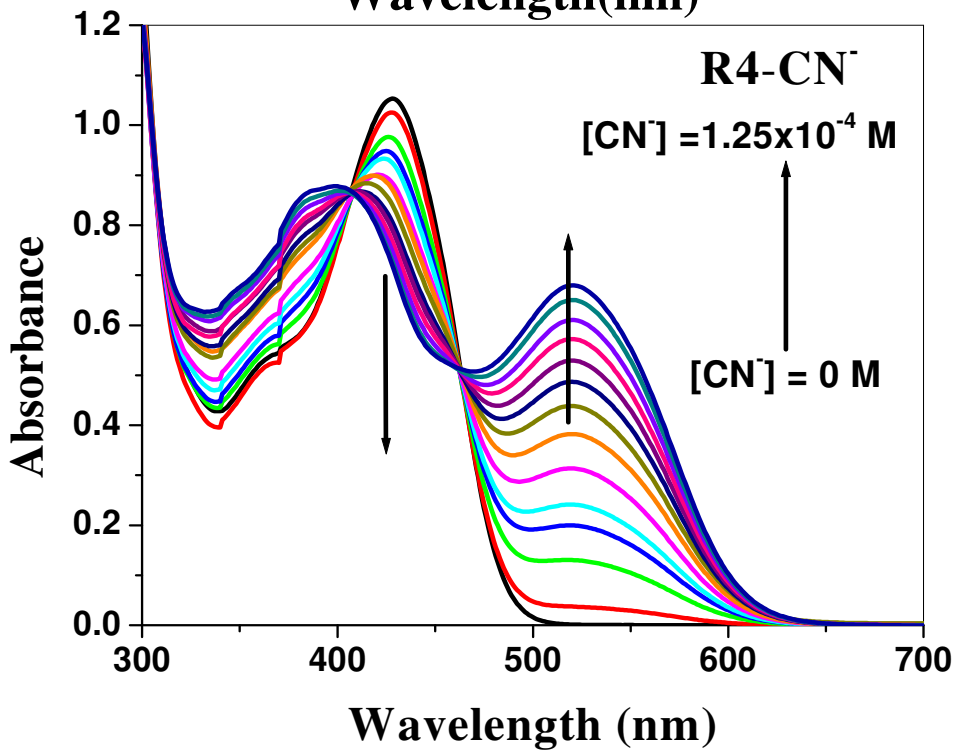
R4-CN-
[CN-] =1.25x10-4 M
[CN-] = 0 M
Absorbance
Wavelength (nm)
1.2
1.0
0.8
0.6
0.4
0.2
0.0
300
400
500
600
700

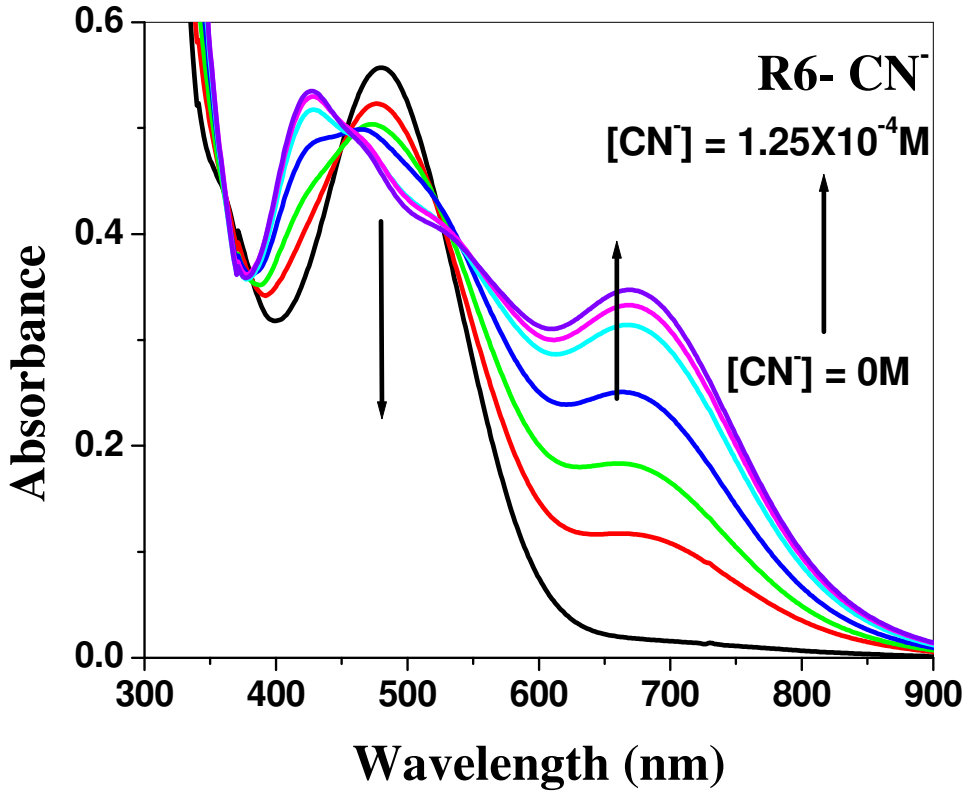

Figure S4. Change in UV-Vis spectra for **R2, R4, R6** (6.25×10^{-5}) in DMF with incremental addition of cyanide ions.

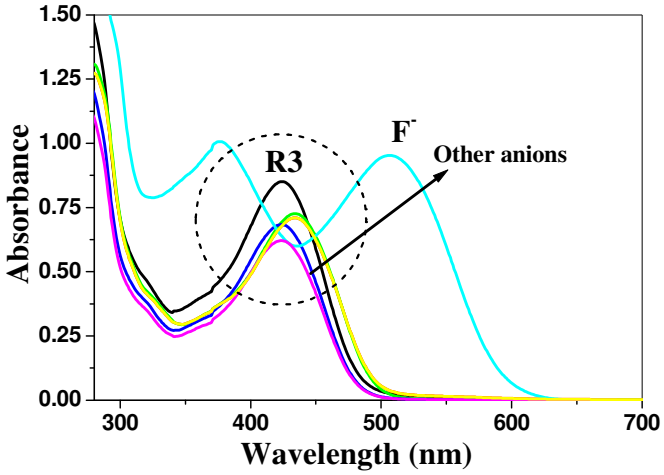

Figure S5. UV-Vis absorption changes of **R3** (6.25×10^{-5} M) upon addition of 1 eqv. of tetrabutylammonium salts of F^-, Cl^-, Br^-, I^-, NO_3^-, $H_2PO_4^-$, AcO^-, CN^-.

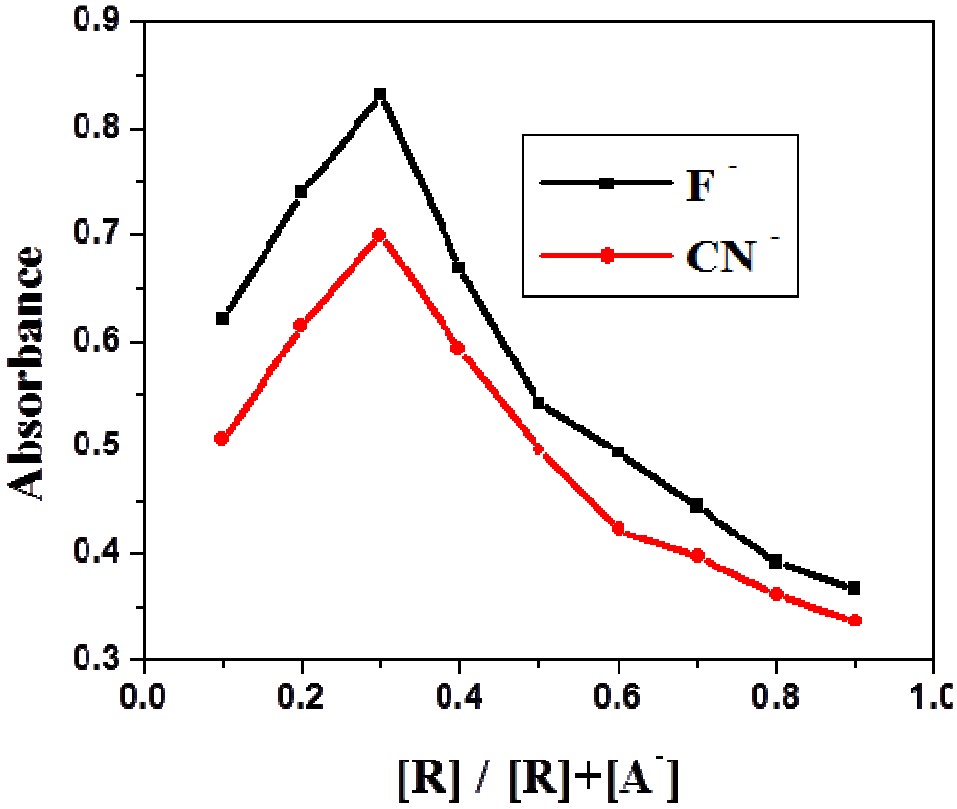

Figure S6. Job's plot for R4 with F^- and CN^-.

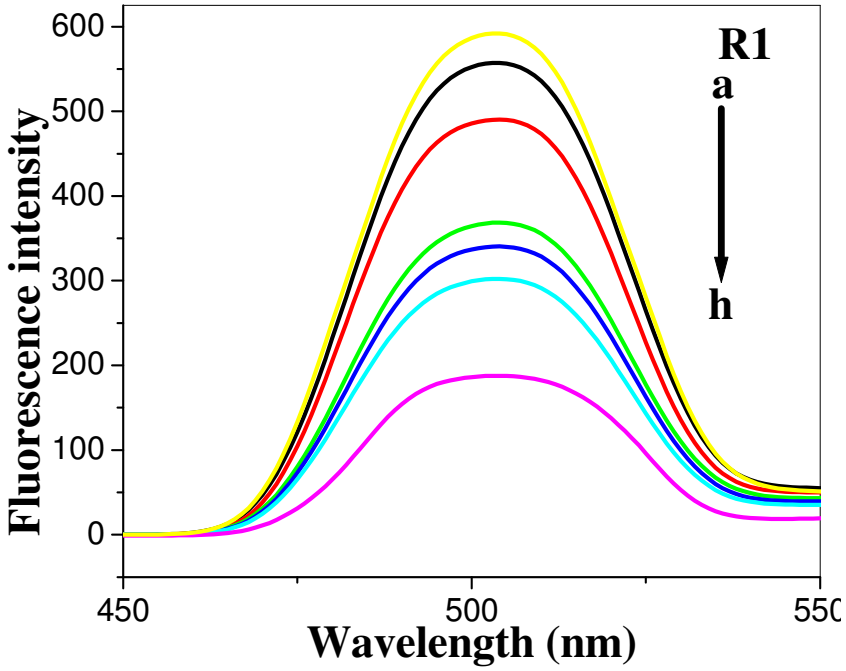
R1
a
h
Fluorescence intensity
Wavelength (nm)
600
500
400
300
200
100
0
450
500
550

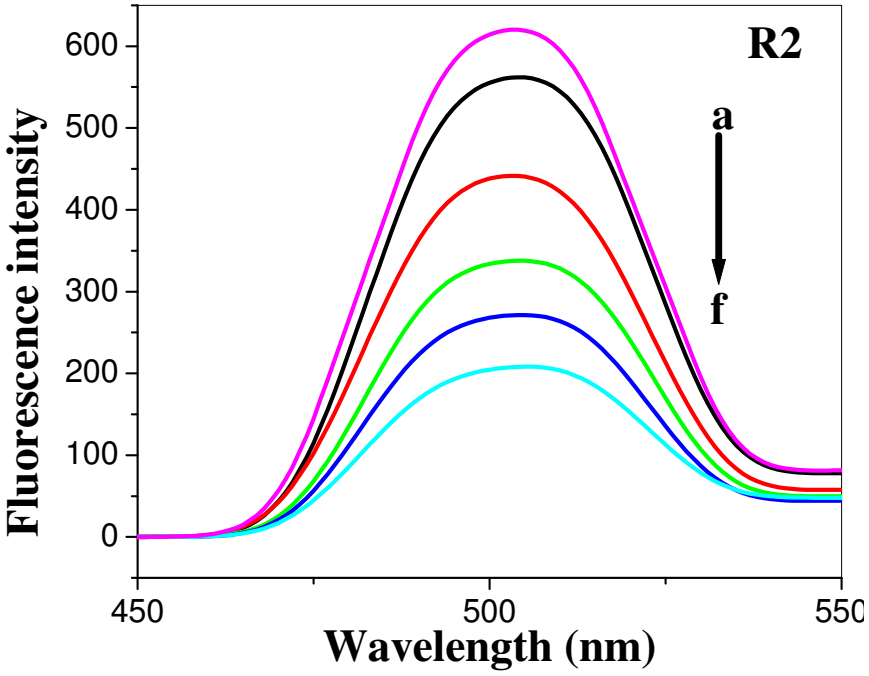
R2
a
f
Fluorescence intensity
Wavelength (nm)
600
500
400
300
200
100
0
450
500
550

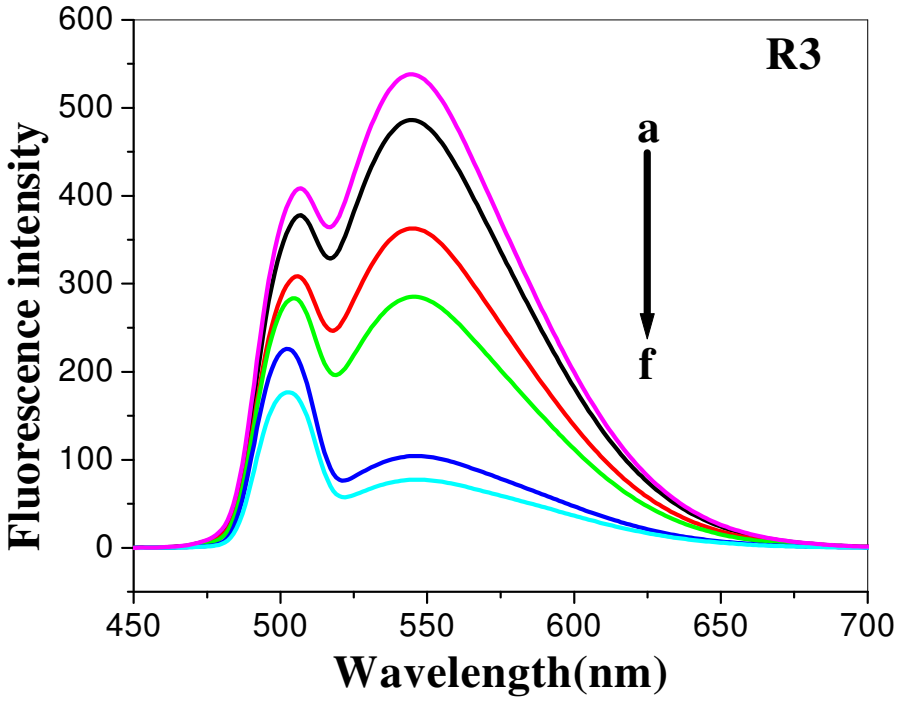
R3
a
f
Fluorescence intensity
Wavelength(nm)
600
500
400
300
200
100
0
450
500
550
600
650
700

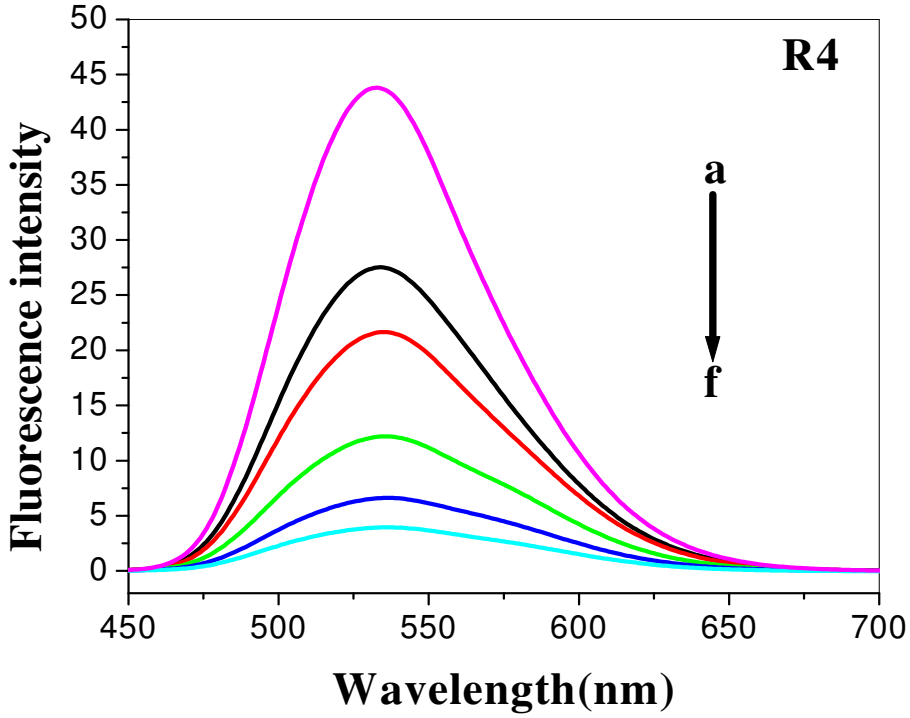
R4
a
f
Fluorescence intensity
Wavelength(nm)
50
45
40
35
30
25
20
15
10
5
0
450
500
550
600
650
700

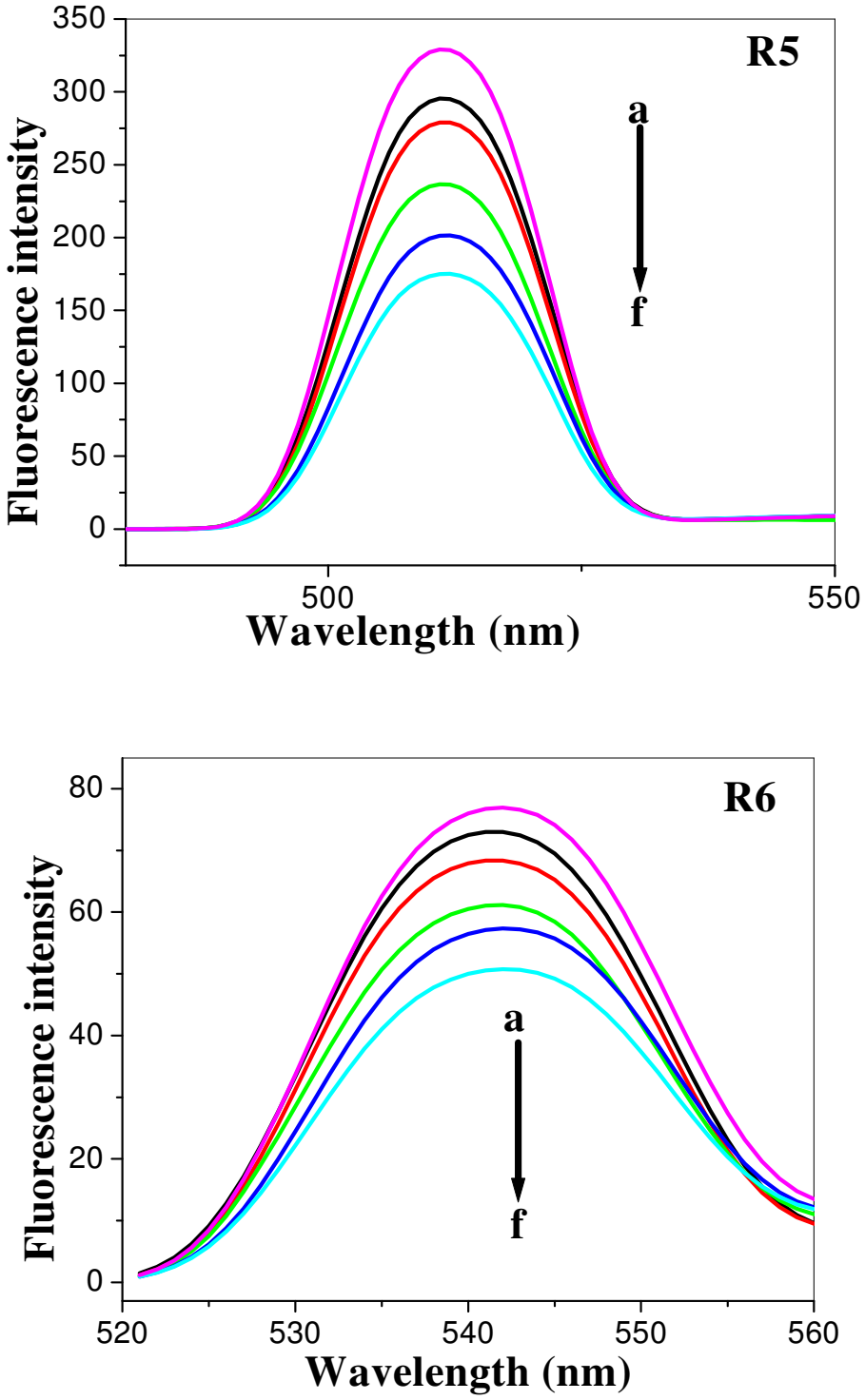

Figure S7. Change in fluorescence emission spectra for R1-R6 (6.25×10^{-5} M) in DMF with addition of $[(Bu)_4N]F$ in DMF from 0 - 12.5×10^{-4} M.

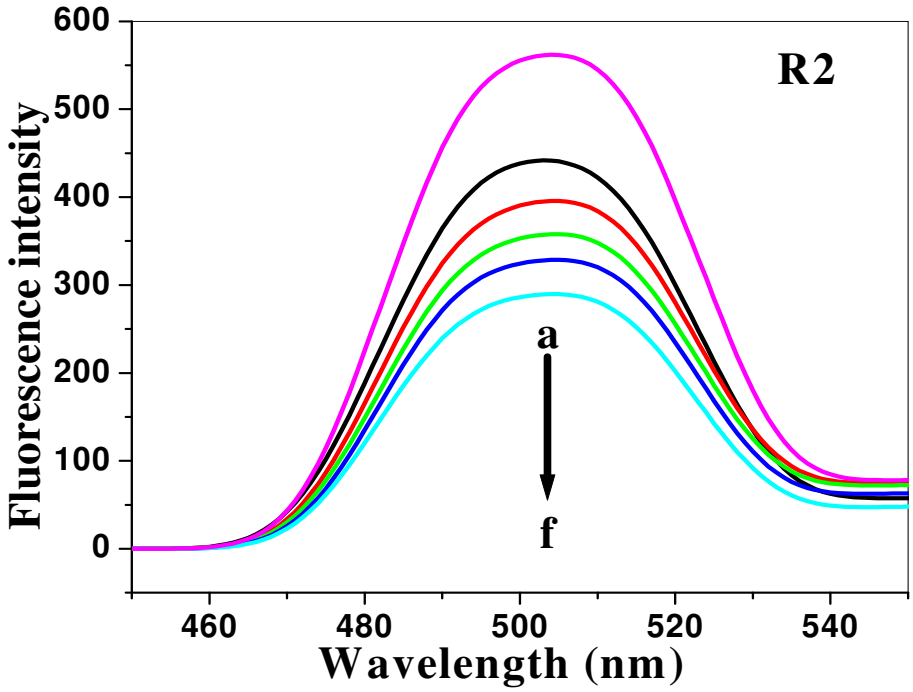
R2
a
f
Fluorescence intensity
Wavelength (nm)
0
100
200
300
400
500
600
460
480
500
520
540

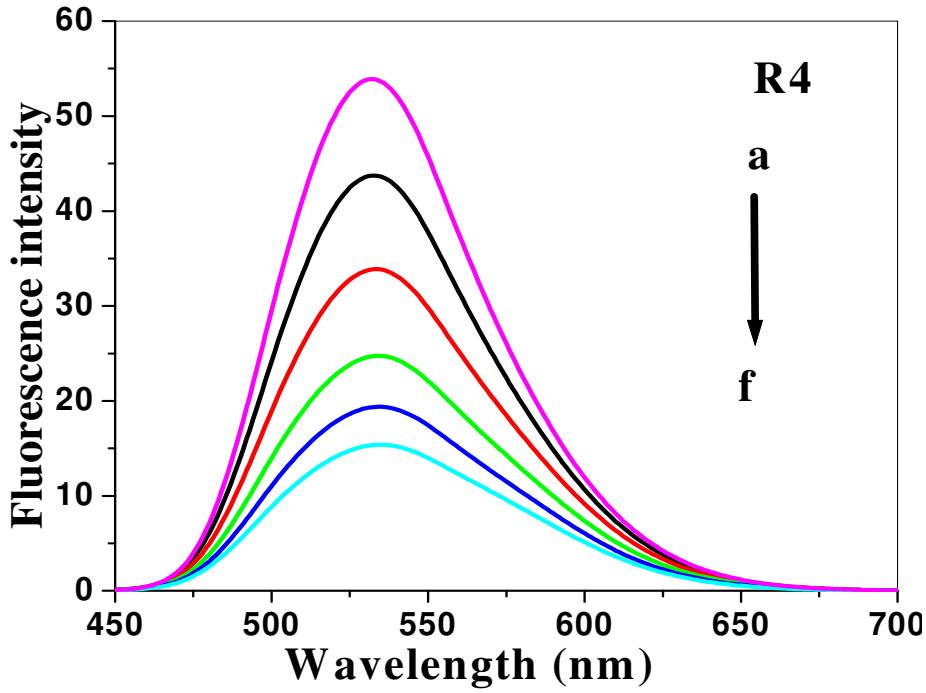
R4
a
f
Fluorescence intensity
Wavelength (nm)
0
10
20
30
40
50
60
450
500
550
600
650
700

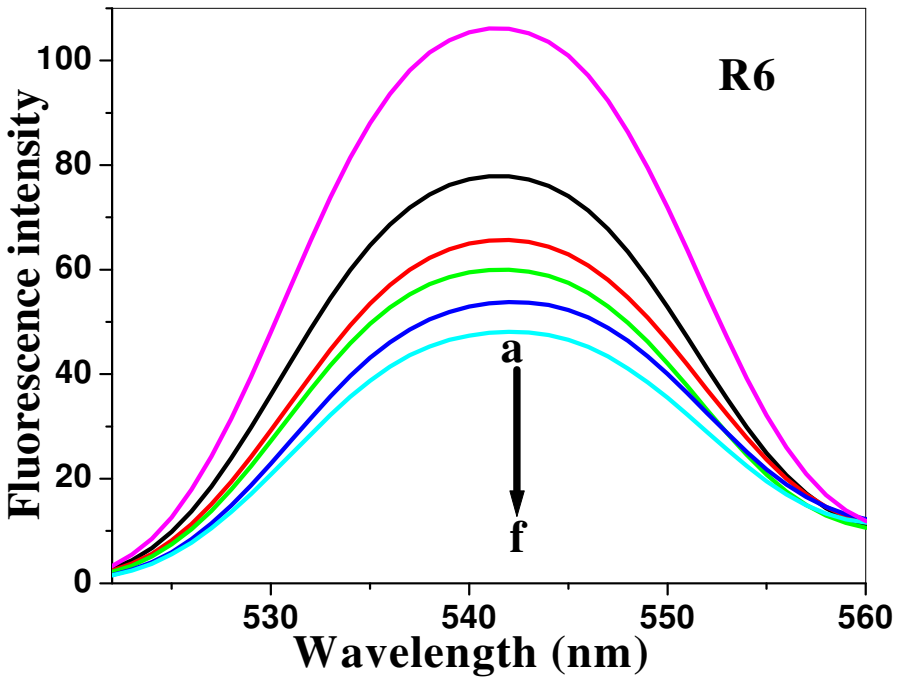

Figure S8. Change in fluorescence emission spectra for R2, R4, R6 (6.25×10^{-5} M) in DMF with addition of [(Bu)4N]CN in DMF from 0- 12.5×10^{-4} M.

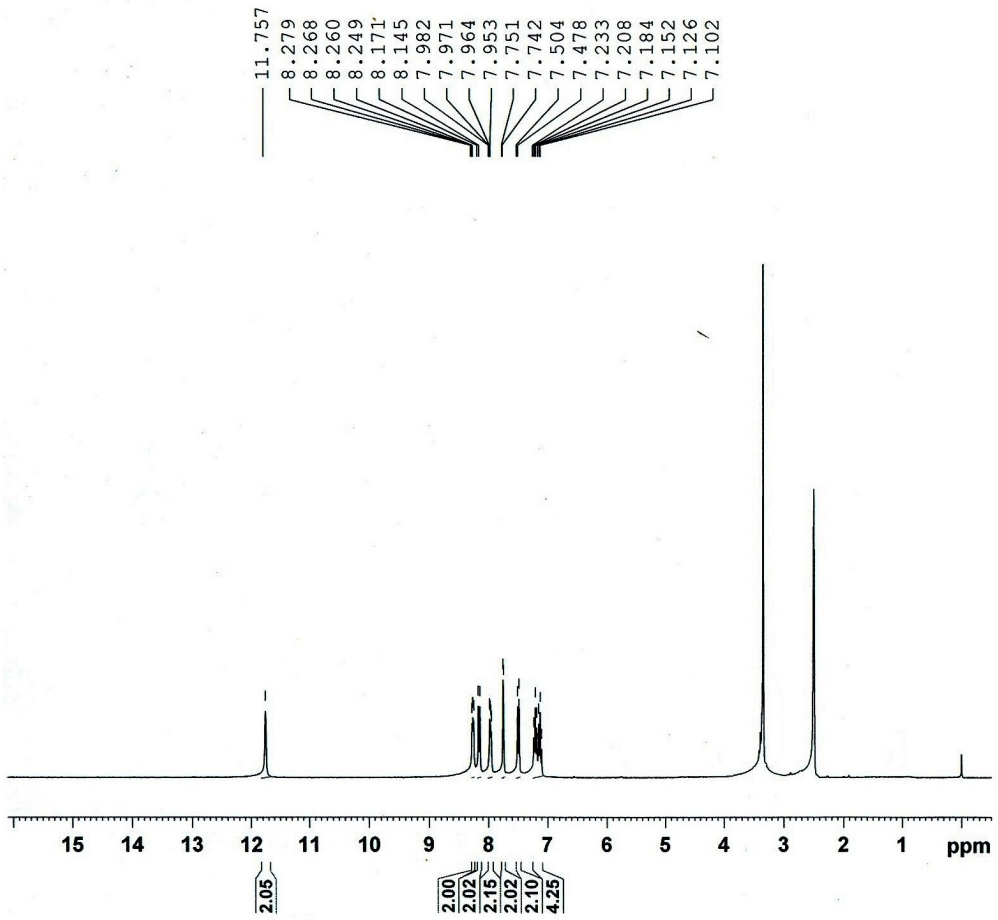

Figure S9. NMR spectrum of R1 with 0 eqv of F^-.

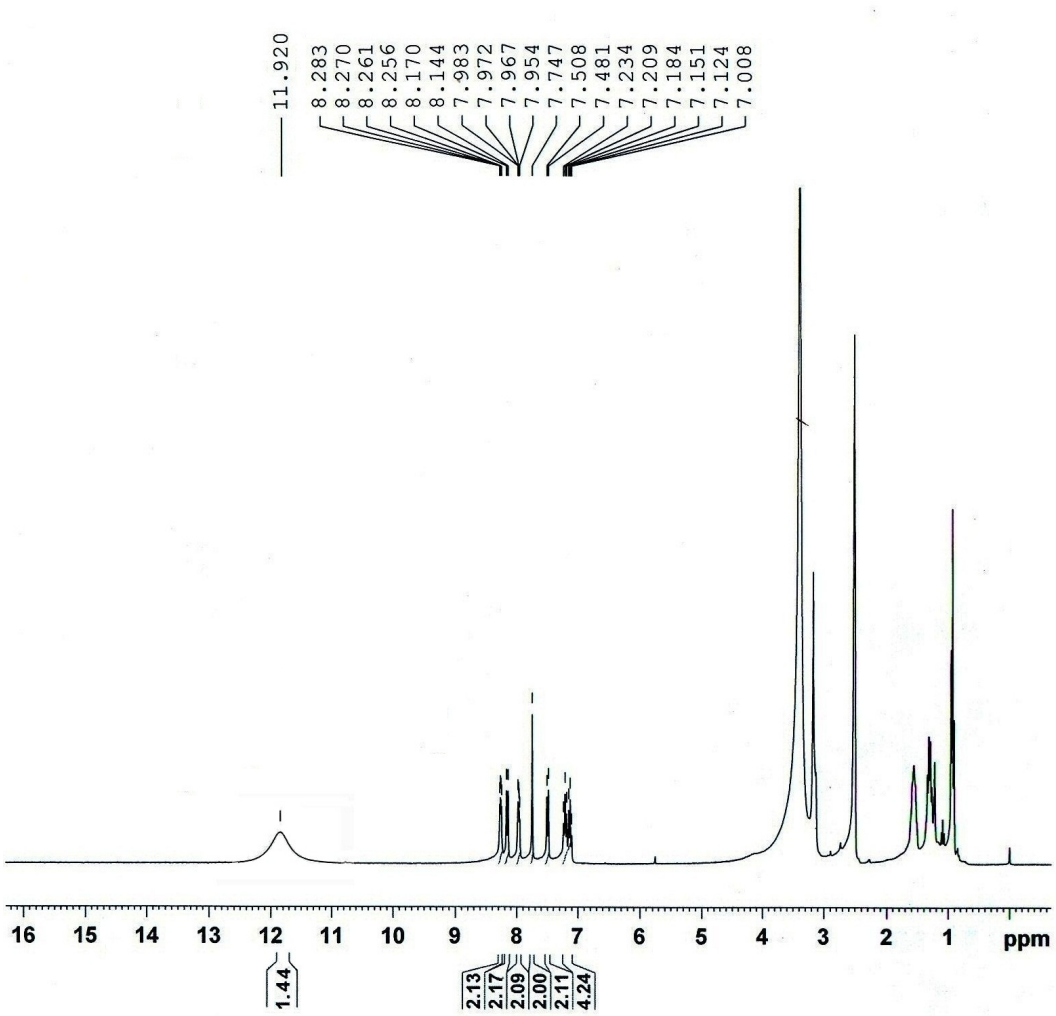

Figure S10. NMR spectrum of R1 with 0.5 eqv of F^-.

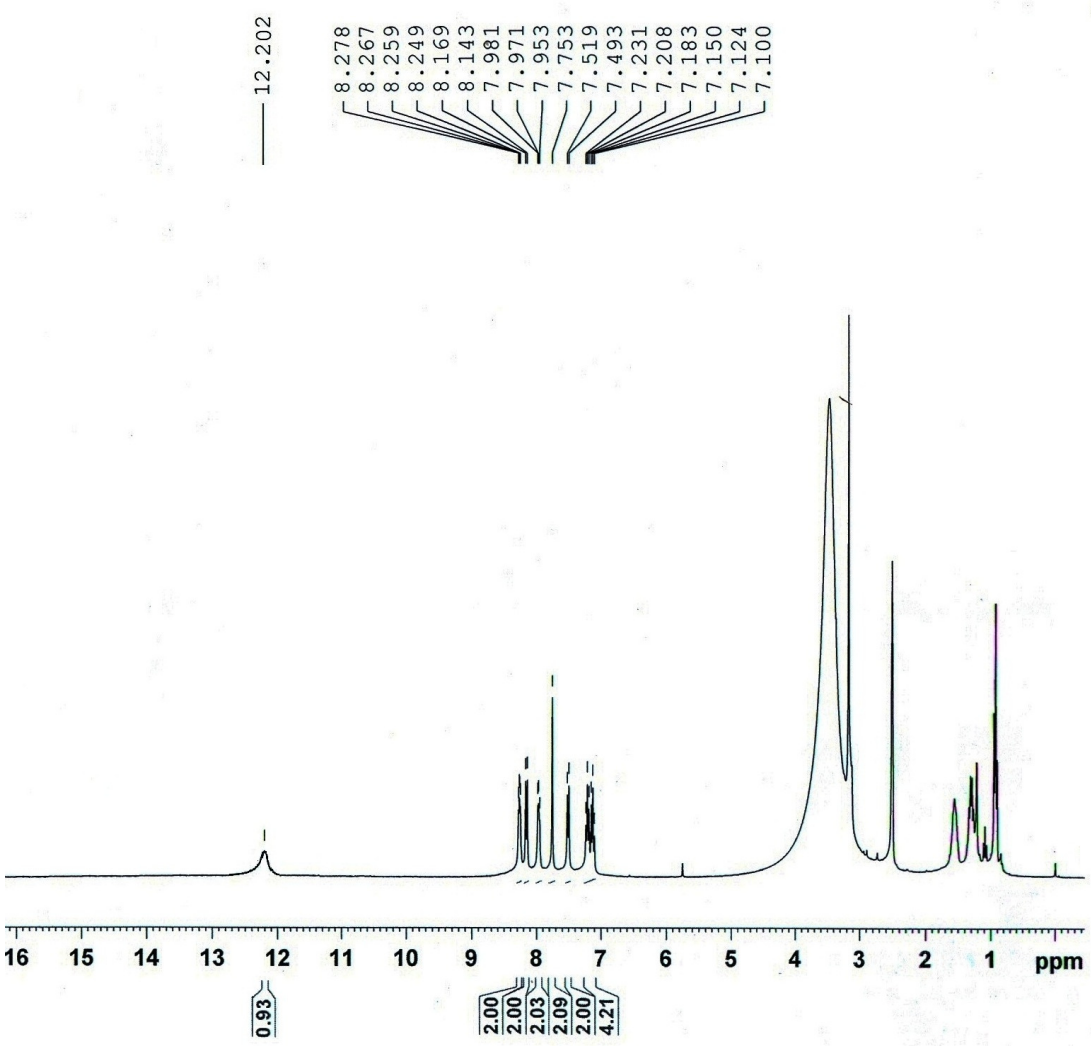

Figure S11. NMR spectrum of R1 with 1.0 eqv of F^-.

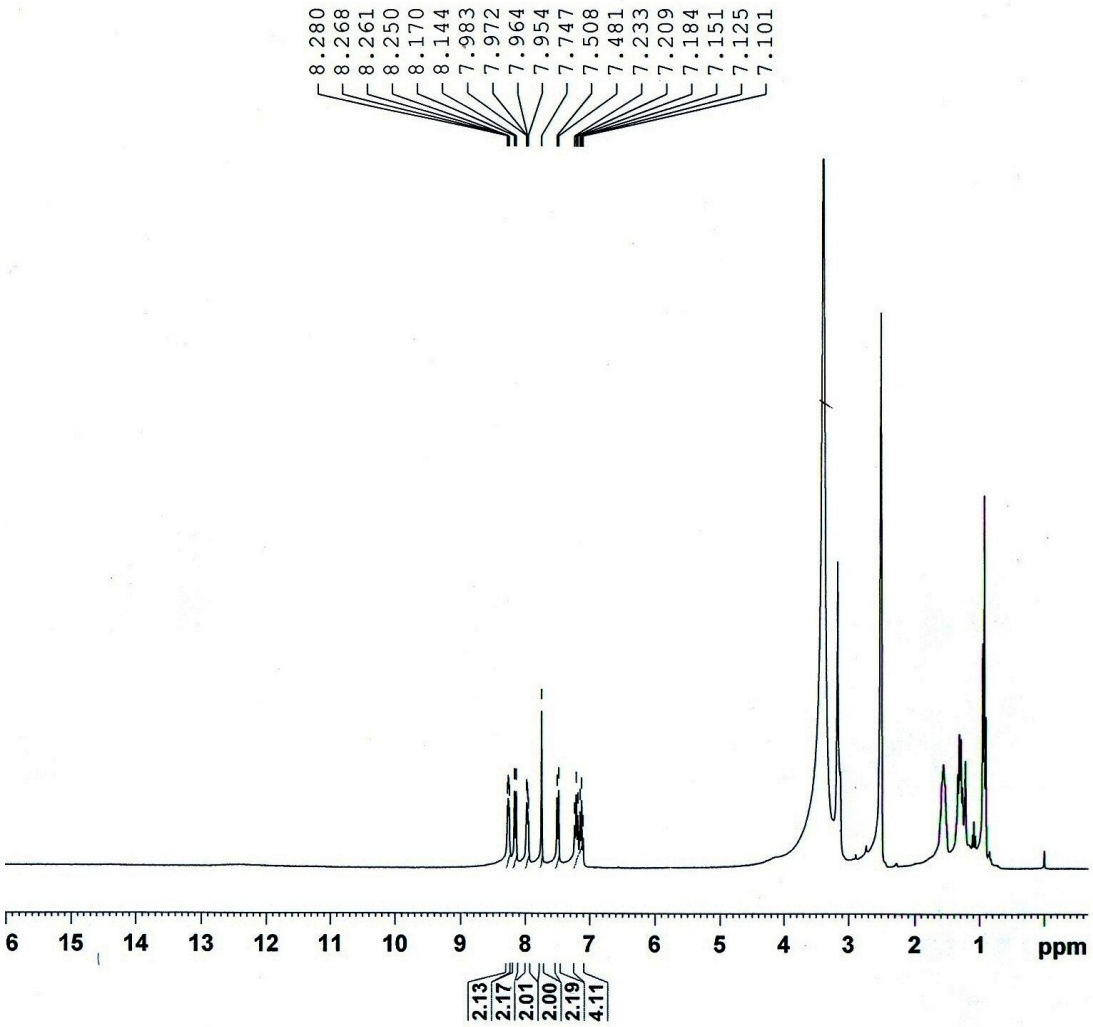

Figure S12. NMR spectrum of R1 with 2.0 eqv of F^-.

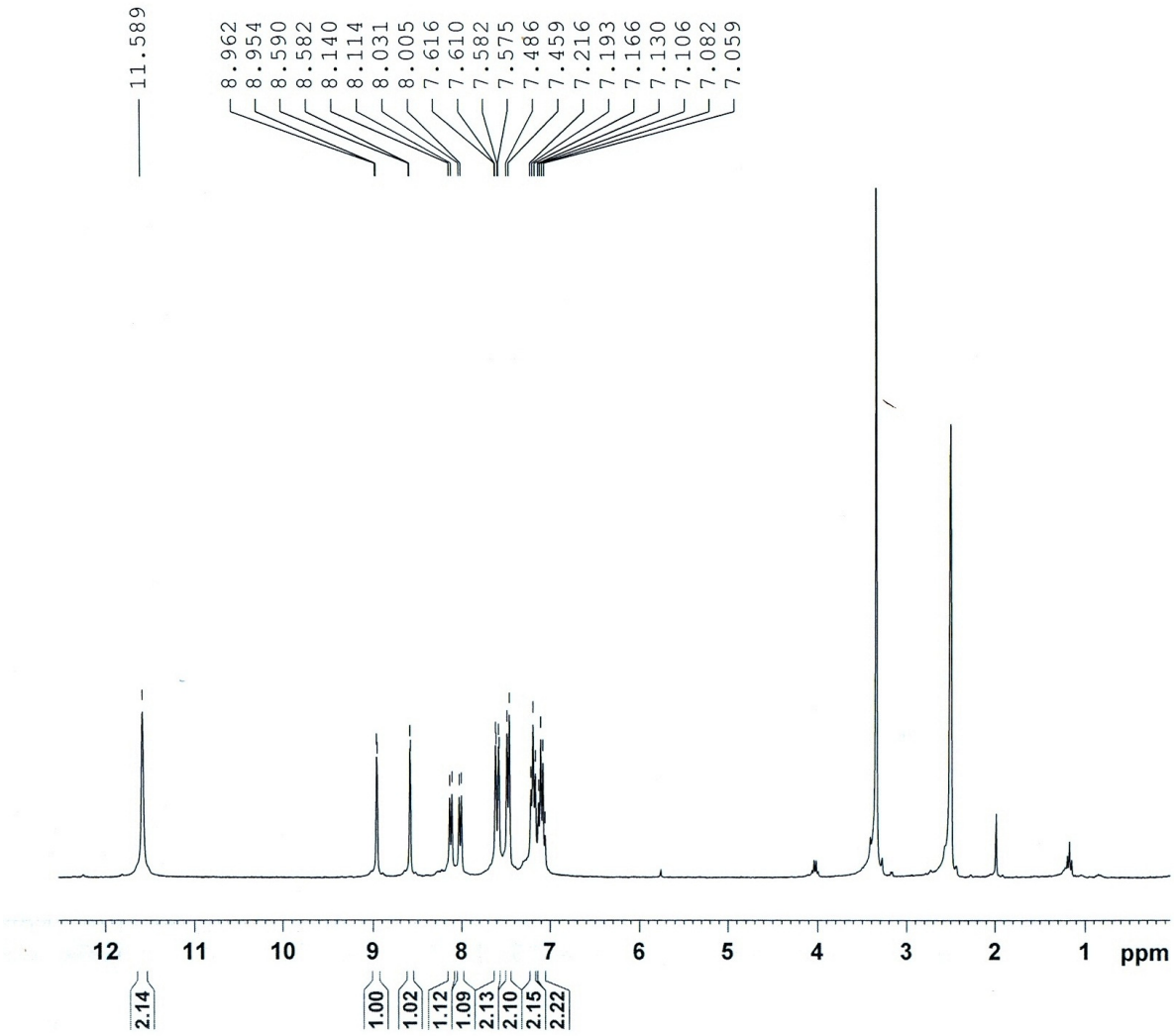

Figure S13. NMR spectrum of R3 with 0 eqv of F^-.

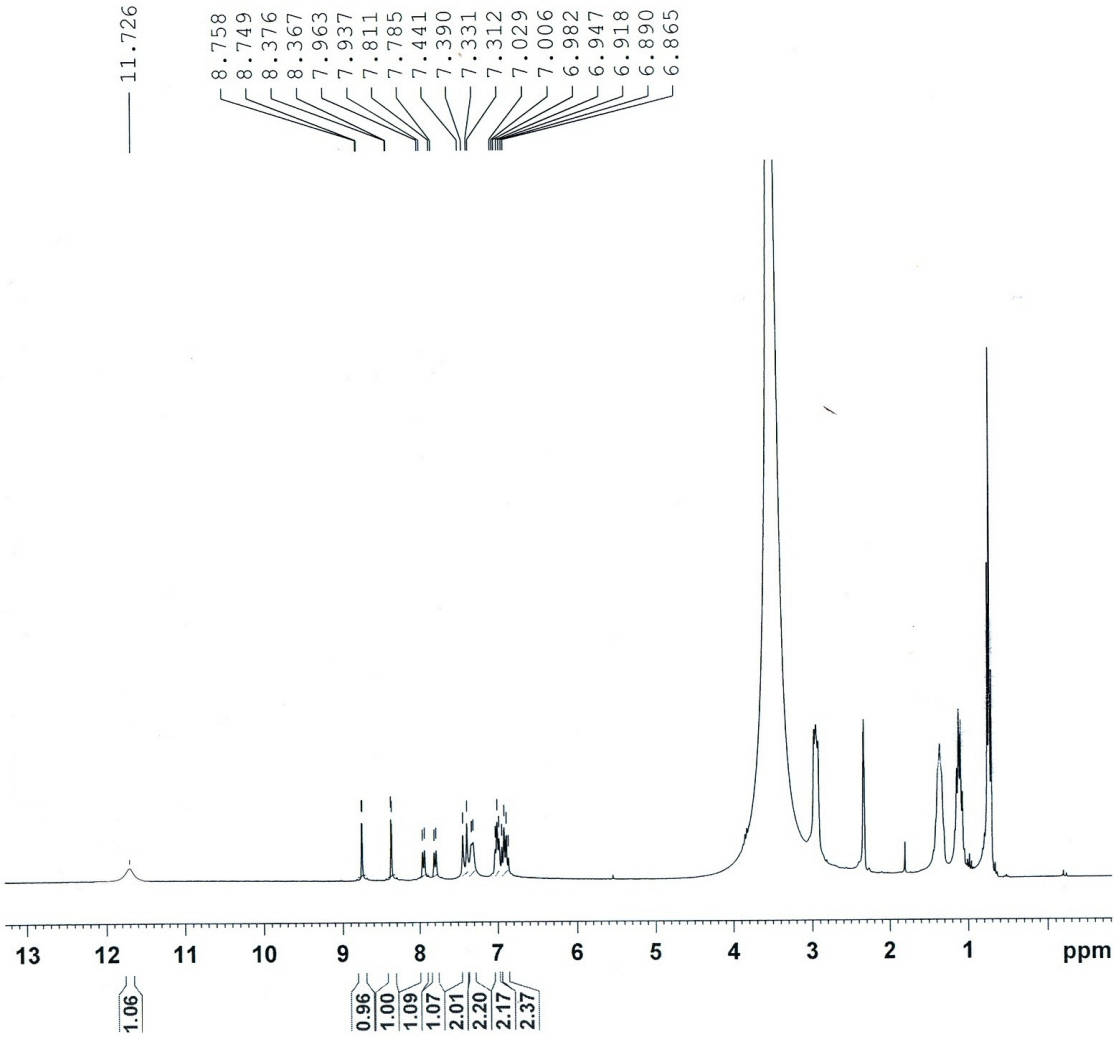

Figure S14. NMR spectrum of R3 with 0.5 eqv of F¯.

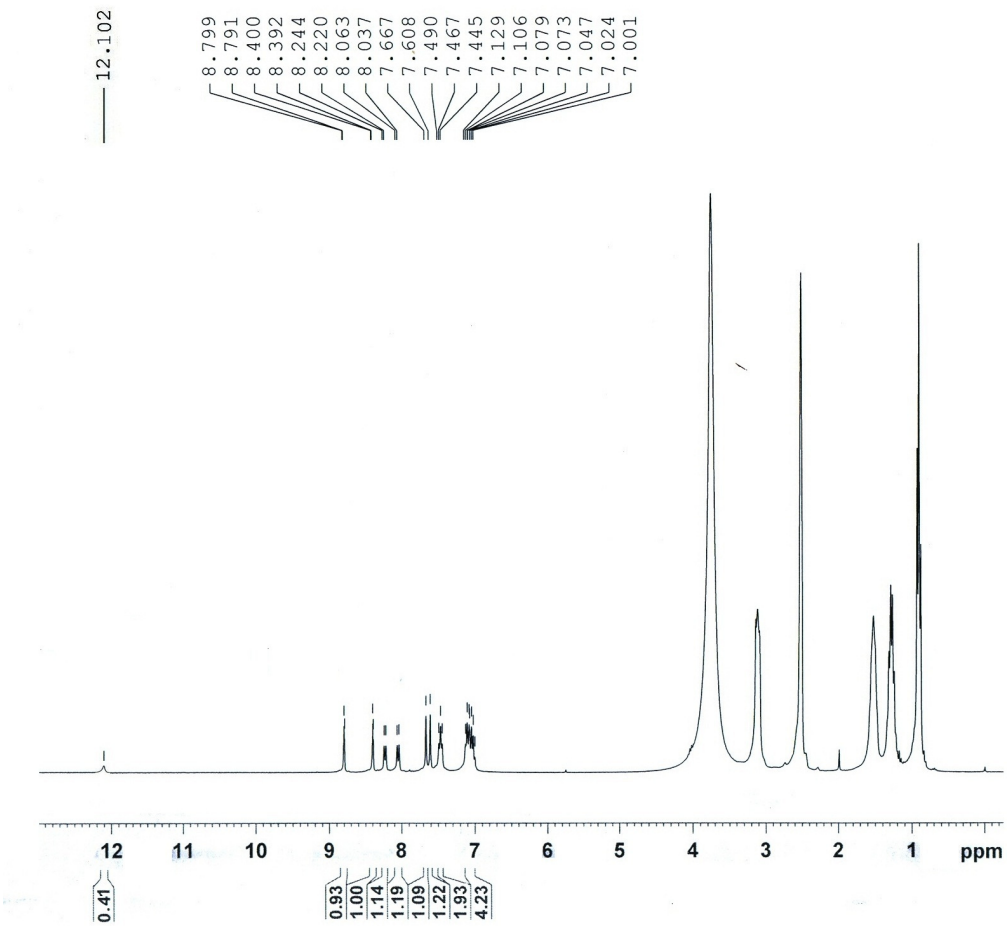

Figure S15. NMR spectrum of R3 with 1.0 eqv of F⁻.

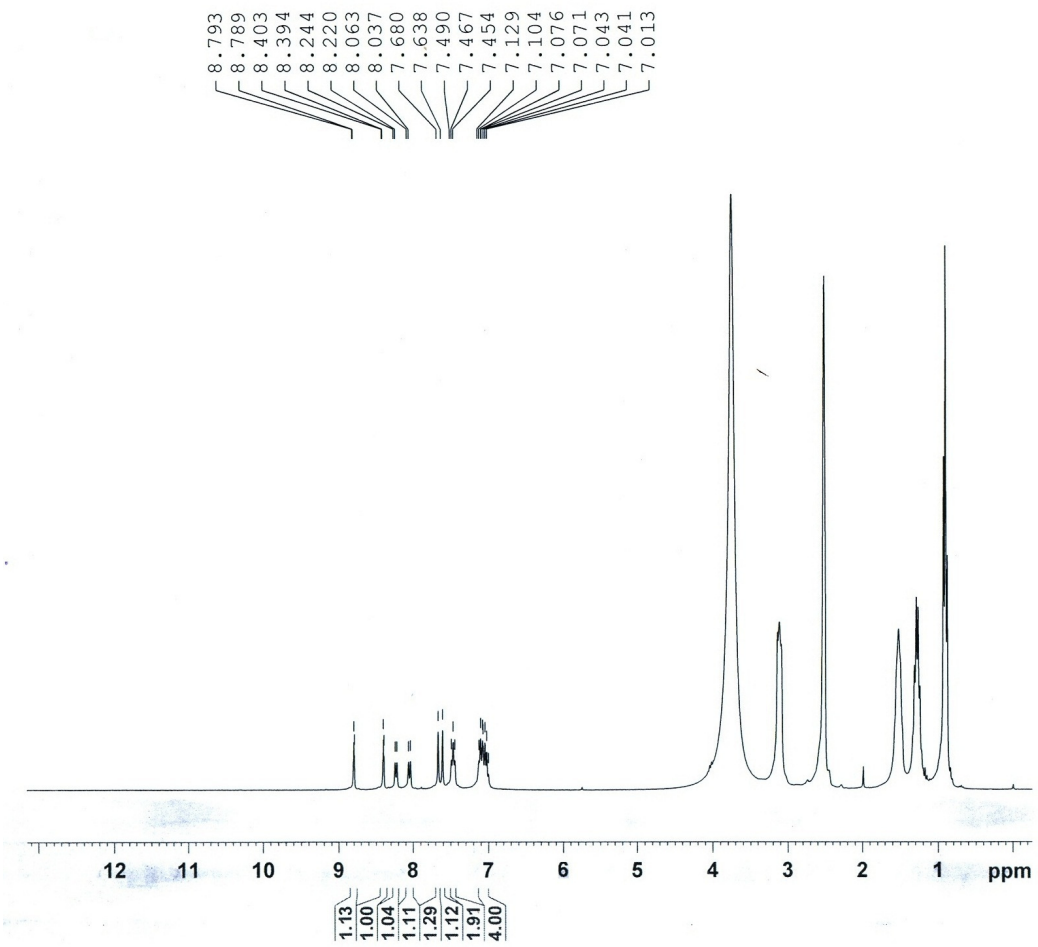

Figure S16. NMR spectrum of R3 with 2.0 eqv of F⁻.

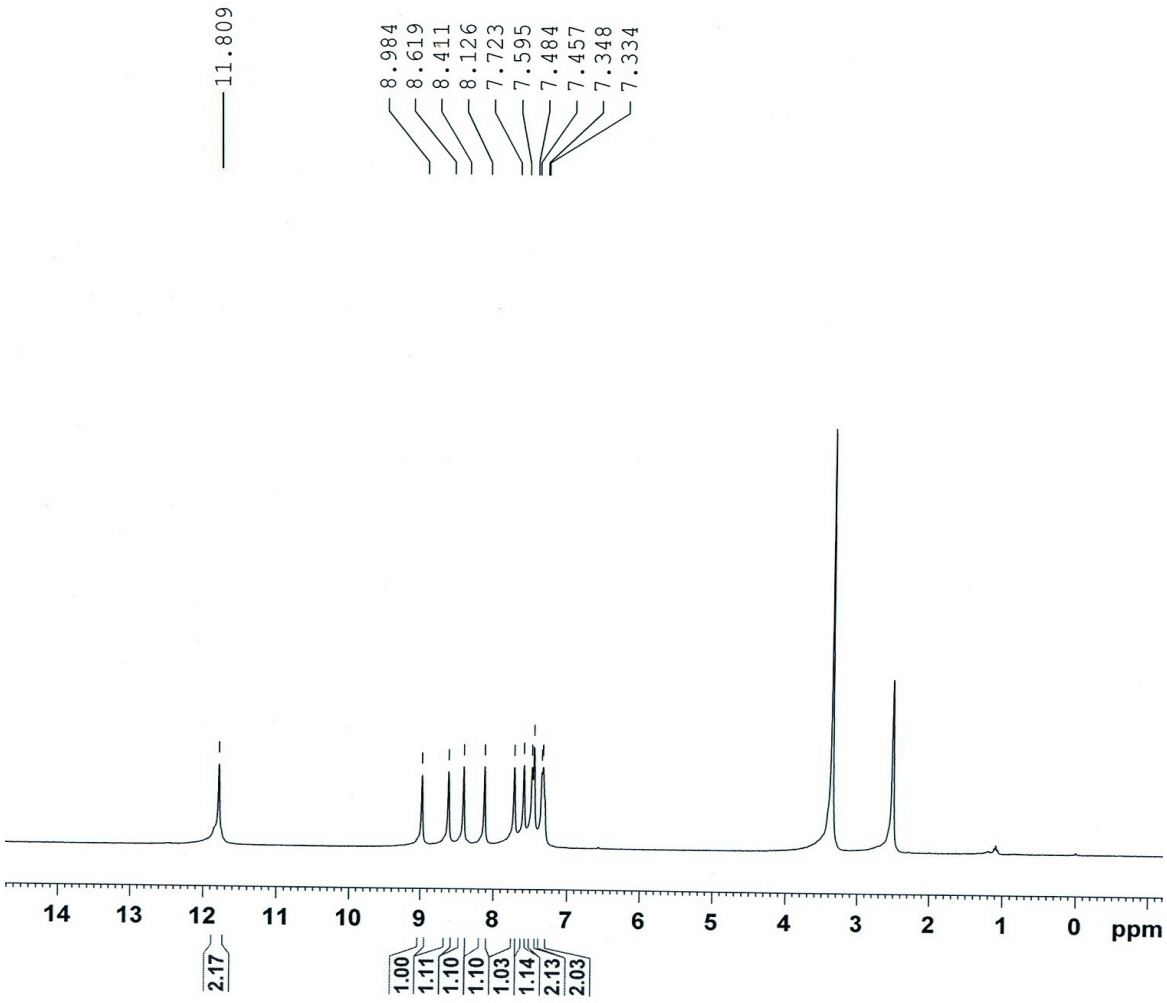

Figure S17. NMR spectrum of R4 with 0 eqv of F^-.

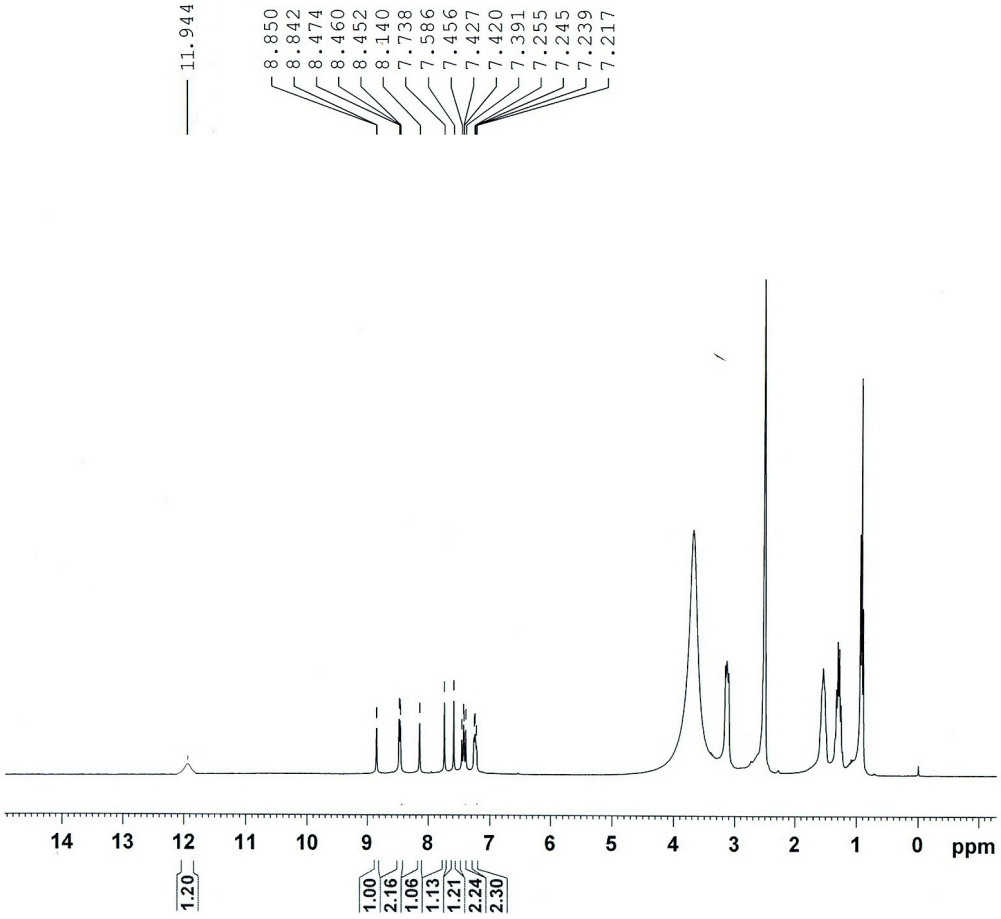

Figure S18. NMR spectrum of R4 with 0.5 eqv of F⁻.

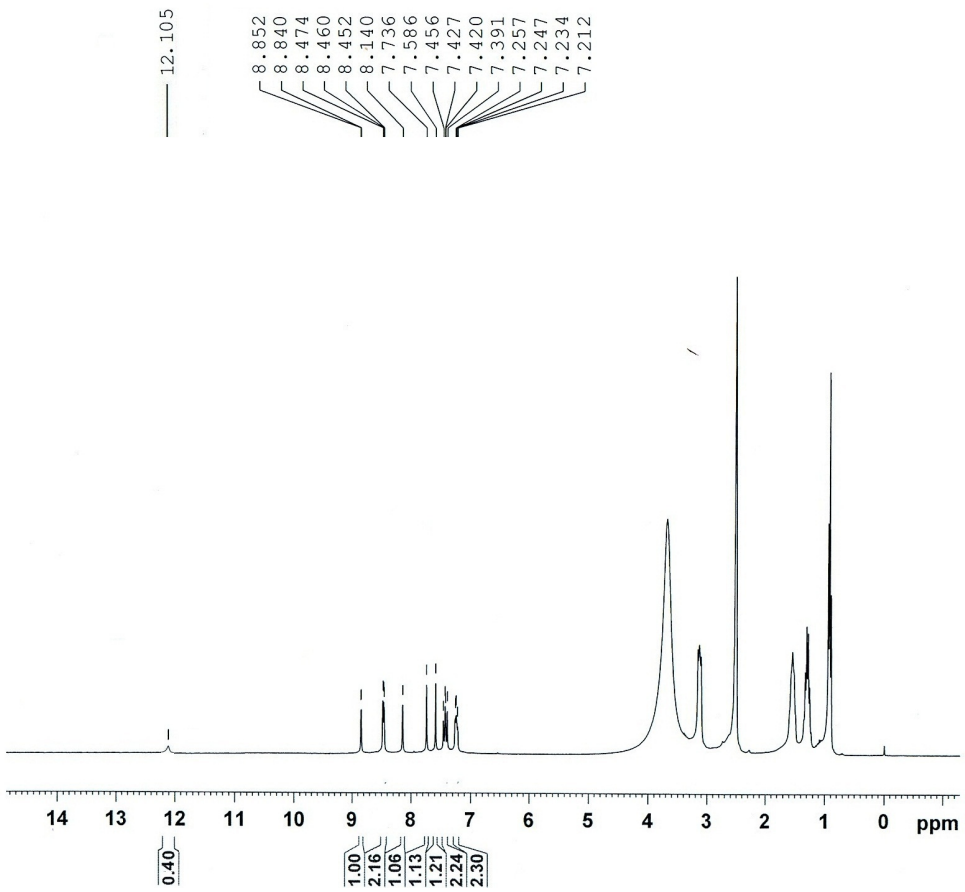

Figure S19. NMR spectrum of R4 with 1.0 eqv of F^-.

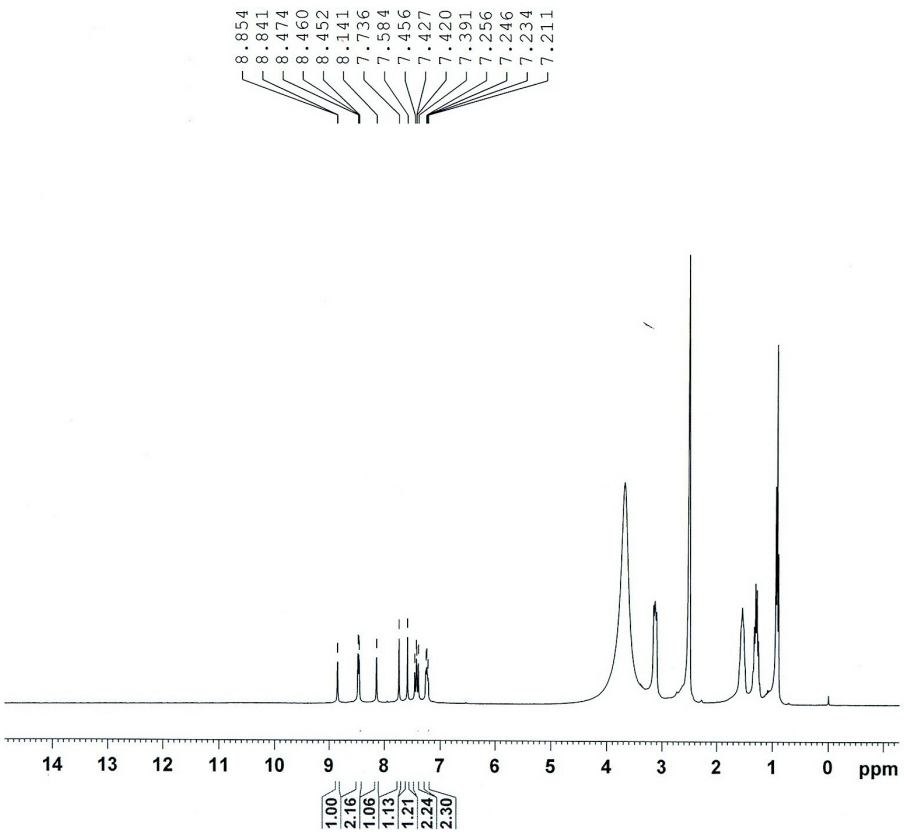

Figure S20. NMR spectrum of R4 with 2.0 eqv of F^-.

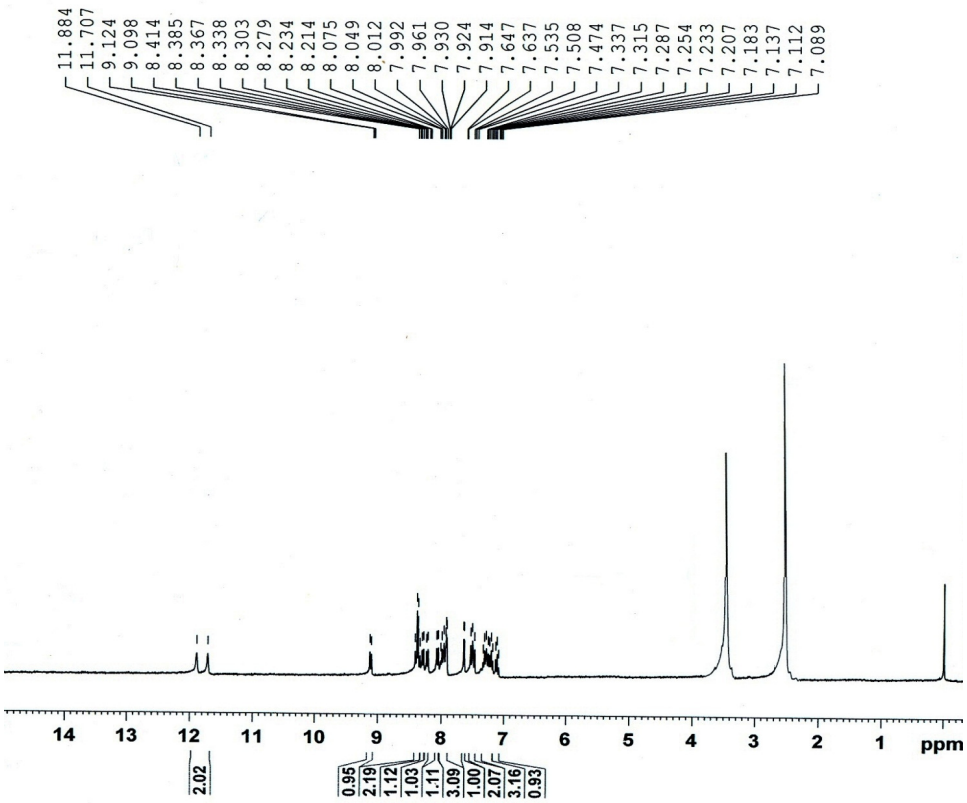

Figure S21. NMR spectrum of R5 with 0 eqv of F^-.

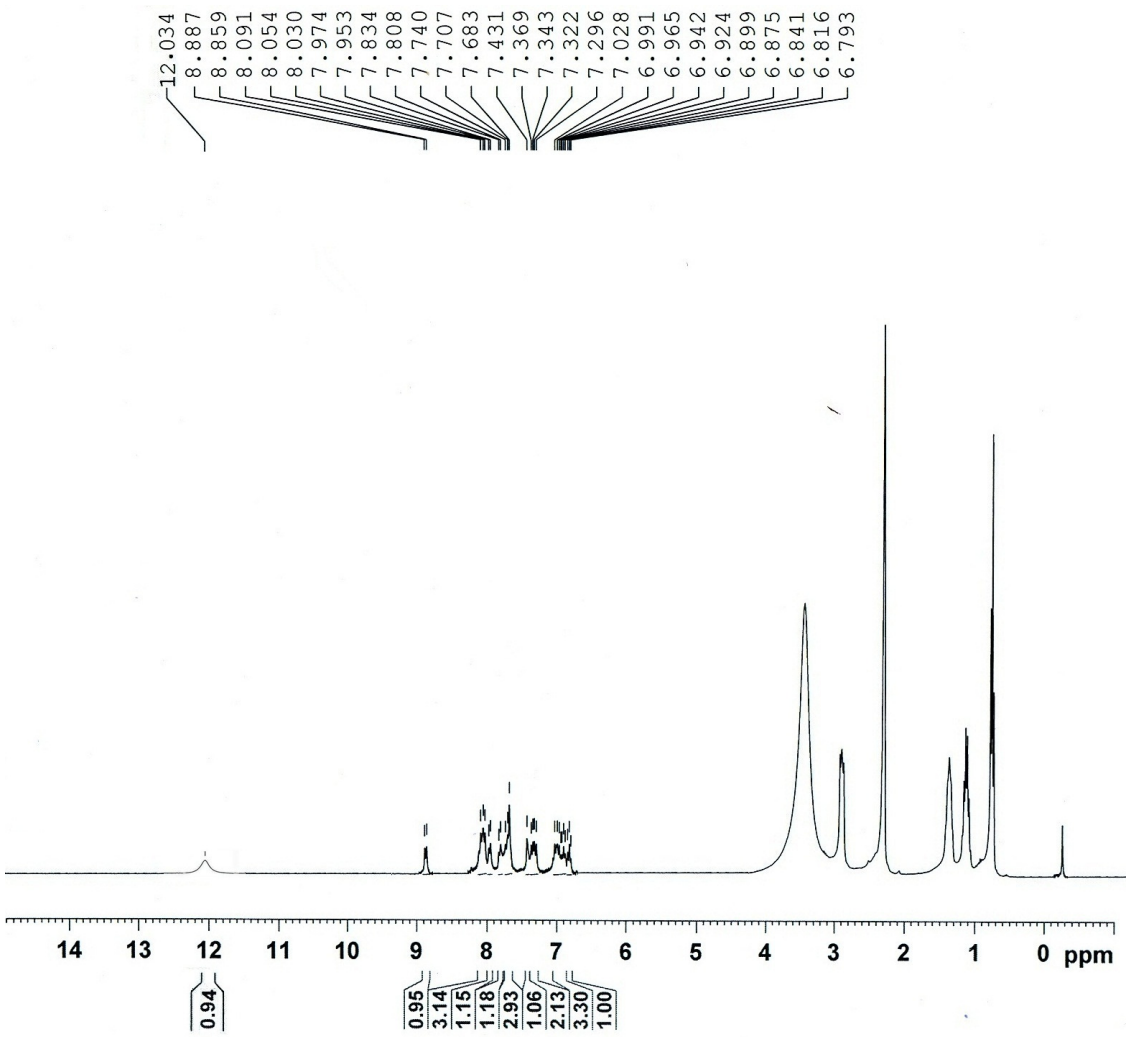

Figure S22. NMR spectrum of R5 with 0.5 eqv of F⁻.

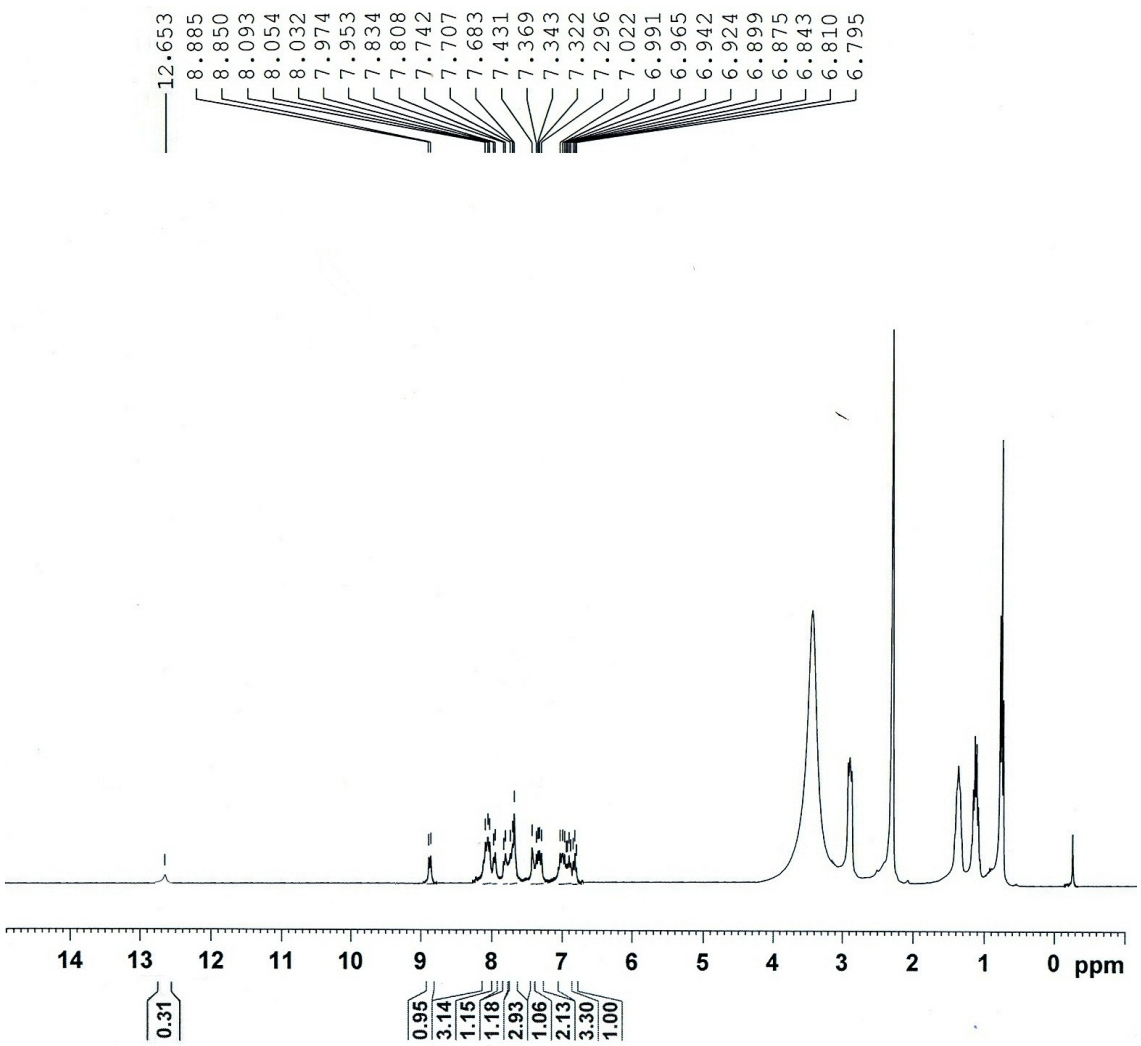

Figure S23. NMR spectrum of R5 with 1.0 eqv of F^-.

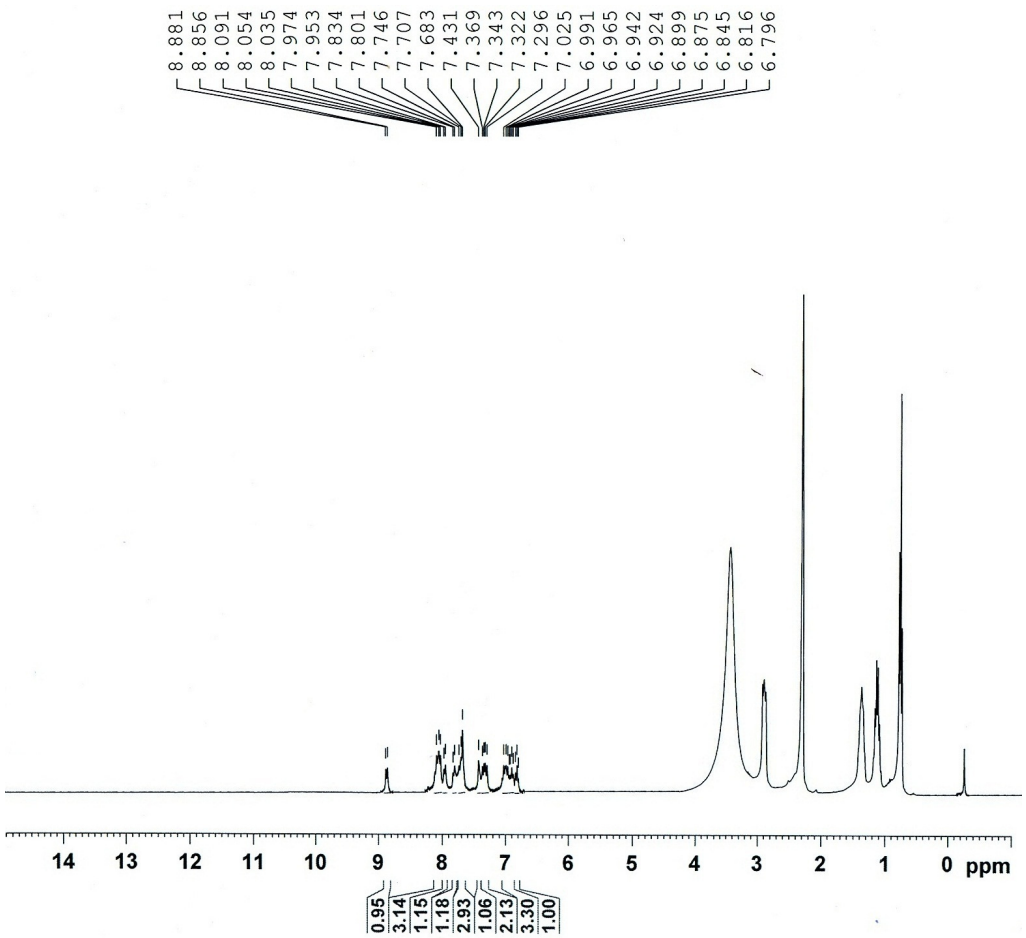

Figure S24. NMR spectrum of R5 with 2.0 eqv of F⁻.

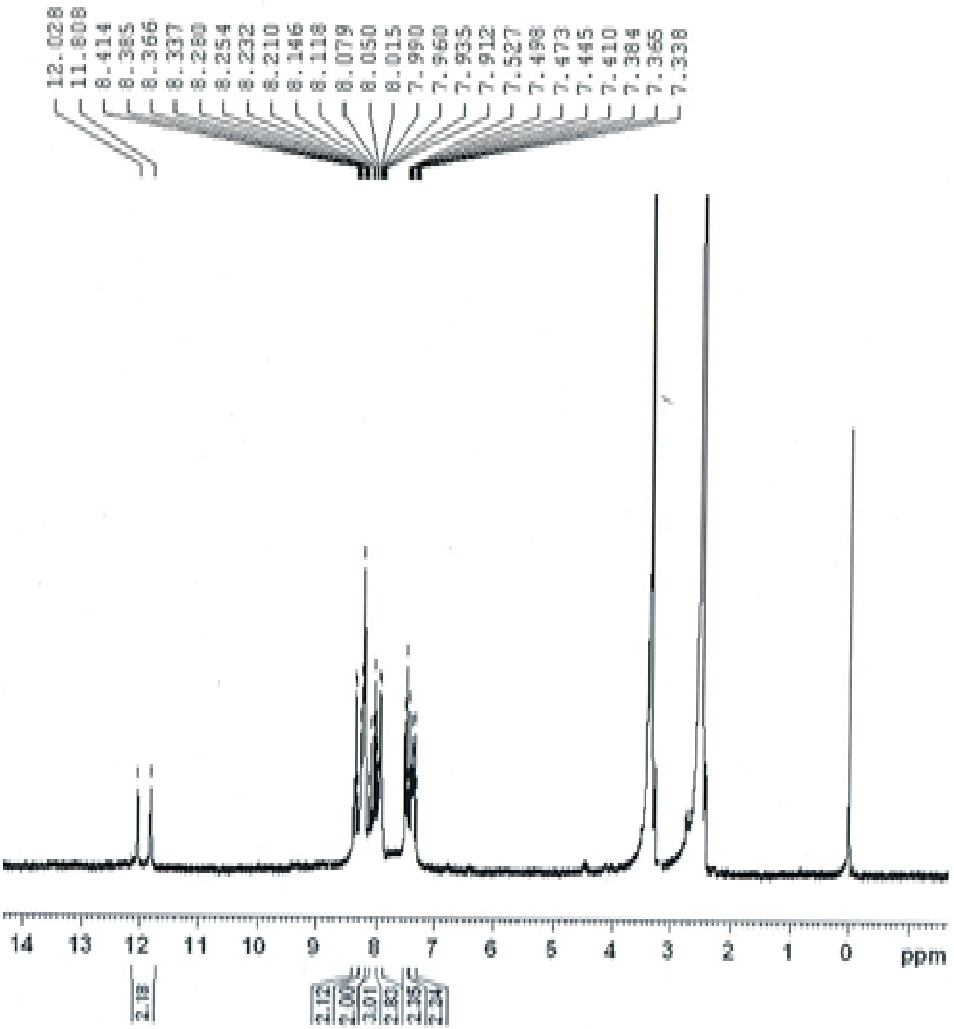

Figure S25. NMR spectrum of R6 with 0 eqv of F^-.

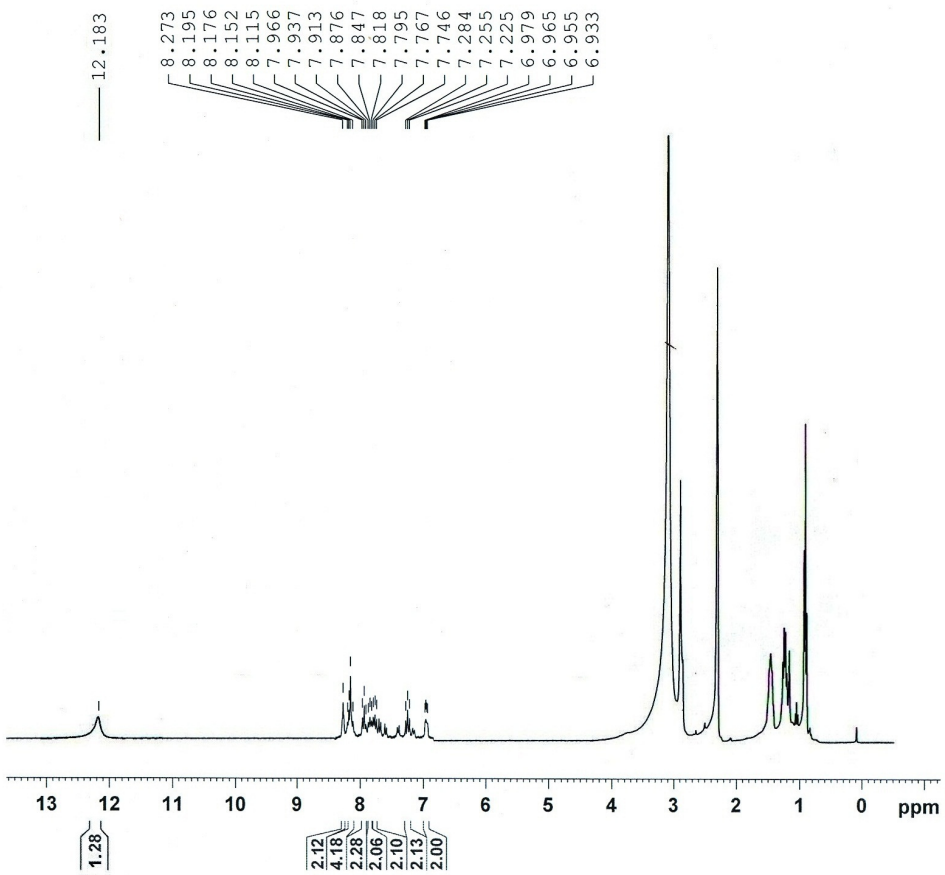

Figure S26. NMR spectrum of R6 with 0.5 eqv of F^-.

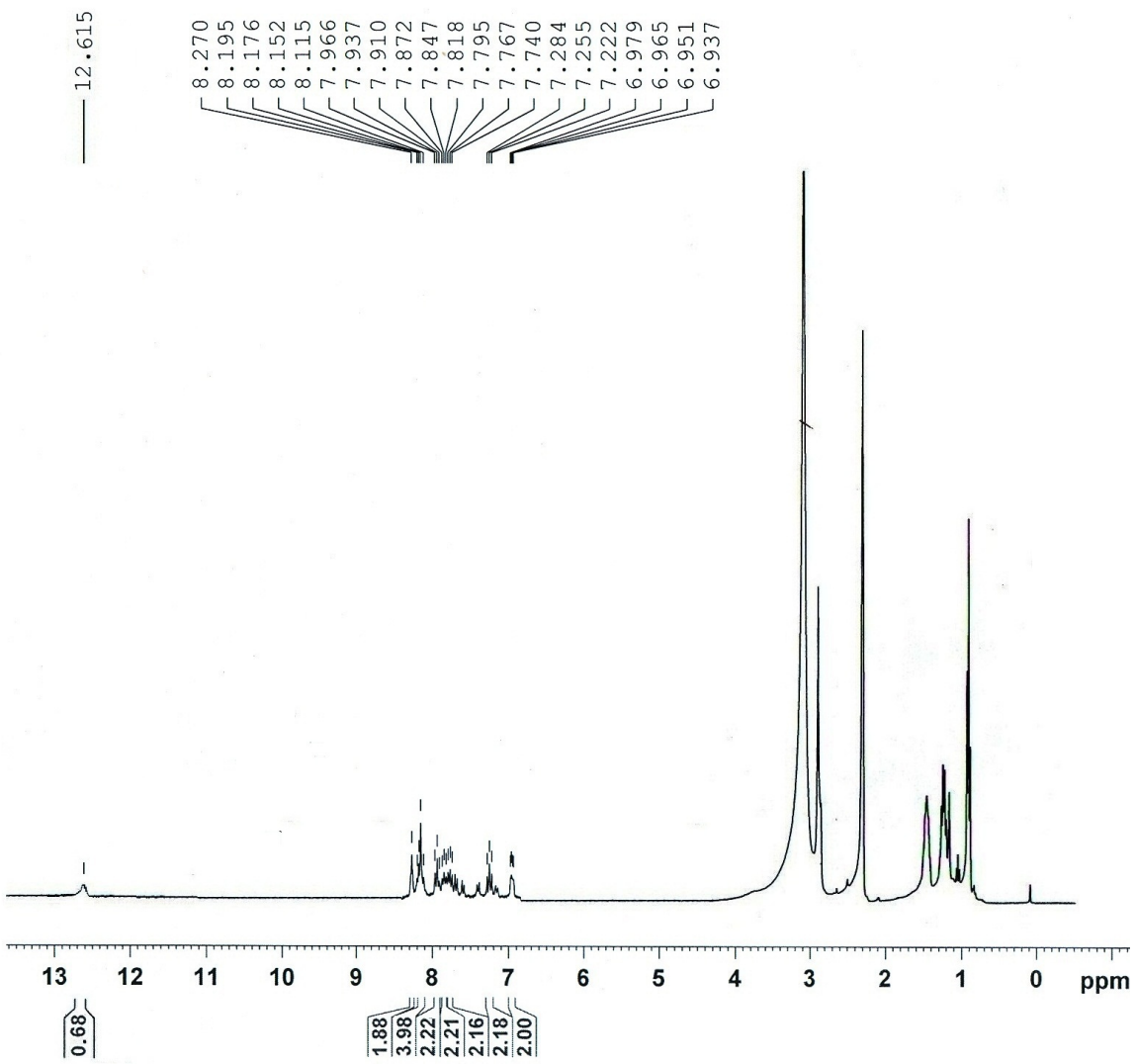

Figure S27. NMR spectrum of R6 with 1.0 eqv of F^-.

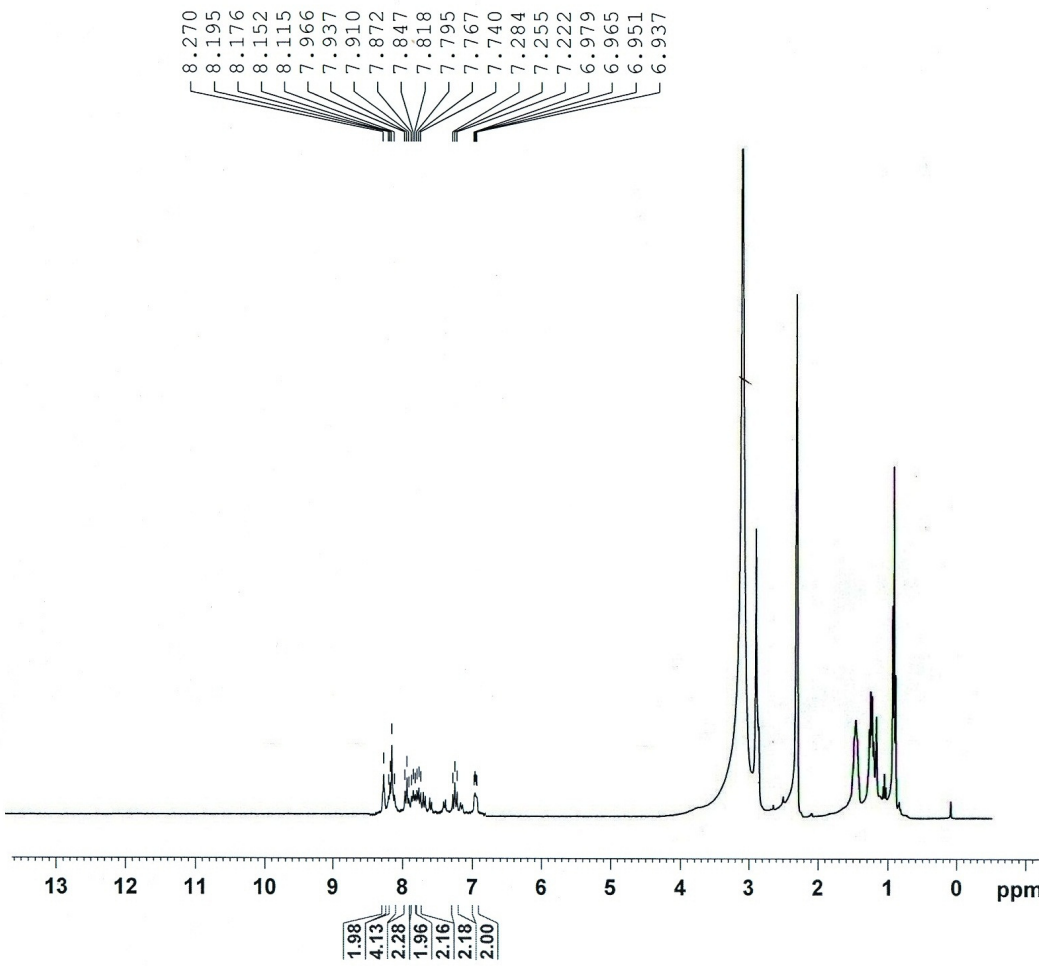

Figure S28. NMR spectrum of R6 with 2.0 eqv of F^-.

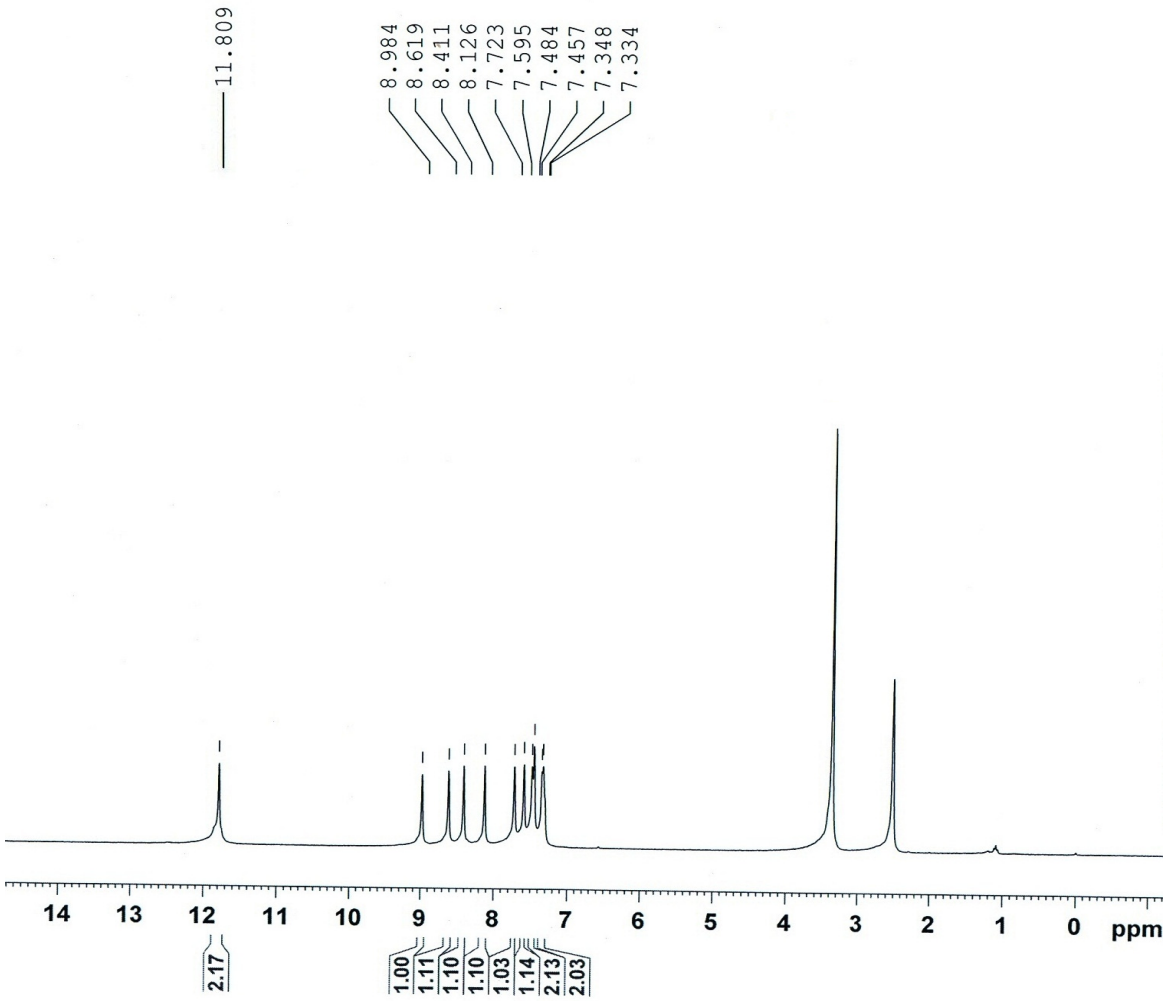

Figure S29. NMR spectrum of R4 with 0 eqv of CN^-.

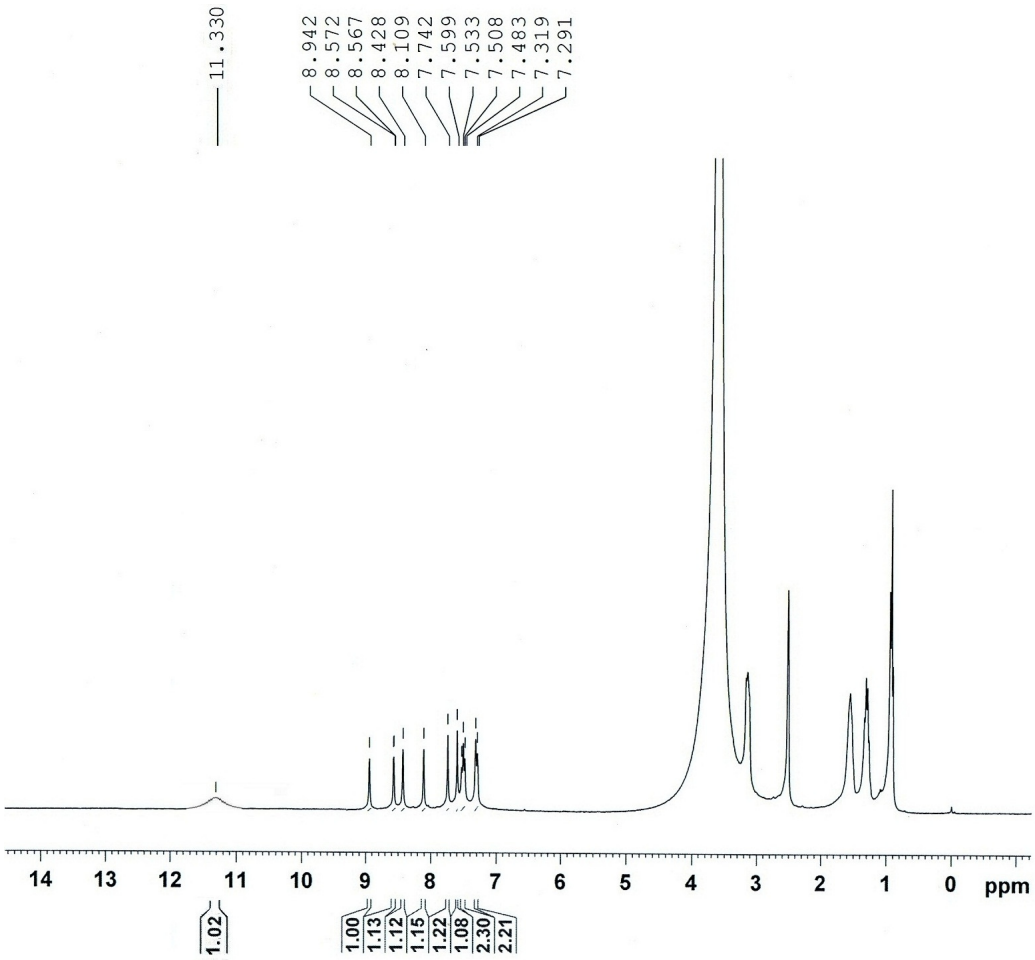

Figure S30. NMR spectrum of R4 with 0.5 eqv of CN^-.

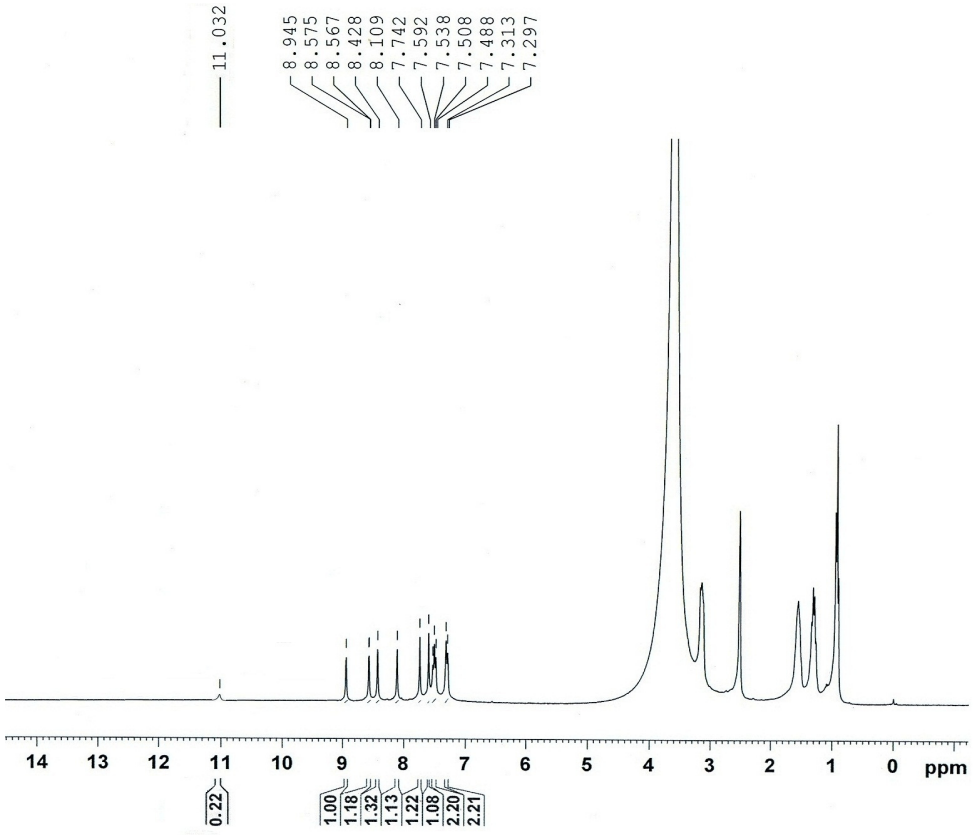

Figure S31. NMR spectrum of R4 with1.0 eqv of CN^-.

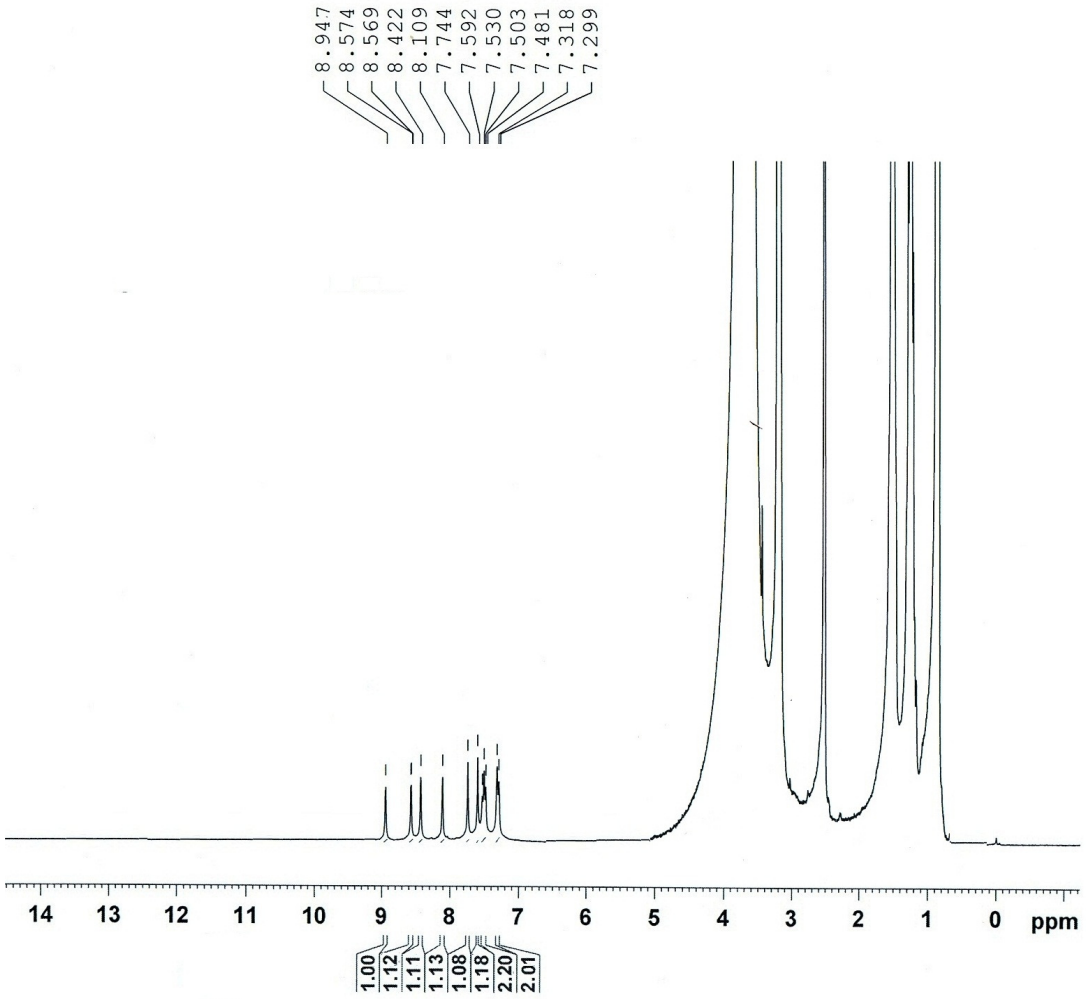

Figure S32. NMR spectrum of R4 with 2.0 eqv of CN^-.

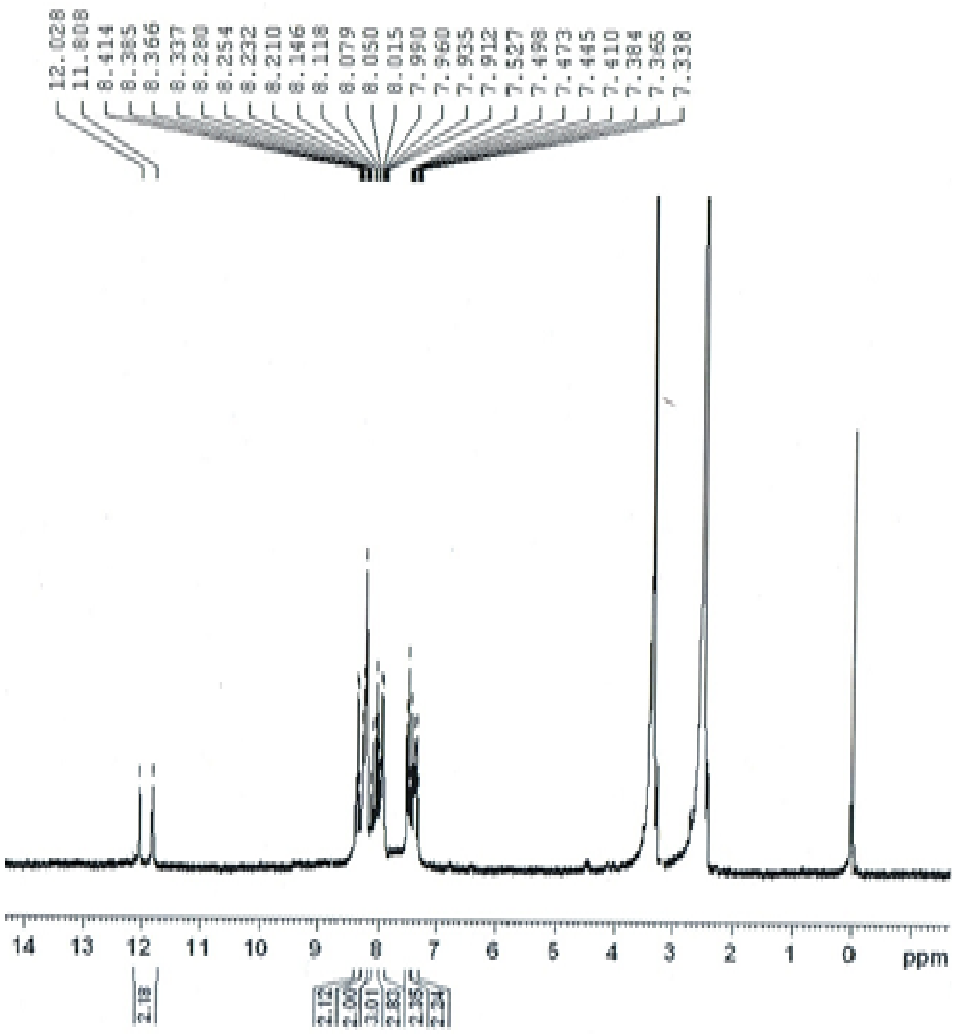

Figure S33. NMR spectrum of R6 with 0 eqv of CN^-.

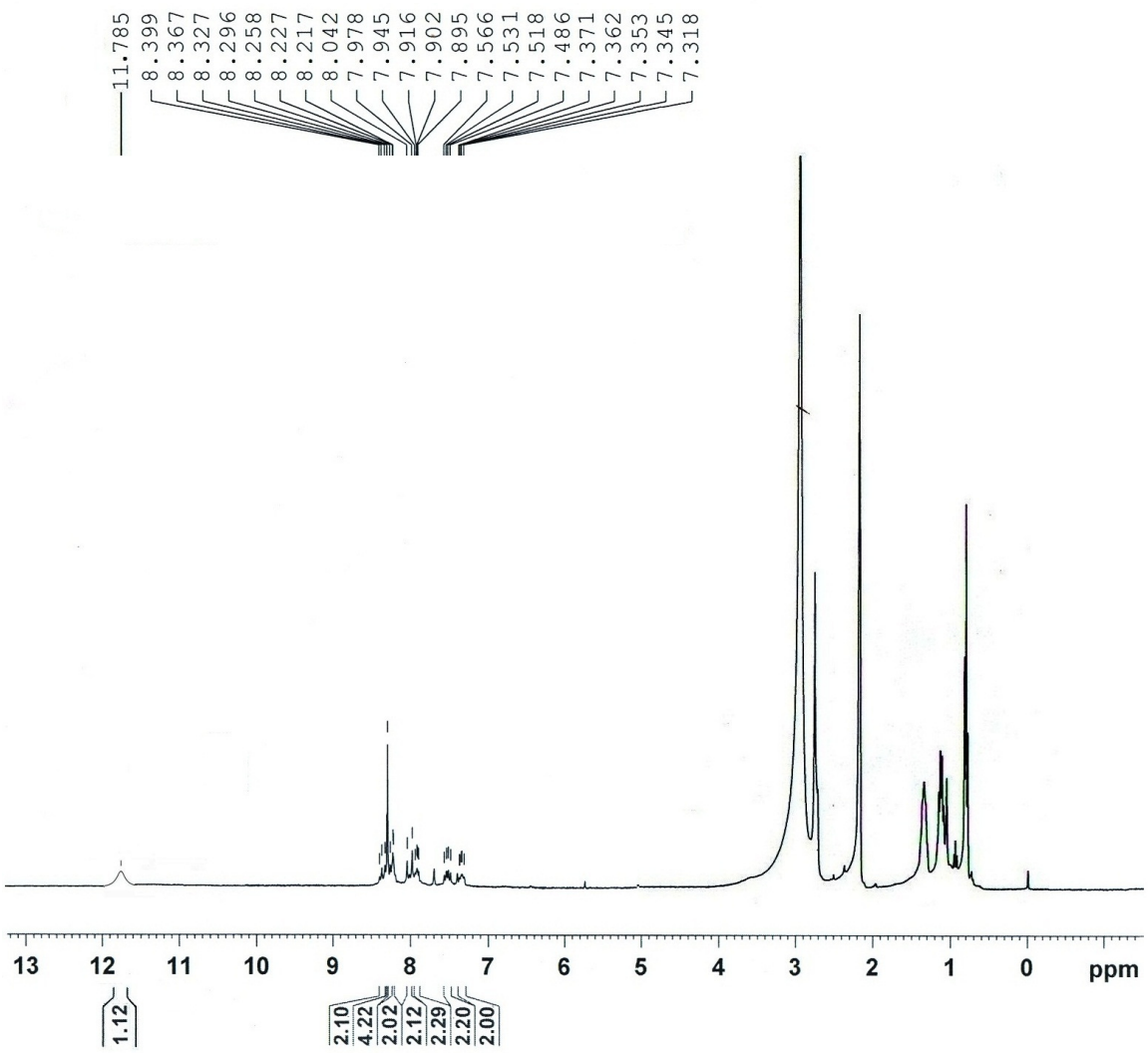

Figure S34. NMR spectrum of R6 with 0.5 eqv of CN^-.

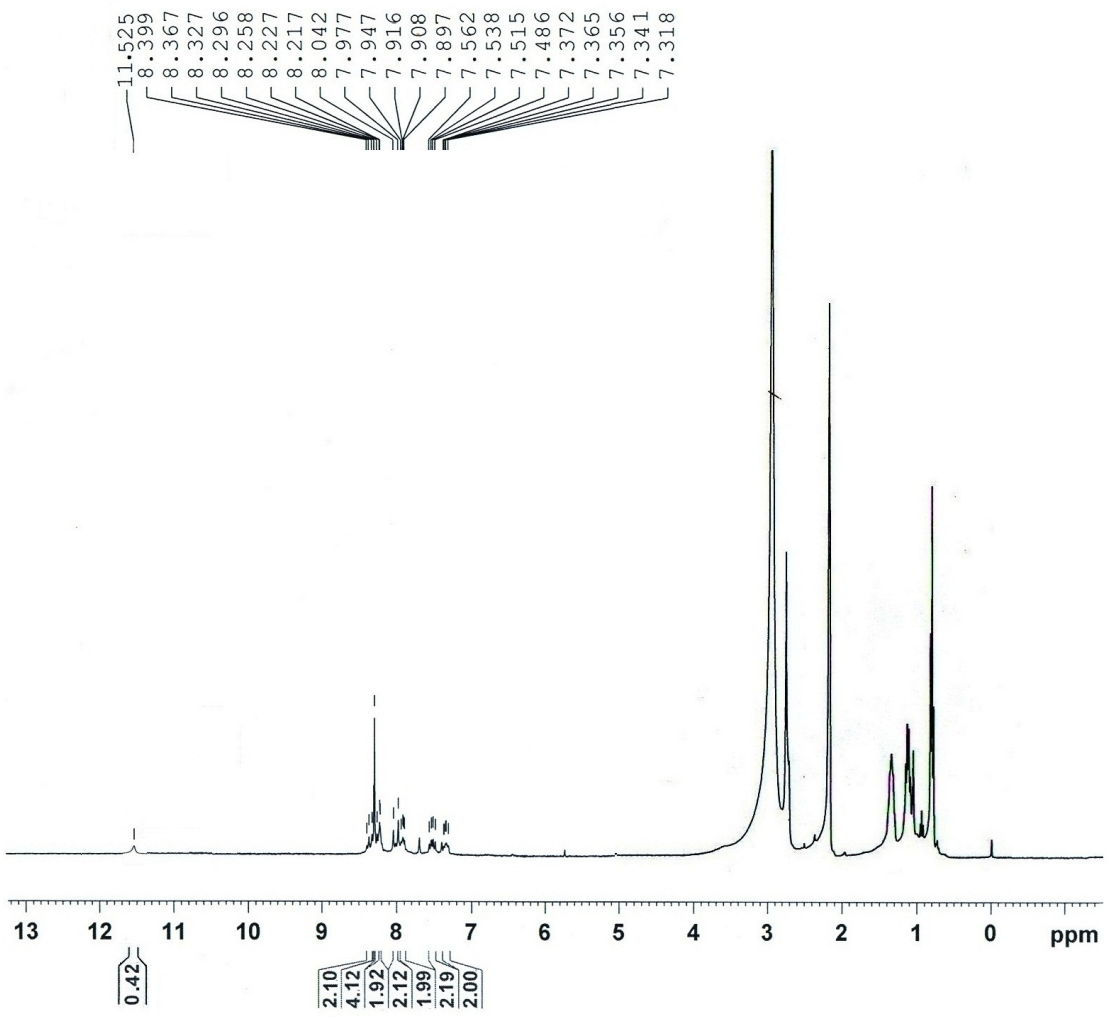

Figure S35. NMR spectrum of R6 with 1. 0 eqv of CN^-.

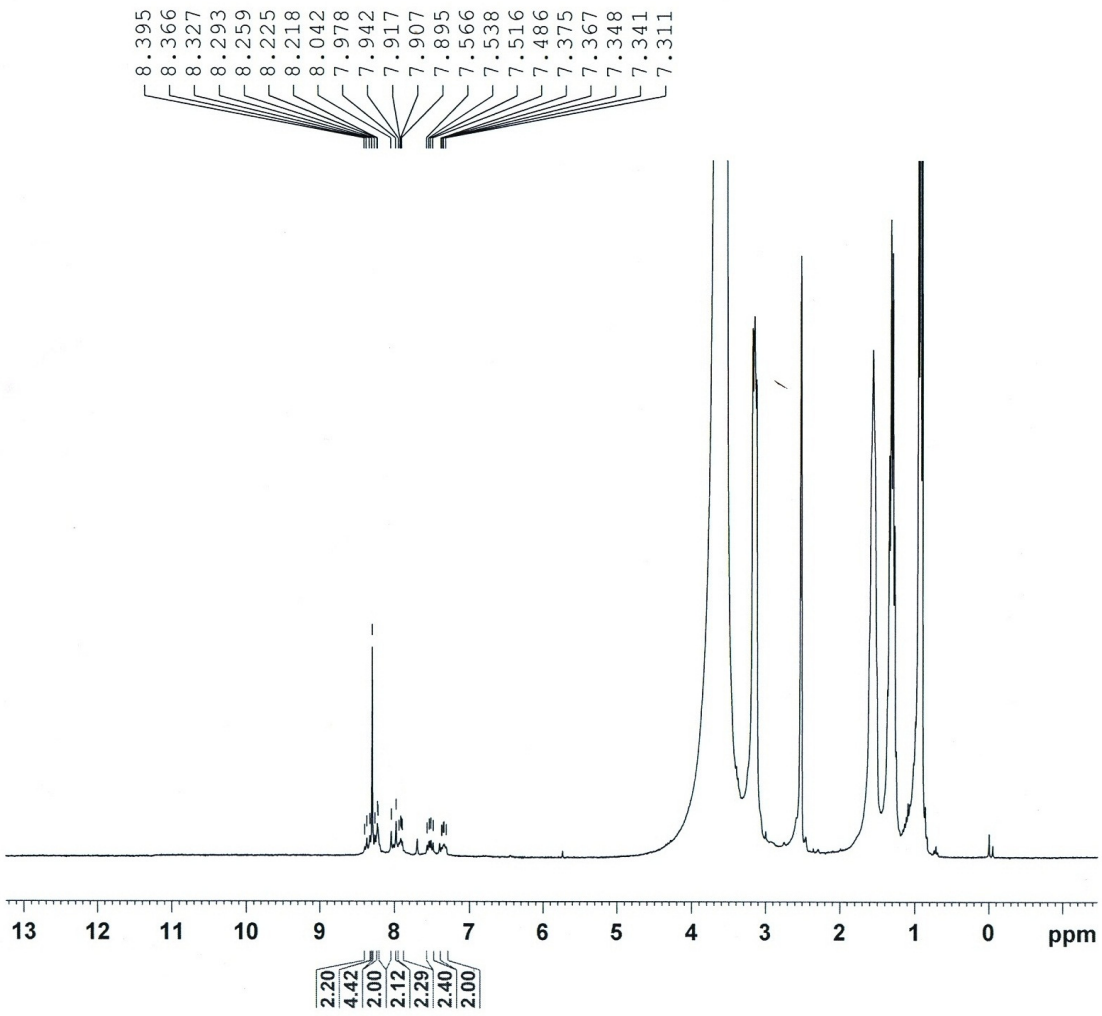

Figure S36. NMR spectrum of R6 with 2. 0 eqv of CN^-.

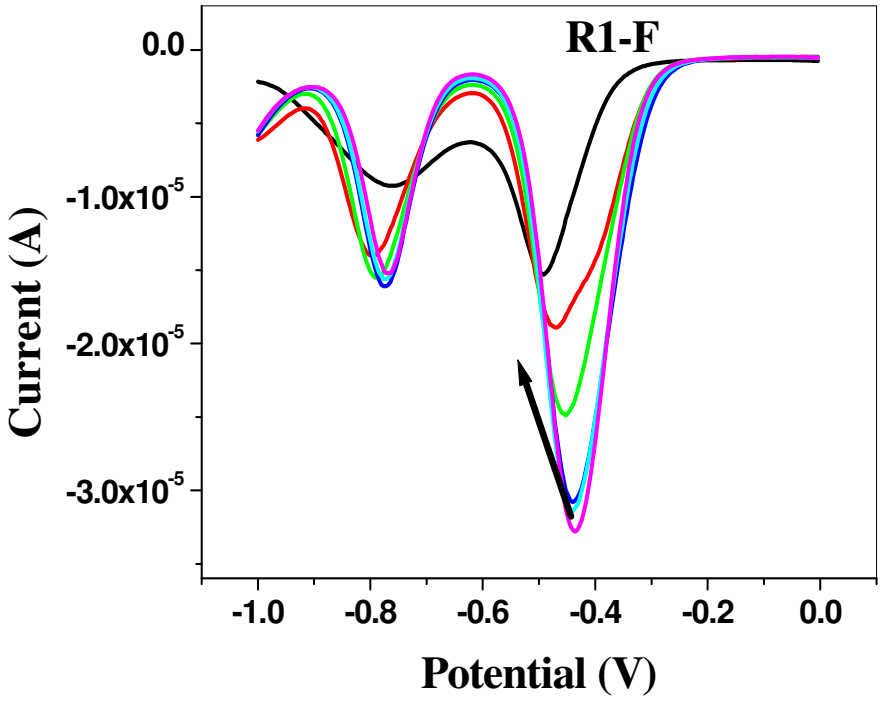
R1-F
0.0
-1.0x10-5
-2.0x10-5
-3.0x10-5
Current (A)
-1.0
-0.8
-0.6
-0.4
-0.2
0.0
Potential (V)

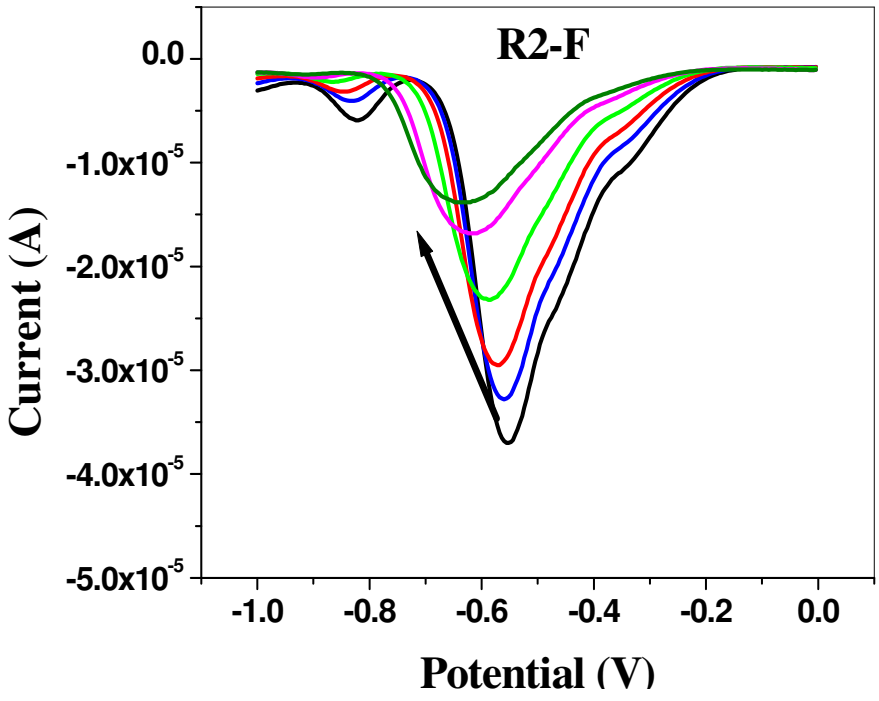
R2-F
0.0
-1.0x10-5
-2.0x10-5
-3.0x10-5
-4.0x10-5
-5.0x10-5
Current (A)
-1.0
-0.8
-0.6
-0.4
-0.2
0.0
Potential (V)

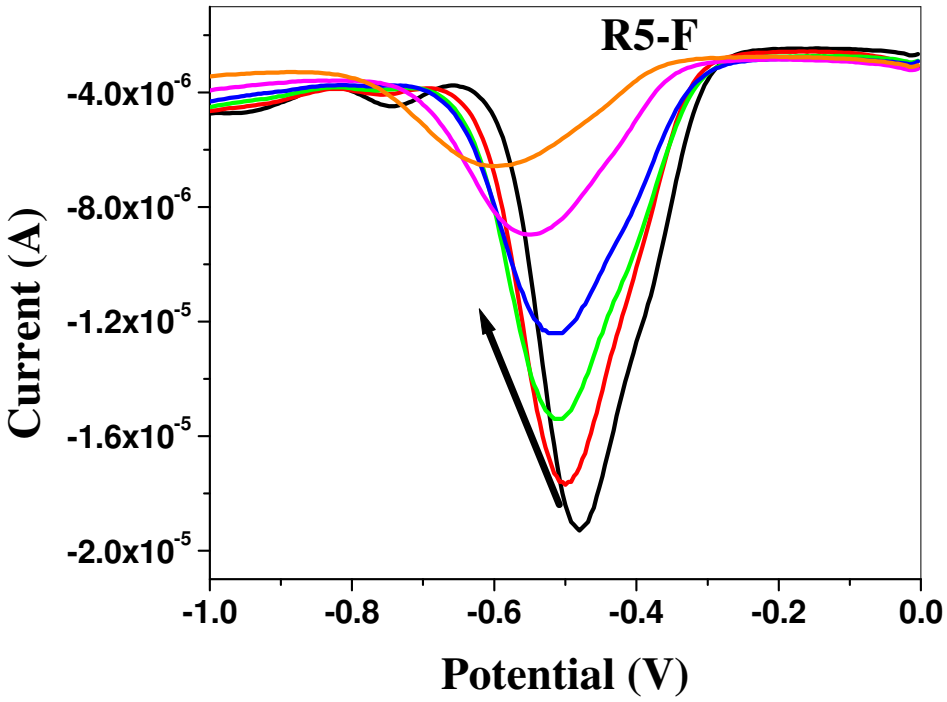
R5-F
-4.0x10-6
-8.0x10-6
-1.2x10-5
-1.6x10-5
-2.0x10-5
Current (A)
-1.0
-0.8
-0.6
-0.4
-0.2
0.0
Potential (V)

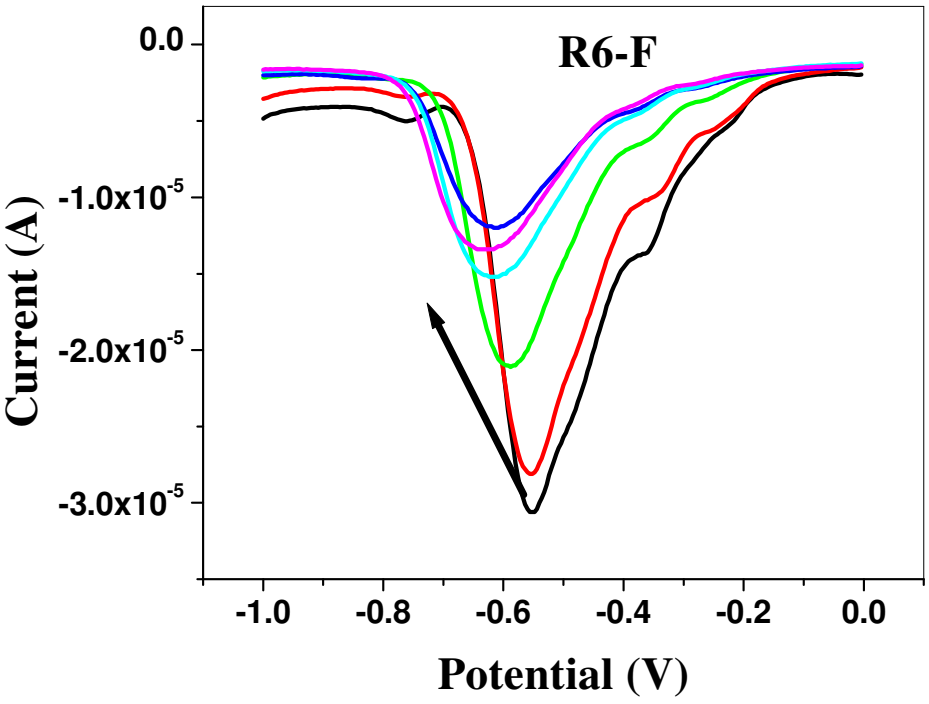
R6-F
0.0
-1.0x10-5
-2.0x10-5
-3.0x10-5
Current (A)
-1.0
-0.8
-0.6
-0.4
-0.2
0.0
Potential (V)

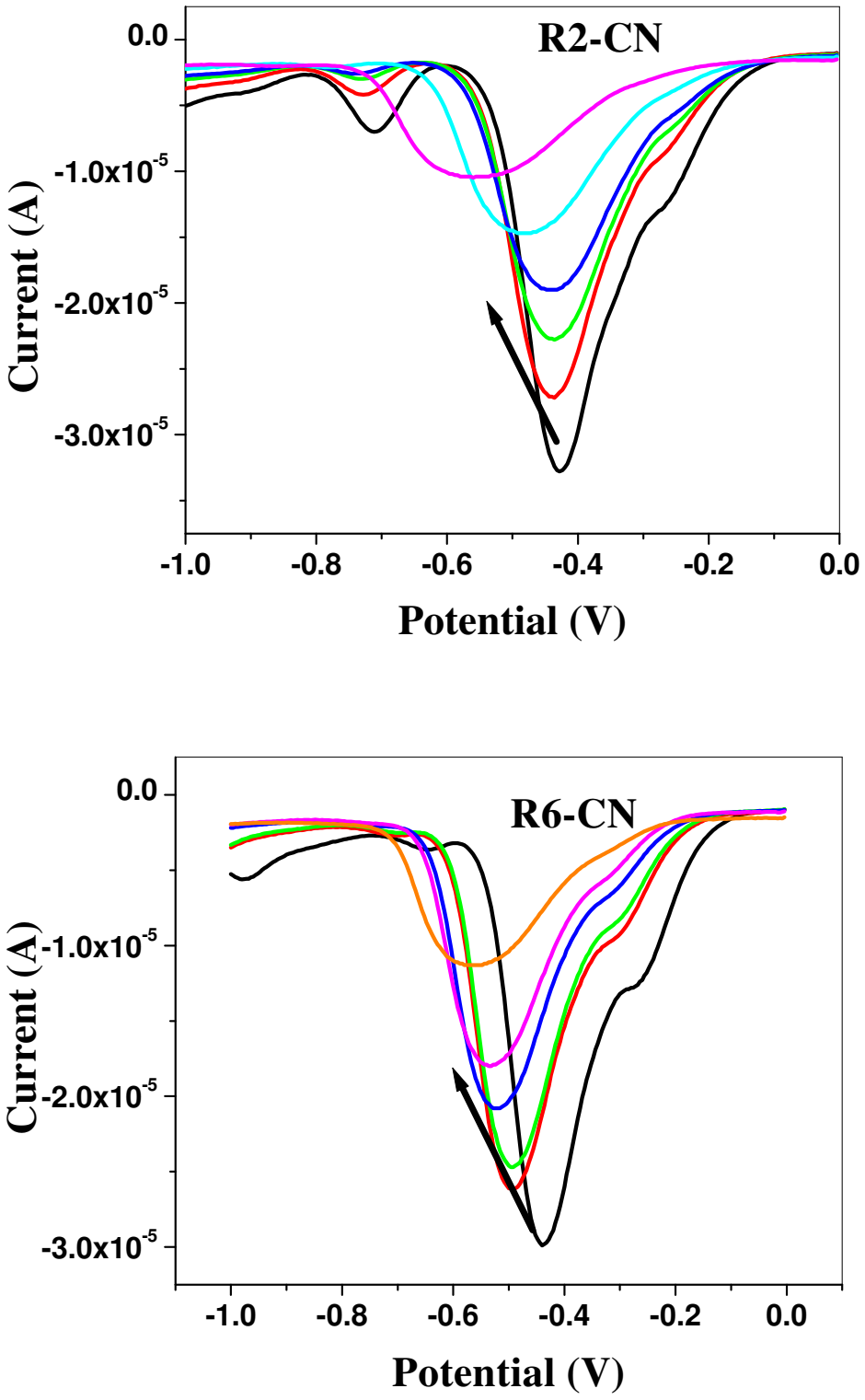

Figure S37. Changes in redox properties of R1, R2, R5, R6 (1 mM) in DMF upon addition of $[(Bu)_4N]F$ in DMF from 0 - $1.25x10^{-4}$ M. R2, R6 (1 mM) in DMF upon addition of $[(Bu)_4N]CN$ in DMF from 0 - $1.25x10^{-4}$ M.

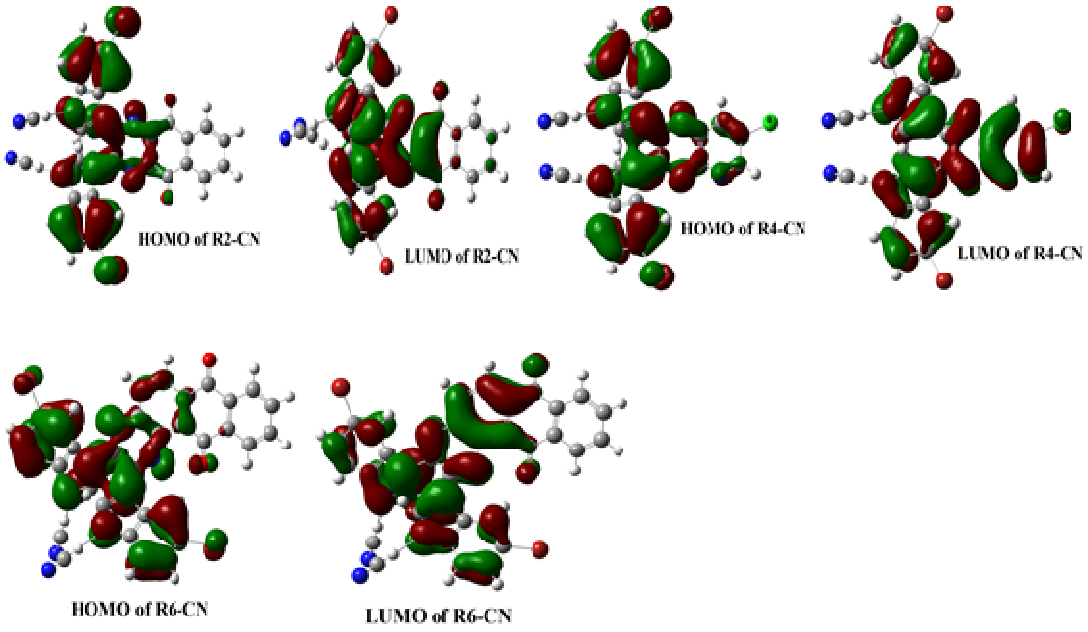

Figure S38. HOMO –LUMO for cyanide complexes of R2, R4 and R6.

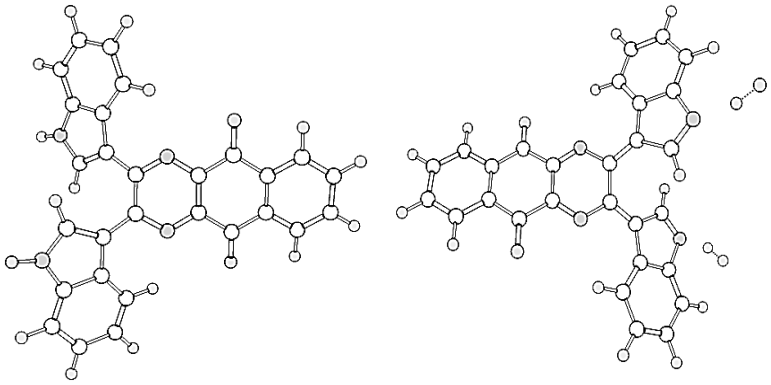

Optimized structure for **R1, R1**-F^-

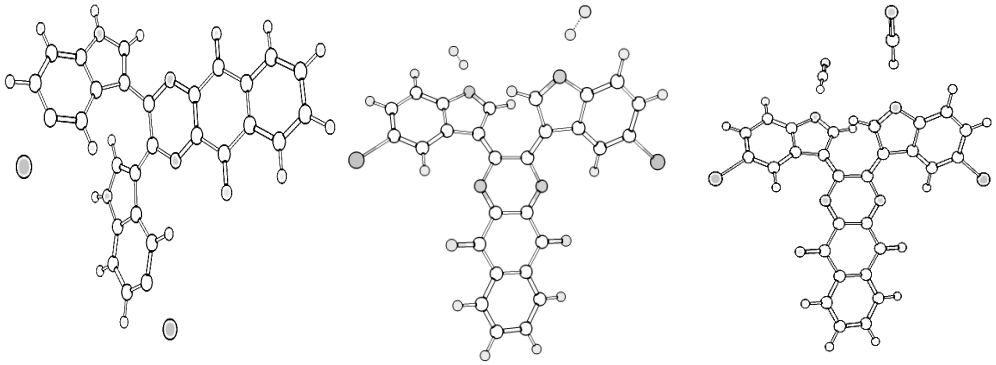

Optimized structure for **R2, R2**-F^-, **R2**-CN^-.

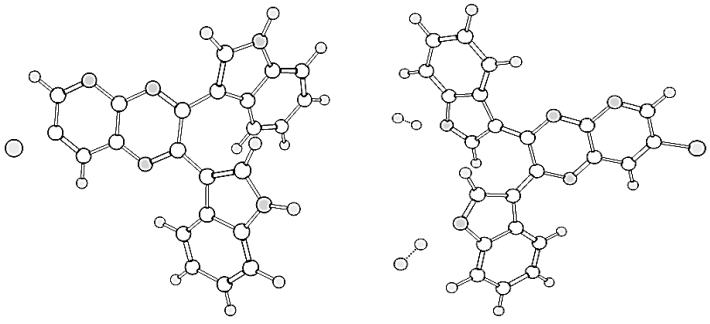

Optimized structure for **R3, R3**-F^-.

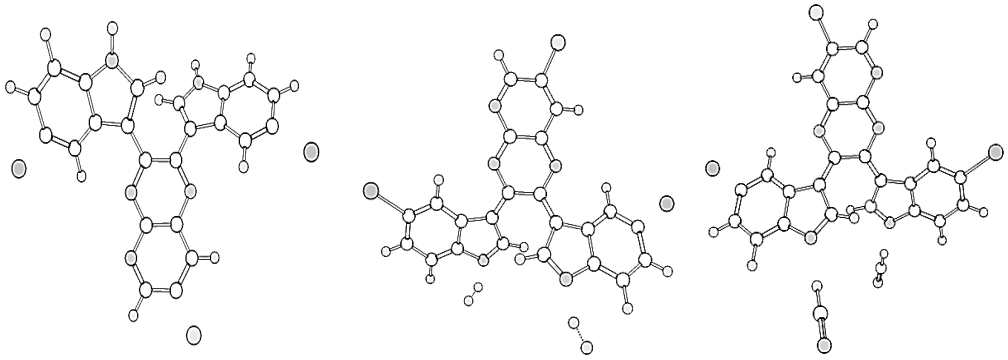

Optimized structure for **R4, R4**-F^-, **R4**-CN^-.

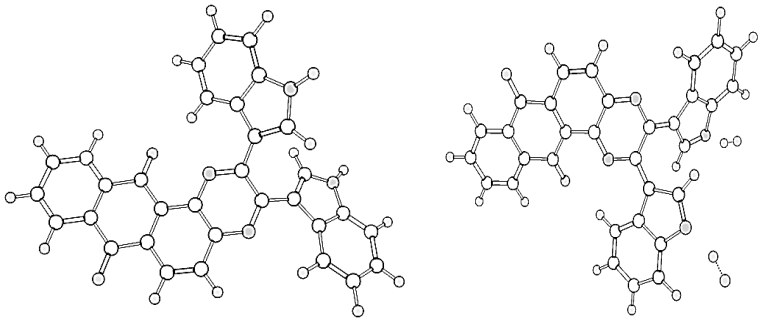

Optimized structure for **R5, R5**-F^-.

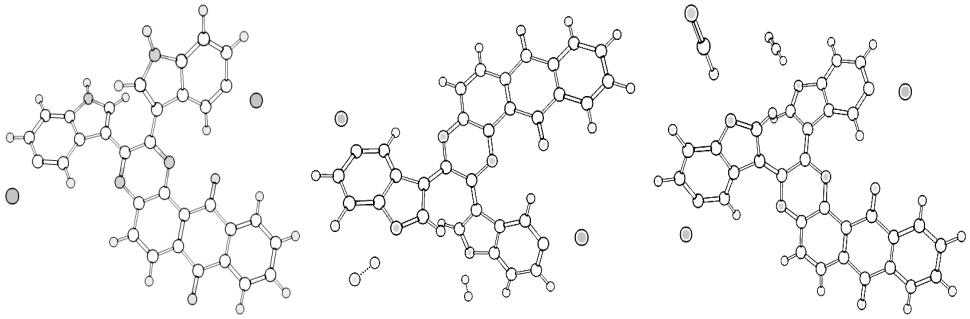

Optimized structure for **R6, R6**-F^-, R6-CN^-.

Figure S39. Optimized structure for R1-R6, and their F^- and CN^- complexes.

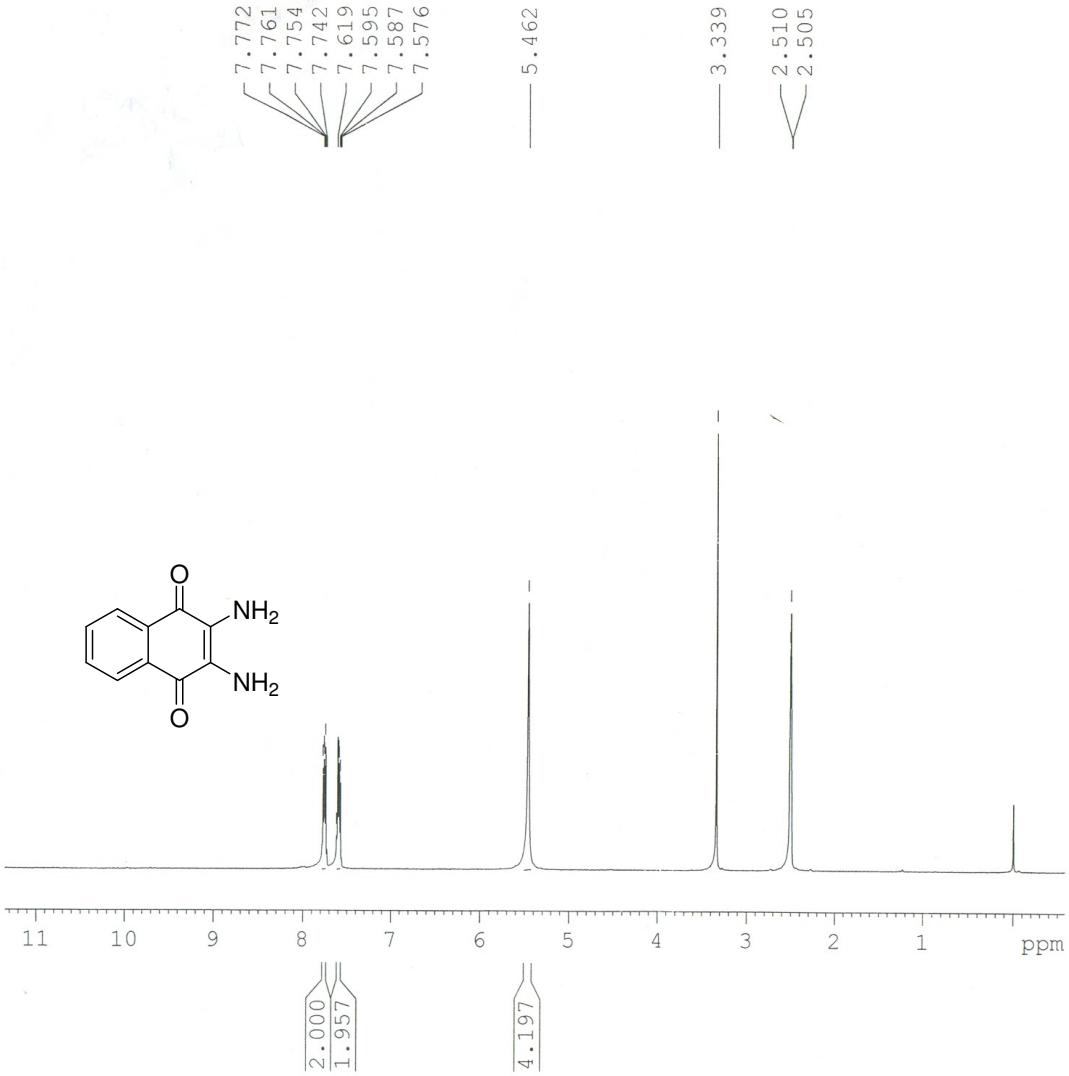

Figure S40. ^{1}H NMR for **1**

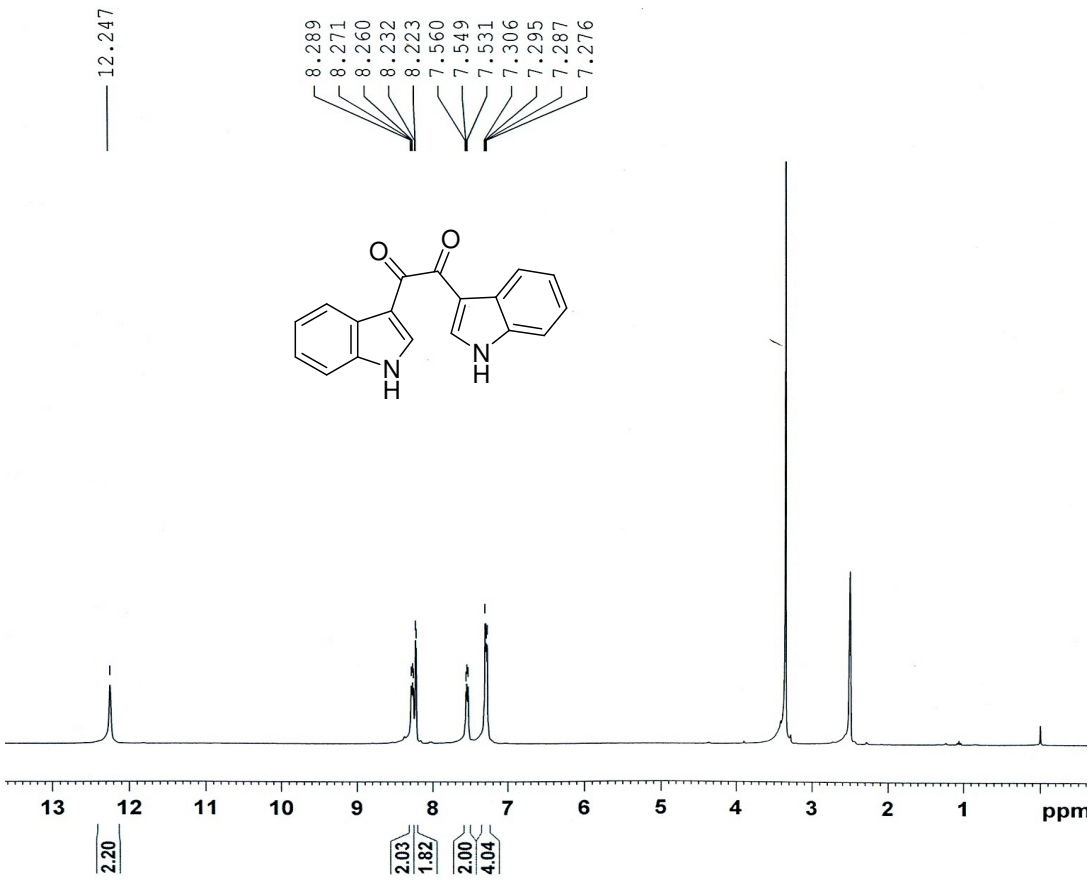

Figure S41. ^{1}H-NMR for **2**

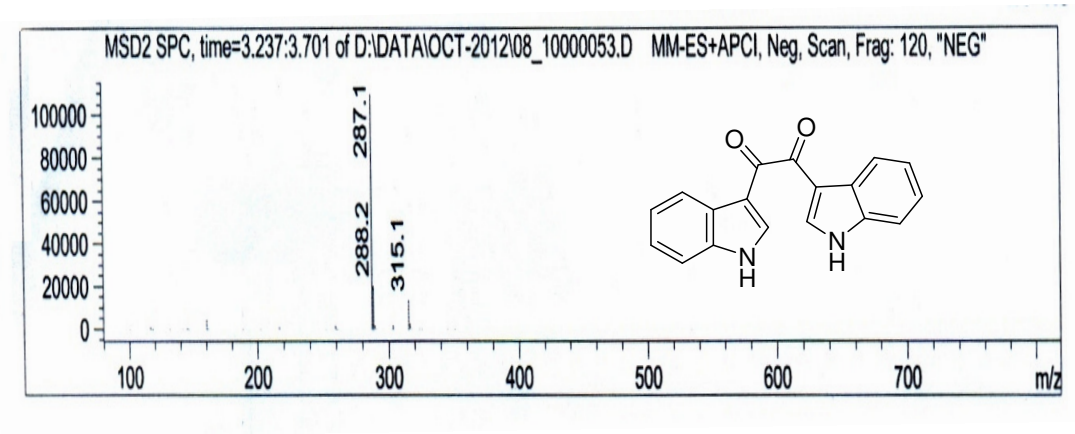

Figure S42.LCMS for **2**

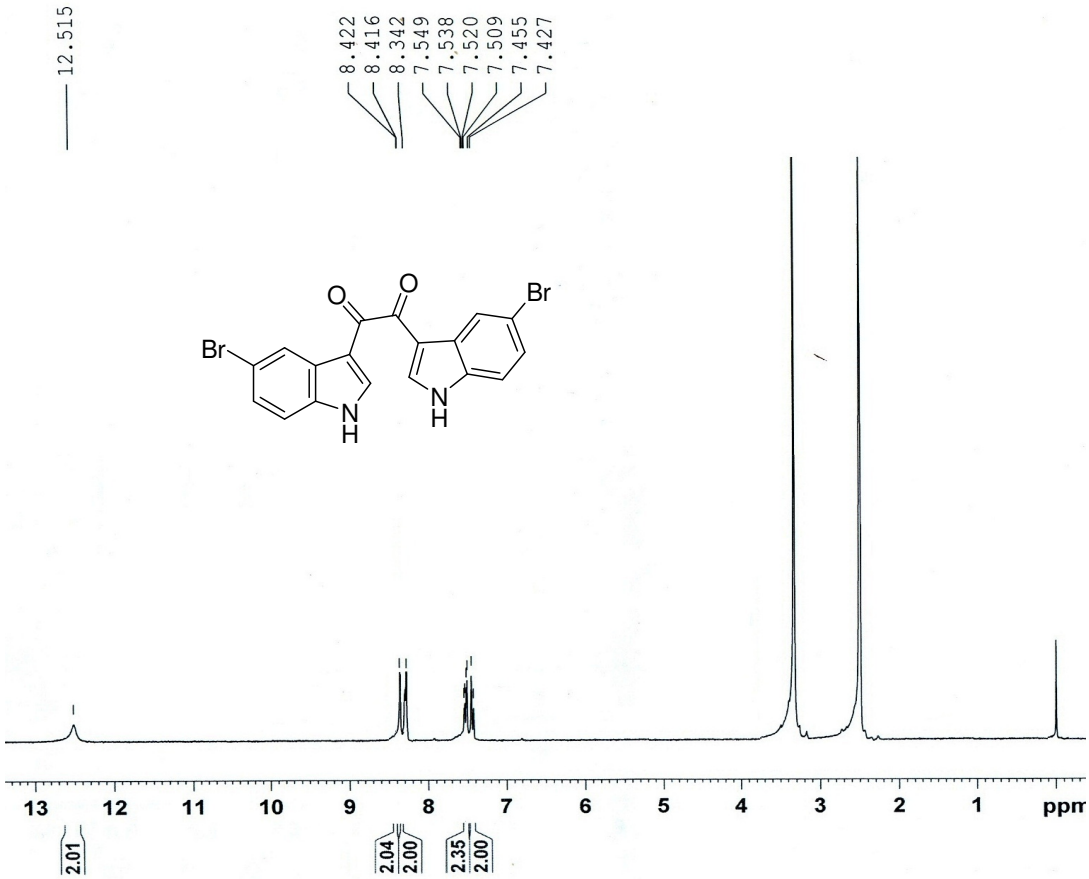

Figure S43. ^{1}H-NMR for **3**

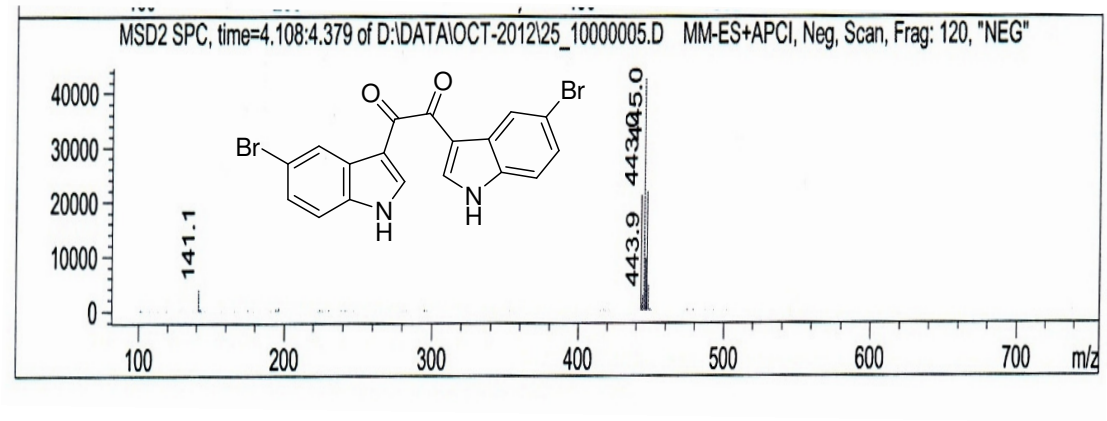

Figure S44. LCMS for **3**

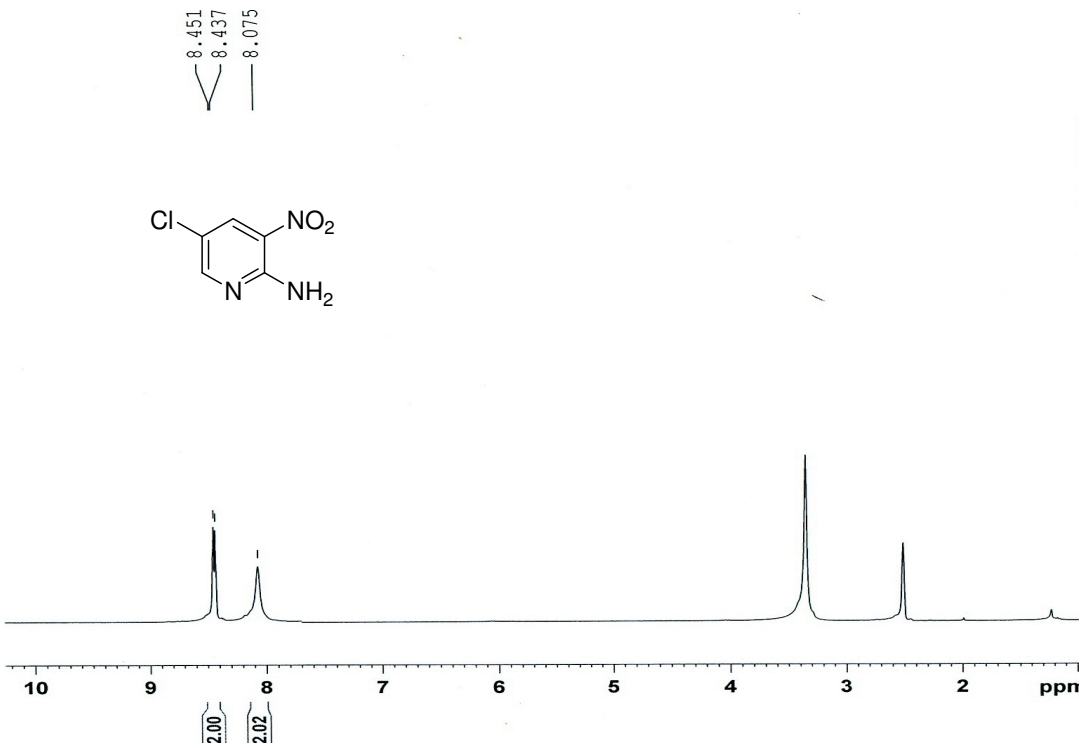

Figure S45. ^{1}H-NMR for **4**

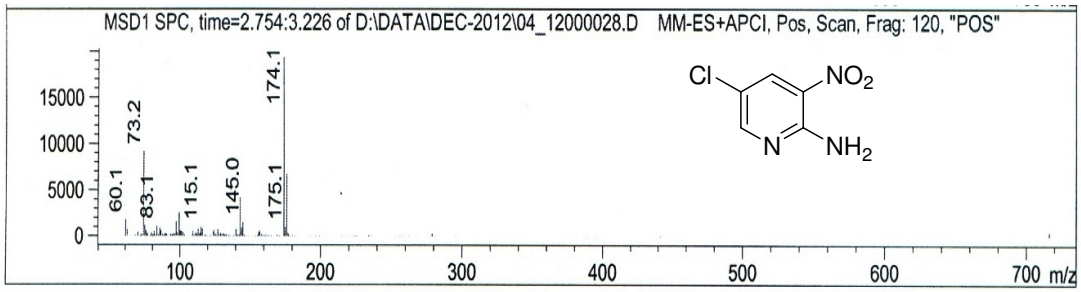

Figure S46. LCMS for **4**

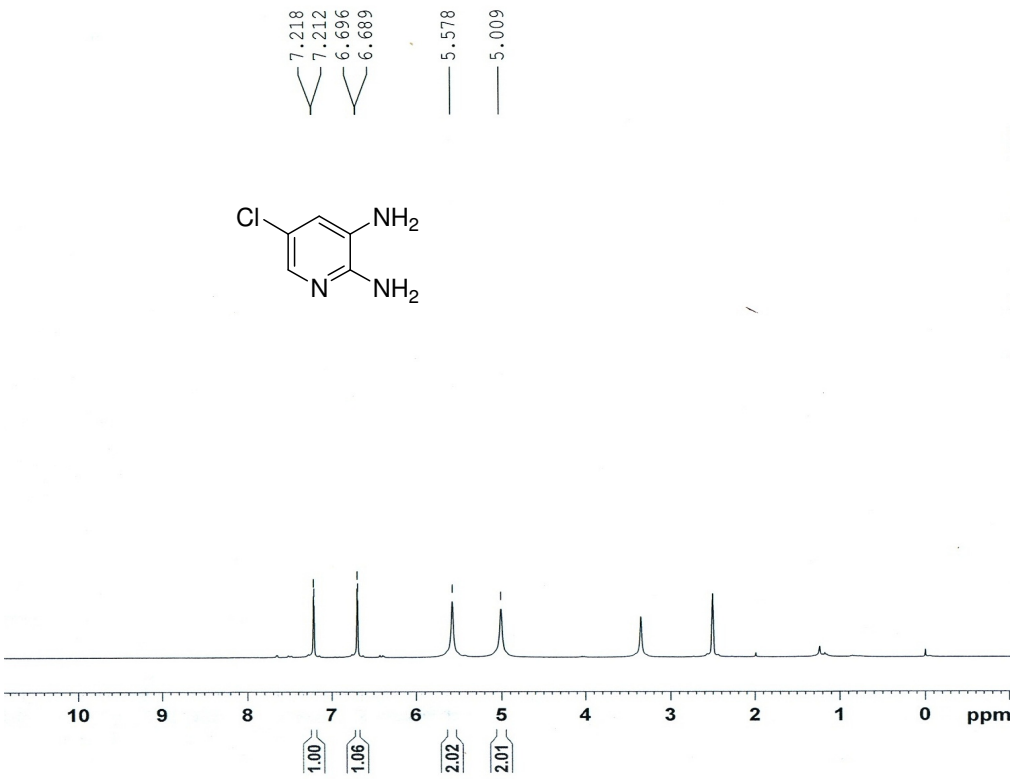

Figure S47. ^{1}H-NMR for **5**

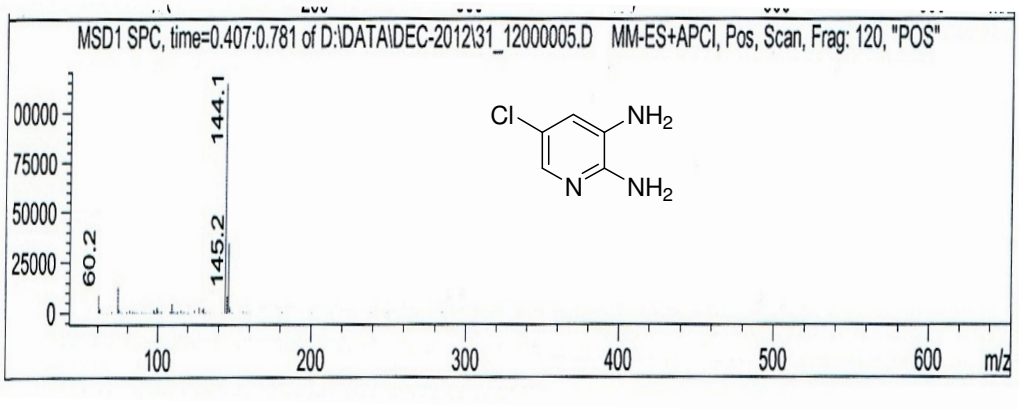

Figure S48. ^{1}H- LCMS for **5**

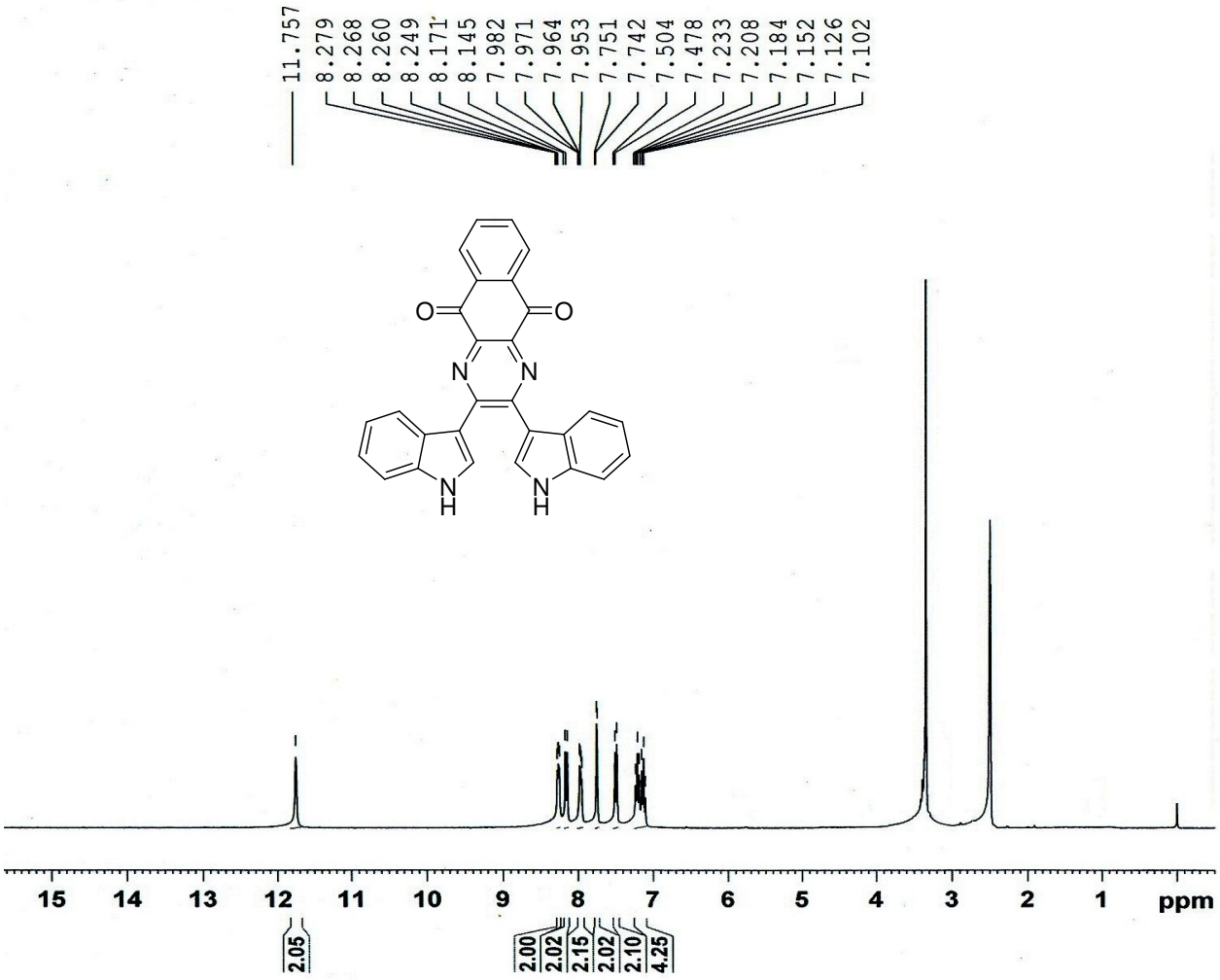

Figure S49. ^{1}H-NMR for **R1**

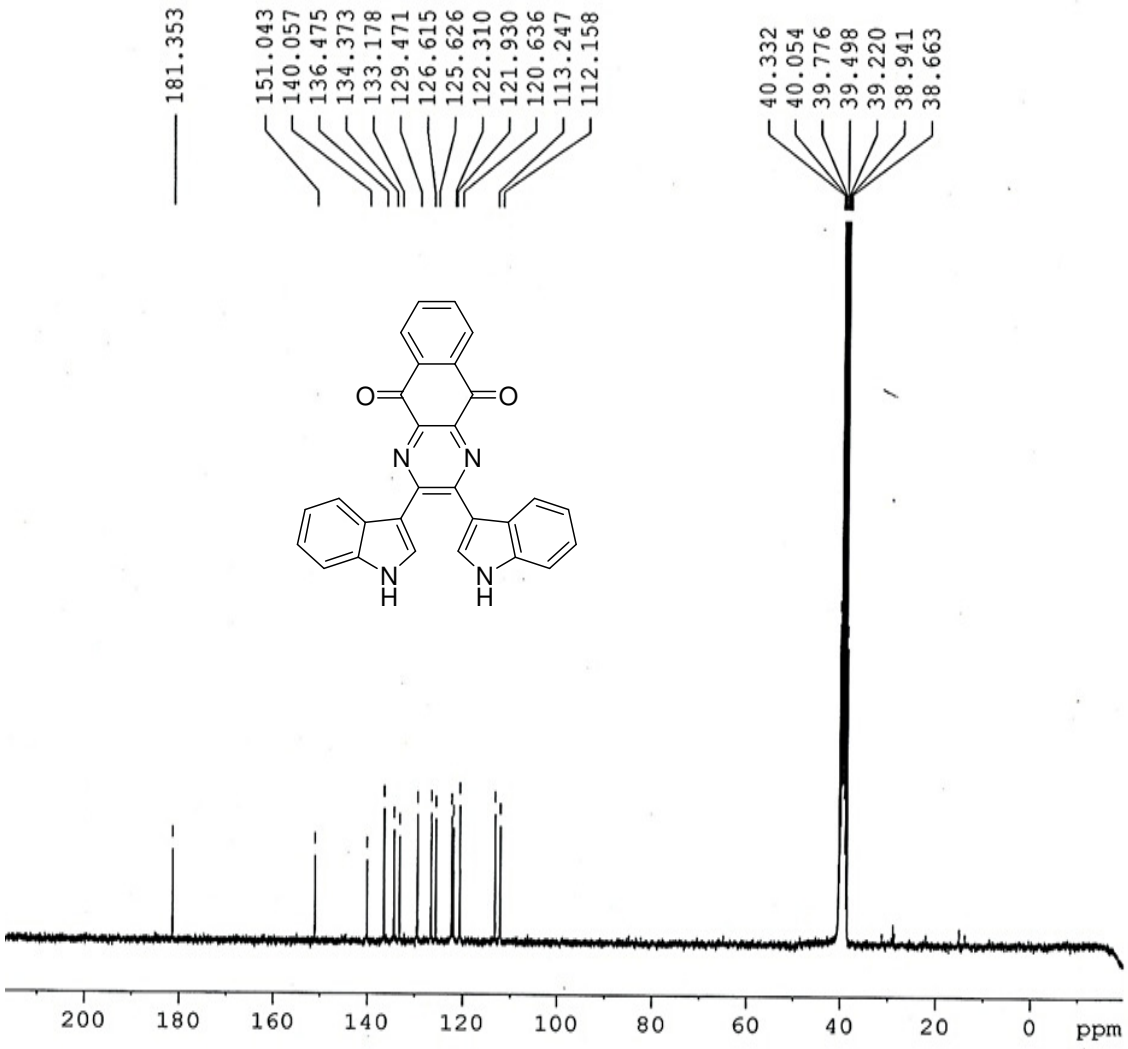

Figure S50. ^{13}C-NMR for **R1**

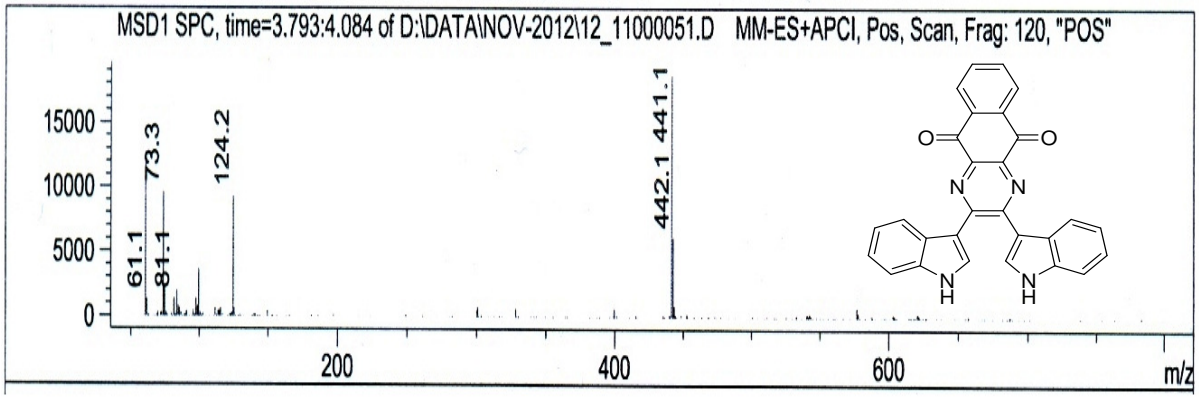

Figure S51. LCMS for **R1**

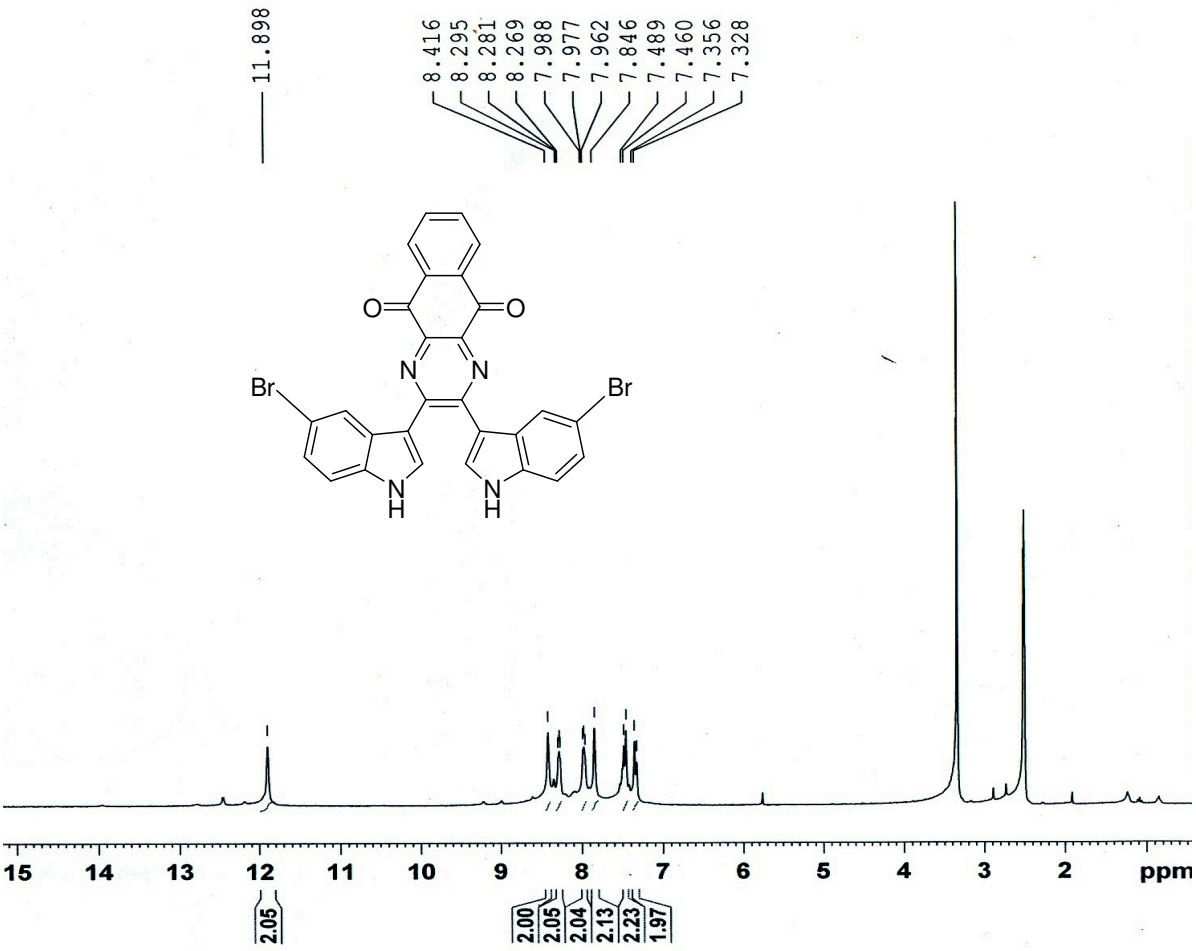

Figure S52. ^{1}H-NMR for **R2**

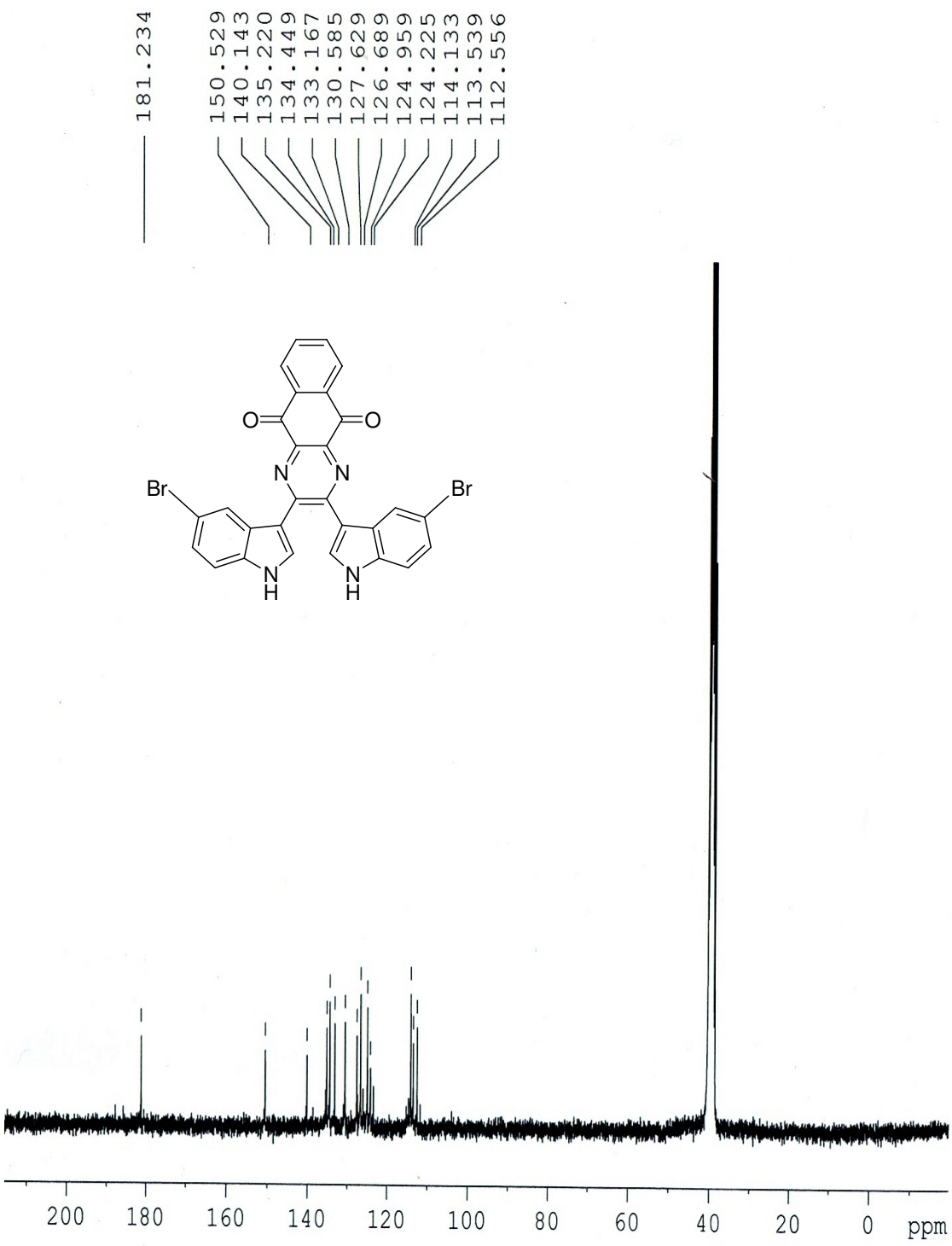

Figure S53. ^{13}C-NMR for **R2**

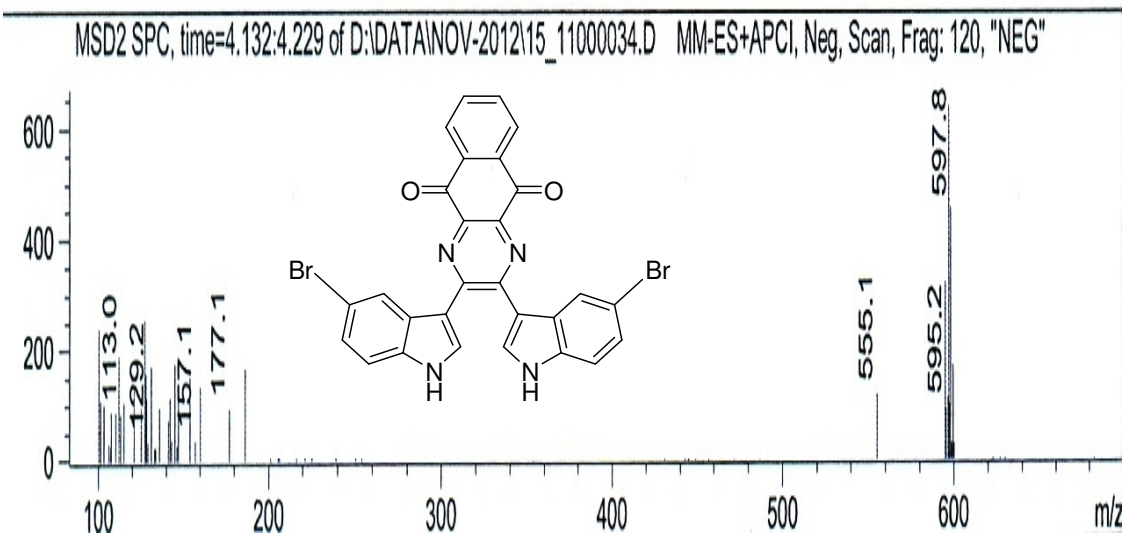

Figure S54. LCMS for **R2**

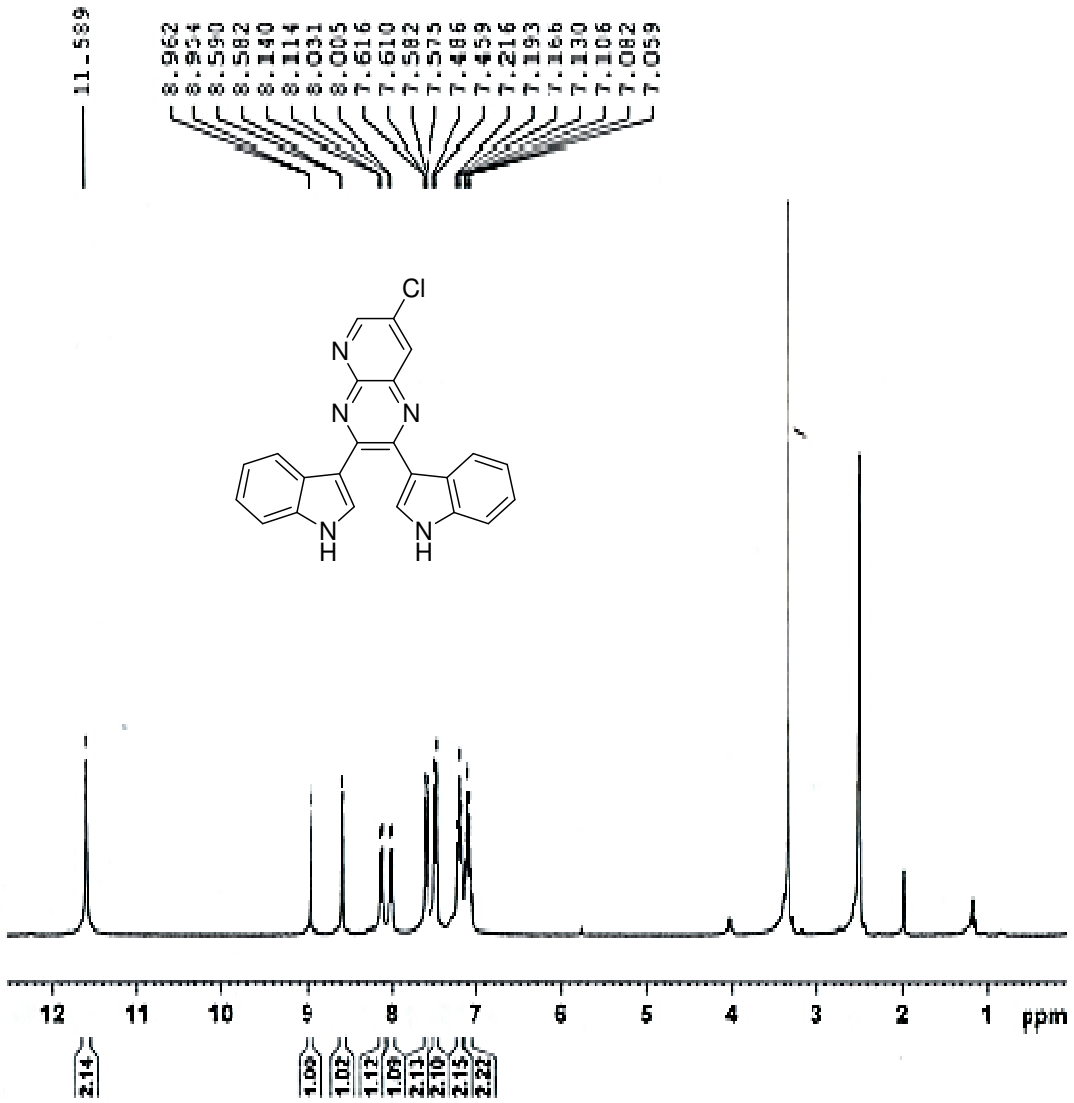

Figure S55. ^{1}H-NMR for **R3**

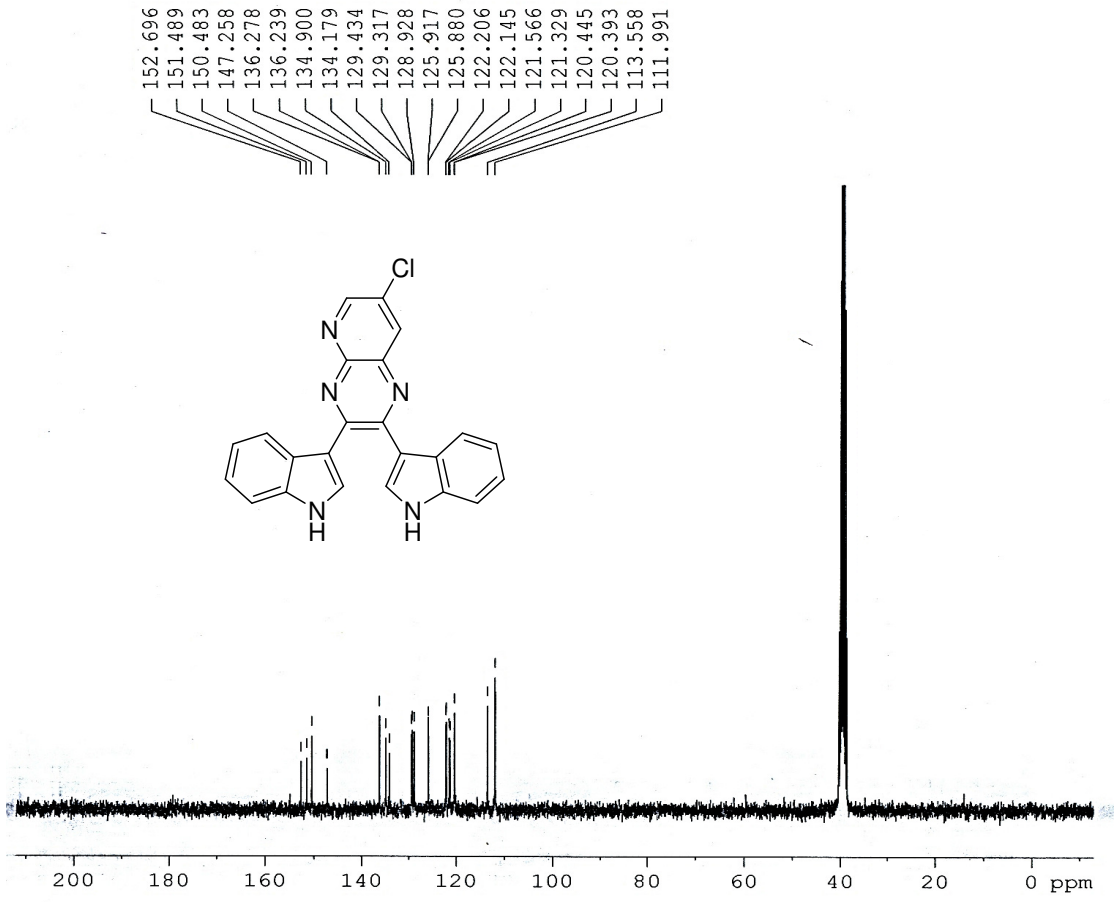

Figure S56.[13]C-NMR for **R3**

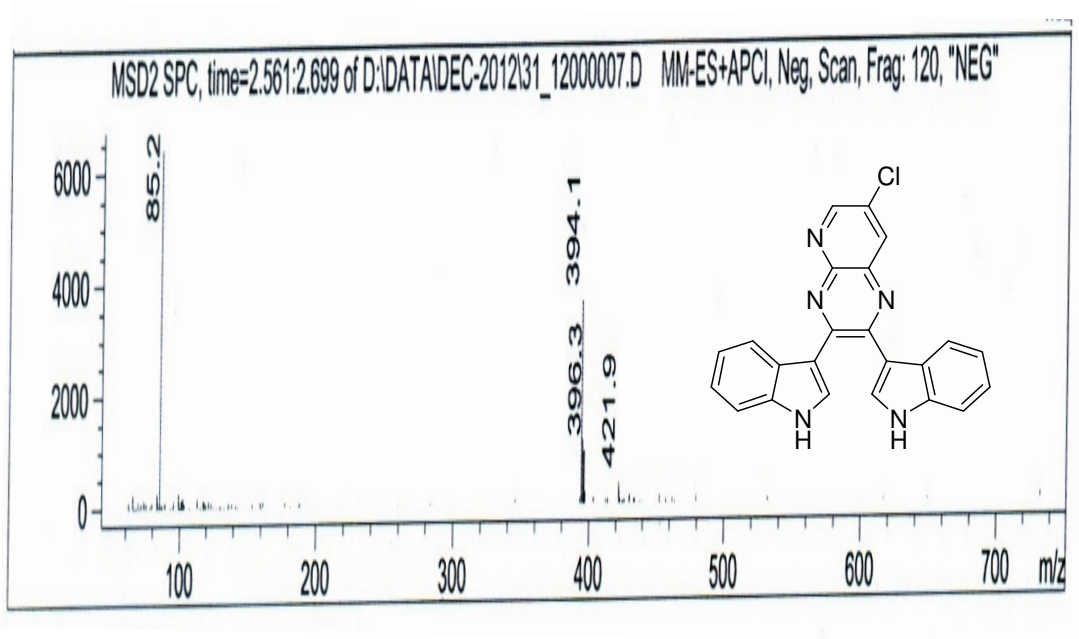

Figure S57. LCMS for **R3**

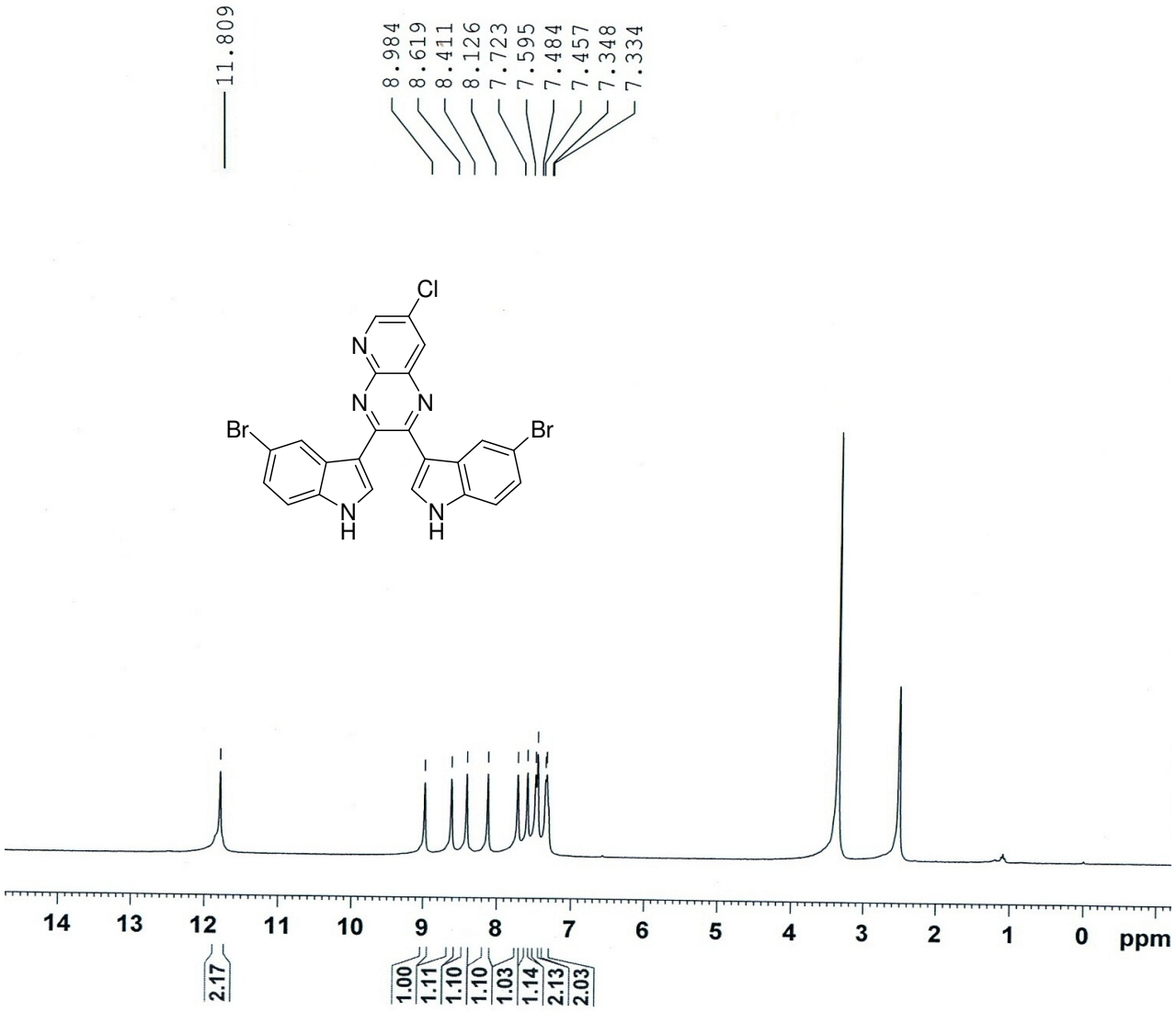

Figure S58. ^{1}H-NMR for **R4**

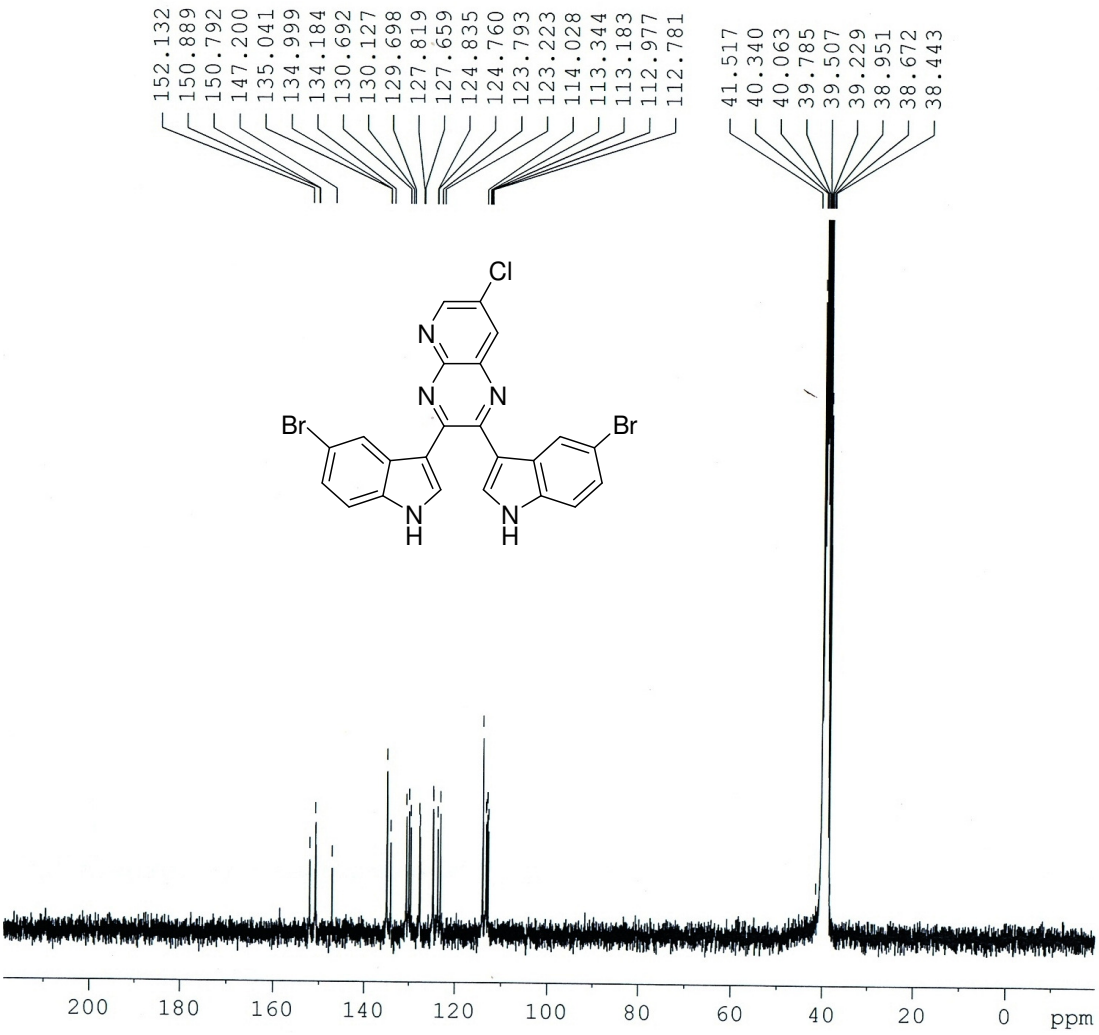

Figure S59. ^{13}C-NMR for **R4**

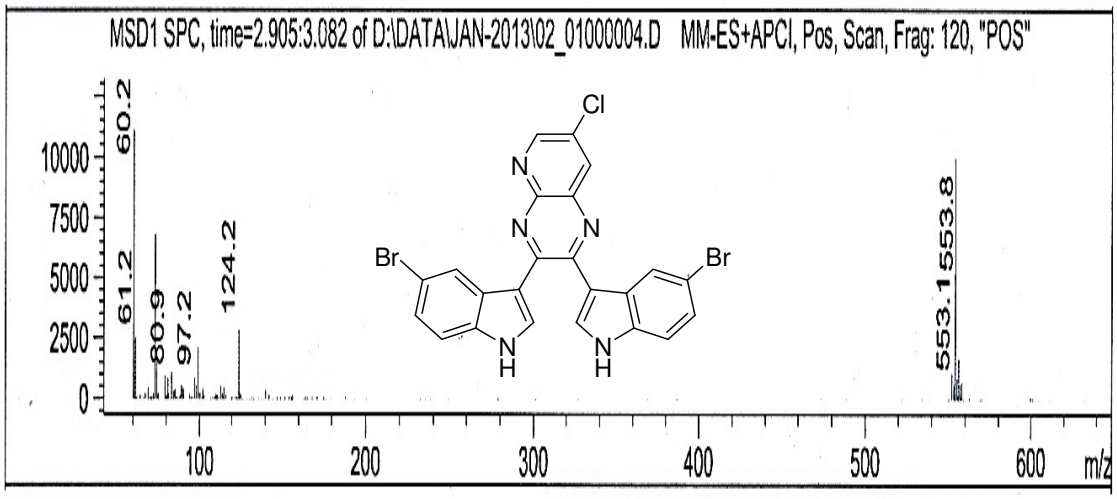

Figure S60. LCMS for **R4**

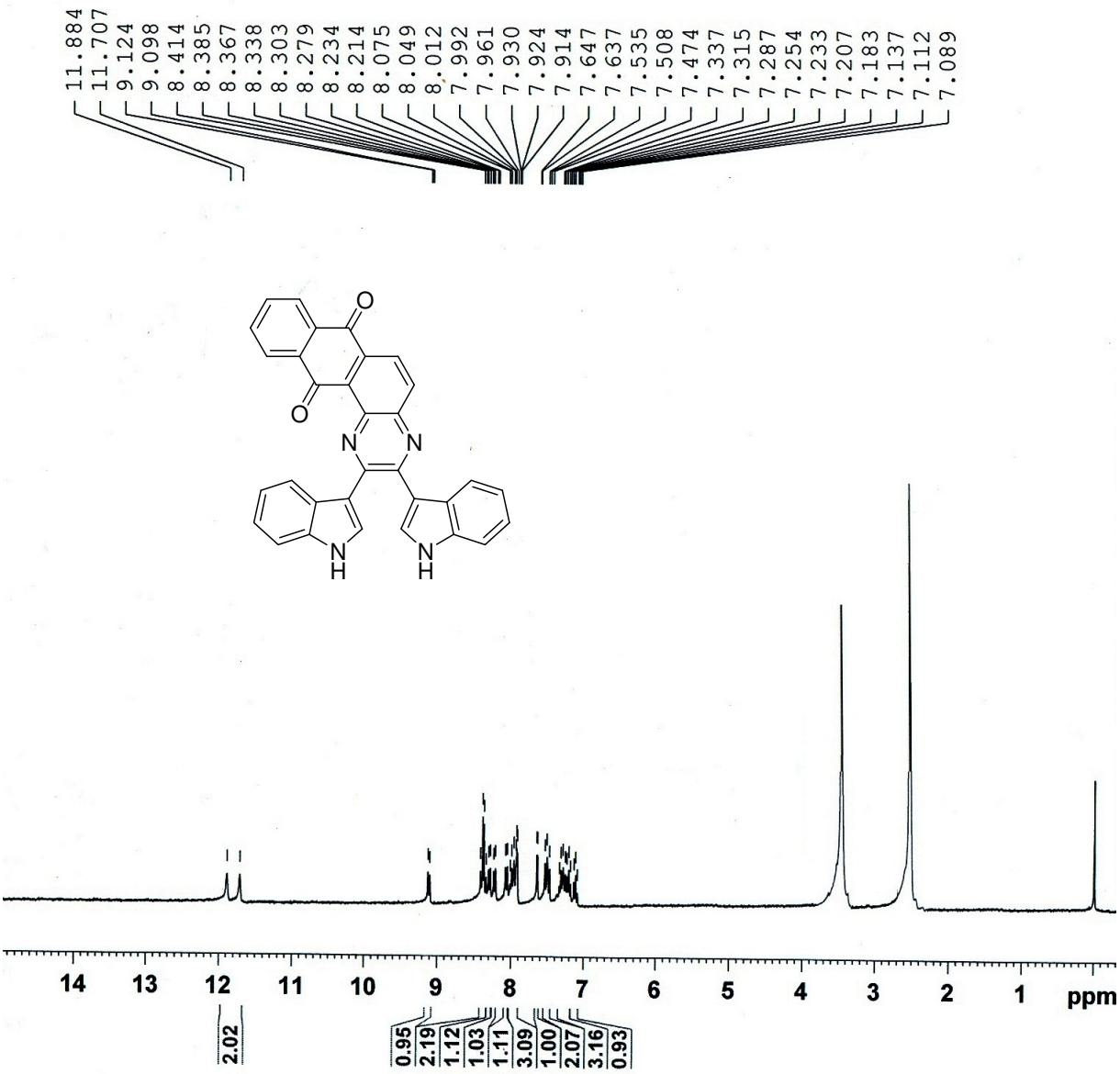

Figure S61. [1]H-NMR for **R5**

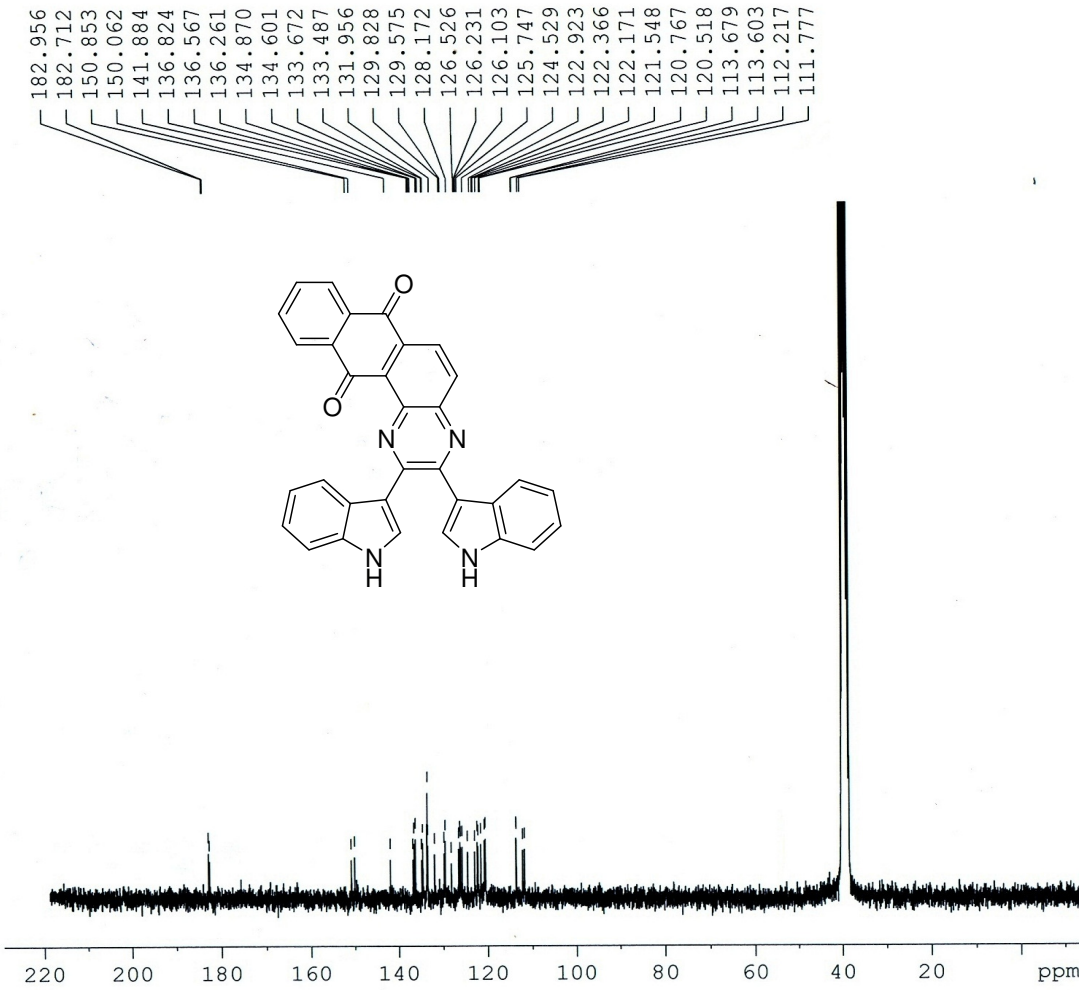

Figure S62. ^{13}C-NMR for **R5**

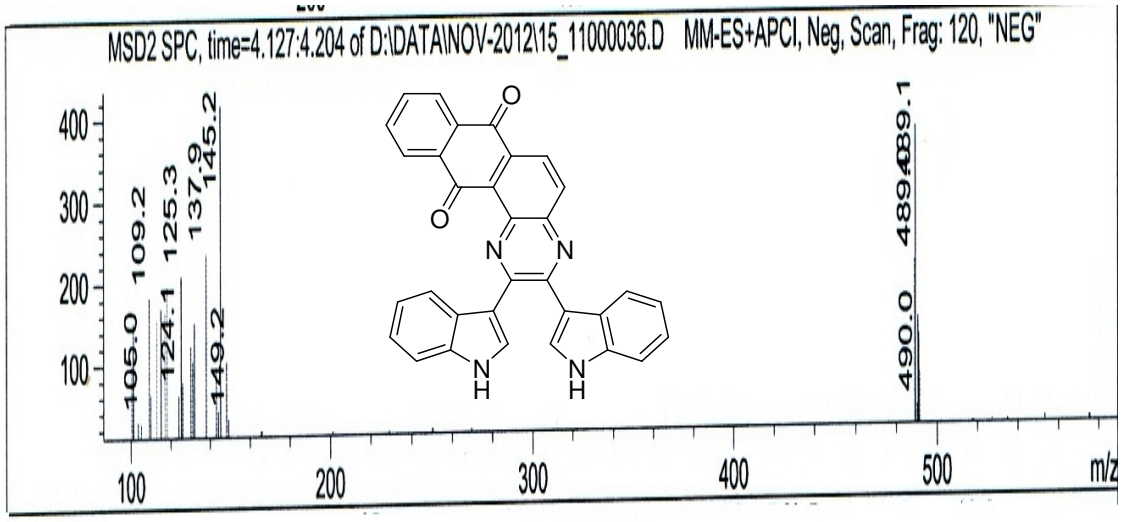

Figure S63. LCMS for **R5**

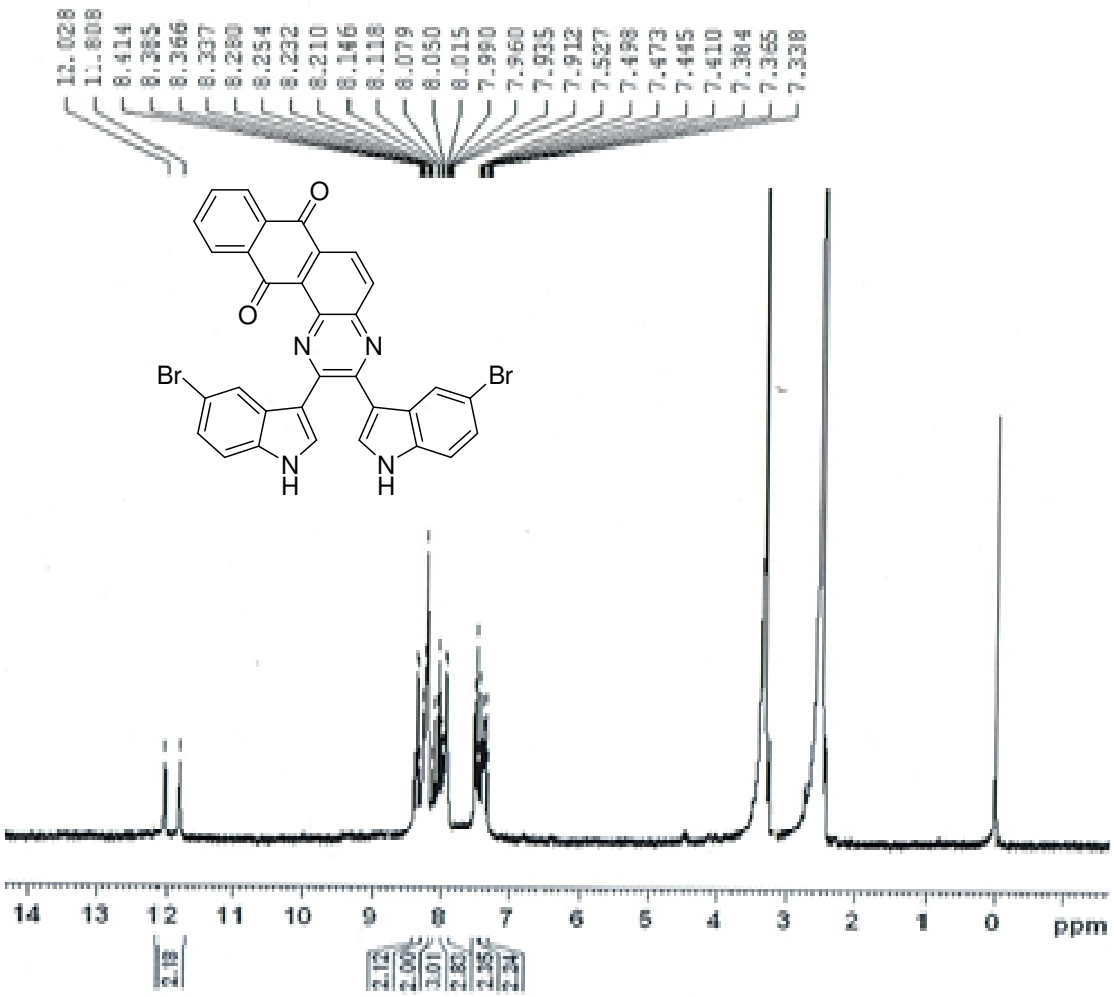

Figure S64. ^{1}H-NMR for **R6**

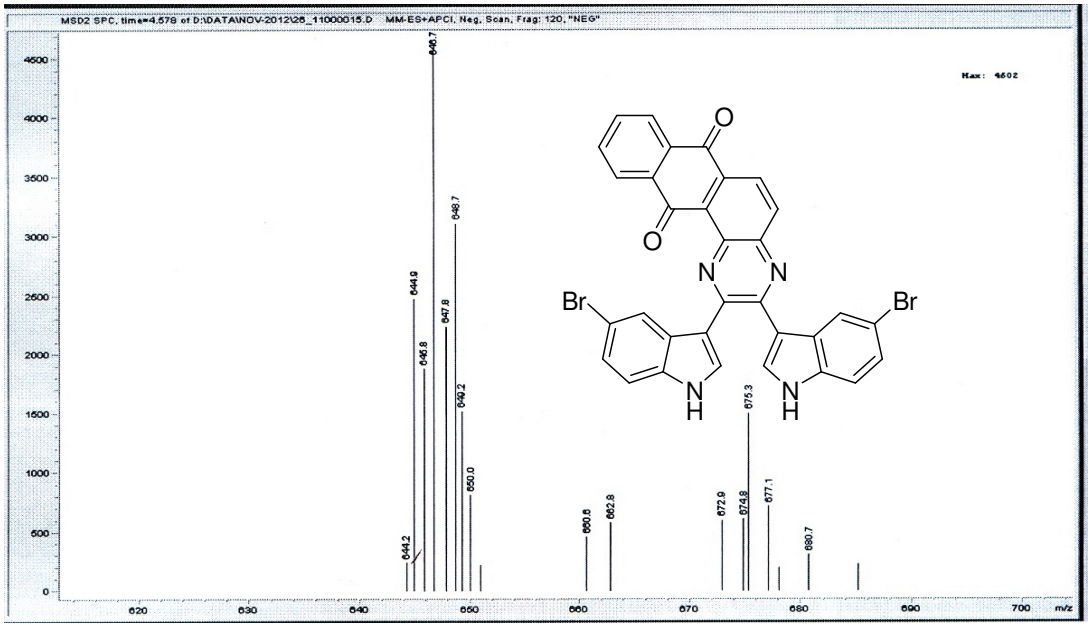

Figure S65. LCMS for **R6.**

Receptor	δ_{N-H} in free receptor	δ_{N-H} in complex	$\Delta\delta$ (ppm)
R1	11.757	11.920	0.163
R2	11.898	12.078	0.180
R3	11.589	11.711	0.122
R4	11.809	11.944	0.135
R5	11.707,11.884	12.034	0.150
R6	11.808,12.028	12.183	0.155

Table S1. ^{1}H NMR spectral data for the interaction of the receptors with F^{-}

Details of data collection and structure refinement

The XRD analysis of the **R4** was done at SAIF, Indian Institute of Technology, Madras. X-ray data collection was performed with Bruker AXS Kappa Apex II CCD Diffractometer equipped with graphite monochromated Mo (Kα) (λ = 0.7107 Å) radiation. Crystal fixed at the tip of the glass fiber using cyanoacrylite adhesive was mounted on the goniometer head with the aid of video microscope and optically centered at the sphere of confusion of the goniometer axes. The automatic cell determination routine, with 36 frames at three different orientations of the detector was employed to collect reflections for unit cell determination. Further, intensity data for structure determination were collected through an optimized strategy which gave an average 4-fold redundancy. The program APEX2-SAINT (Bruker, 2004) was used for integrating the frames. Four-fold redundancy per reflection was utilized for achieving good multi-scan absorption correction using the program SADABS (Bruker, 2004). Besides absorption, Lorentz, polarization and decay corrections were applied to intensity during data reduction. The structures were solved by direct methods using SIR92 (Altormare et al., 1993)) and refined by full-matrix least squares techniques using SHELXL-2014 computer program. Molecular graphics were drawn using ORTEP3. The relevant details of data collection and refinement are given in Table 1 (Main text).

Refinement details

In the indole rings, the carbon atoms of benzo -moities and bromines connected to the ring are disordered over two site occupancies. The disorder was resolved by successive Fourier electron density maps and least squares refinements. Sum of the occupancies of the disordered components were restrained as 1 during refinement.

The occupancies of major components of the groups C12 - C15 & Br1 and

C19 - C22 & Br2 are 0.78 and 0.82 respectively. The C-C and C-Br bond distances in indole moieties were restrained using DFIX and SADI commands with the effective standard deviations 0.02 and 0.01 A^0 respectively. Anisotropic displacement parameters (U_{ij}) of atoms in the disordered groups were restrained to be equal within the limits of allowed standard deviation. The thermal parameters of the disordered atoms were restrained to show approximate isotropic behavior within an effective standard deviation of 0.01 A^{2o} . The FLAT instruction is used to restrain the atoms of the benzo moieties to lie in a plane. The solvent (acetone) was also modeled as disordered and sum of the occupancies of the disordered components were restrained as 1 during refinement using appropriate restrains wherever necessary.

References.

1. Altormare, A., Gascarano, G., Giacovazzo, C. & Guagliardi, A. (1993).

SIR92. J. Appl. Cryst. 26, 343-350.

2. Bruker (2004). SADABS. Bruker AXS Inc., Madison, Wisconsin, USA.

3. Bruker (2004). APEX2 and SAINT-Plus (Version 7.06a). Bruker AXS